Lithium-ion Traction Battery Design for FSAE Racing Car

M.Sc. DEGREE IN AUTOMOTIVE ENGINEERING

Marco Maglio

Department of Mechanical Engineering

Polytechnic of Turin

Academic Advisor:

Prof. Andrea Tonoli

Abstract

This thesis work discusses the detailed design of the Traction Battery of the 2018 FSAE season car, a project on which I have been working as Technical Director of the PoliTO racing team in the academic year 2017-2018. The starting point for the car development was the analysis of the weaknesses of the previous car, with a focus on the improvement of the vehicle handling, aerodynamic, control as well as on weight reduction. The Traction Battery resulted to have a huge impact on the vehicle weight and packaging. A new design has been crucial to lower the centre of gravity and allow the integration of a diffuser which increased the vehicle downforce.

Power and Energy targets were established using data from the previous season races, and the safety requirements were updated according to the current FSAE regulations. Together, these factors drove most of the technical choices.

The Traction Battery used a new cell chemistry, which resulted in an overall increased specific energy while keeping the same nominal energy and specific power. Cell selection was done based on literature review to understand cell behaviour and characteristics at different operating conditions. Experimental tests were performed to validate an equivalent model for electric and thermal simulations, conducted to deliver the best parallel and series configuration along with an optimized cooling system.

Cells connection was found to play a fundamental role in the design choices. A new cell bonding technology was adopted, which provided the best performance and reliability outcomes, simplifying the manufacturing and assembly processes. The achieved results show that the designed Traction Battery could withstand the maximum power request during all dynamic events and store enough energy to complete the endurance event with remarkable results in efficiency.

Aknowledgements

The work presented here represents a milestone in my career as well as in my personal life. Indeed, this thesis represents my first complete work as an automotive engineer and my last as a student. It is the result of two years spent in the PoliTO racing team and my biggest achievement as the Technical Director of the team for the academic year 2017-2018.

I'd like to thank Professor Andrea Tonoli for his support throughout my entire experience in the racing team, as well as his advises during the development of this work and his expertise in automotive field which drove every technical aspect of the SC18 design. Although these years have been tough and very intense, I'm grateful to the Polytechnic of Turin for the opportunities, knowledge and cultural stimuli it gave to students. Being part of this excellence community has been an honour for me.

A big thank goes to the PoliTO racing team and to the many people it is composed of. They have been a family for me during these last two years and the experiences made together allowed me to grow under the technical and personal points of view, developing skills that would certainly become fundamental during my career and my entire life.

I'd like to thank FCA®, which represented the team main sponsor and provided us all with the facilities needed to manufacture and assemble the car. Moreover, I'm grateful to Podium Advanced Technologies, another PoliTO racing team partner, for providing me the technical support as well as the testing and manufacturing facilities without which this work wouldn't have been done.

Finally, I'd like to thank Francesca, my father Paolo, my mother Anna and my brother Luigi for believing in me and for being always supportive throughout my study career and life. In particular, Francesca has been the needle of my compass.

Contents

1 Introduction

1.1 FSAE Electric Competition

The Formula SAE Electric competition is an international student competition that challenges universities to conceive, develop and produce small, Formula style electric vehicles and compete against each other [1]. The competition allows the teams to show their creativity and engineering skills, applying cutting edge technologies and research findings to design racing electric cars. Each vehicle should ensure safety, high performances and durability to complete all Formula SAE examinations. In particular, two are the main events each team has to face during the competition: Static and Dynamic.

The Static events are divided in three categories and meant to introduce the team's vehicle and give an overview of the manufacturing and designing processes [1]: the Business Presentation, the Cost Analysis and the Engineering Design event. Each category has a maximum score, summarised in Table 1.

During the Business Presentation event, the teams have to present to a jury the vehicle's concept and provide a comprehensive business, logistical, production and technical case to convince potential external funders to invest in the team's concept. Moreover, the event represents a good opportunity for students to attend a business pitch in front of market's experts.

Before the beginning of the competition, each team submits a cost analysis document with a detailed cost-breakdown of every component of the car, as well as the manufacturing and assembly expenditures. During the Cost Analysis event, the teams are evaluated for their capacity to make trade-off decisions between content and cost based on the performance of each part, on the assembly and the overall manufacturing process.

Finally, during the Engineering Design event the teams discuss their design choices in front of a group of experts. The aim is to judge how their choices met the intent of the market both in terms of vehicle performance and overall value. Usually, the main areas considered for the evaluation are aerodynamics, chassis, electrical, ergonomics, management, powertrain and suspension.

Event Name	Points
Business Presentation	75
Cost Analysis	100
Engineering Design	150

Table 1: FSAE Electric Competition: Static Events

The Dynamic events evaluate the car during the competition based on its performance and involve five different events (Table 2).

- The Acceleration event tests the vehicle acceleration in a straight line and on a flat pavement over 75m from the starting to the finish line.
- The Skidpad event measures the vehicle cornering ability on a flat surface. Drivers have to complete a course of two pairs of concentric circles in a figure-eight pattern.
- The Autocross judges the car's manoeuvrability and handling performance over a 0.805 km course, which consists of numerous corners, hairpins and slaloms.
- The Endurance event evaluates the overall performance of the vehicle, its durability and reliability. It consists of 20 laps of a closed course to a total distance of approximately 22km. Meanwhile, the energy efficiency is measured to determine how well the team tuned its car.

Event Name	Points
Acceleration	100
Skid Pad	75
Autocross	125
Efficiency	100
Endurance	275

Table 2: FSAE Electric Competition: Dynamic Events

As of 2017, 172 were the registered teams in Formula SAE, of which 153 participated to the competition [2]. Table 3 shows the main characteristics of the racing cars of the five top world competitors. The last two columns present the same parameters of the cars designed by the PoliTO racing team in 2016 and 2017. Clearly, the weight represents the parameter by which the PoliTO racing vehicles differ the most compared to the top teams.

	TU Delft 2017	*ETH Zurich 2017*	*KIT Karlsruhe 2017*	*Universität Stuttgart 2017*	*DHBW Stuttgart 2017*	***PoliTO (2016)***	***PoliTO (2017)***
Traction	4WD	4WD	4WD	4WD	4WD	**4WD**	**4WD**
Motors and Inverters	AMK	Self-developed	Self-developed	AMK	AMK	**AMK**	**AMK**
Weight [kg]	171	181	173	172	193	**258**	**223**
Energy [kWh]	7.4	6.4	7.0	6.8	6.7	**6.7**	**7.4**

Table 3: FSAE Top competitors comparison

In a racing car, an increase of its performance is based on the weight-power ratio. While, many competitions limit the vehicle minimal weight to ensure a Balance of Performance, Formula SAE does not provide restriction on mass, which makes weight the main parameter on which teams focus to achieve the best performance. In the last competitions, racing teams from other universities have indeed presented vehicles with weights spanning from 300kg to 160kg.

In 2015, the PoliTo racing team presented its electric car, equipped with an AMK Powertrain with a 4WD traction, which weighted 260kg (Figure 1). In 2016, the team didn't design a new car but rather worked on the improvement of the previous model reliability. In 2017, it was both conceived a new design and the overall weight was reduced of 40kg. The aim of the team for the competition of 2018 consisted of a further weight reduction of 20kg, to reach 200kg.

Figure 1: PoliTo racing car for the years 2015 and 2016.

Figure 3: Racing car designed by the team for the FSAE Competition of 2017.

The project design of the 2018 started from the previous season car, which achieved high performance and showed high reliability during the 2017 races. It was carried out a detailed analysis of the elements with high influence on the overall car's weigh (Figure 2). It turned out that the battery pack was the most impacting element, followed by the monocoque and the unsprung masses.

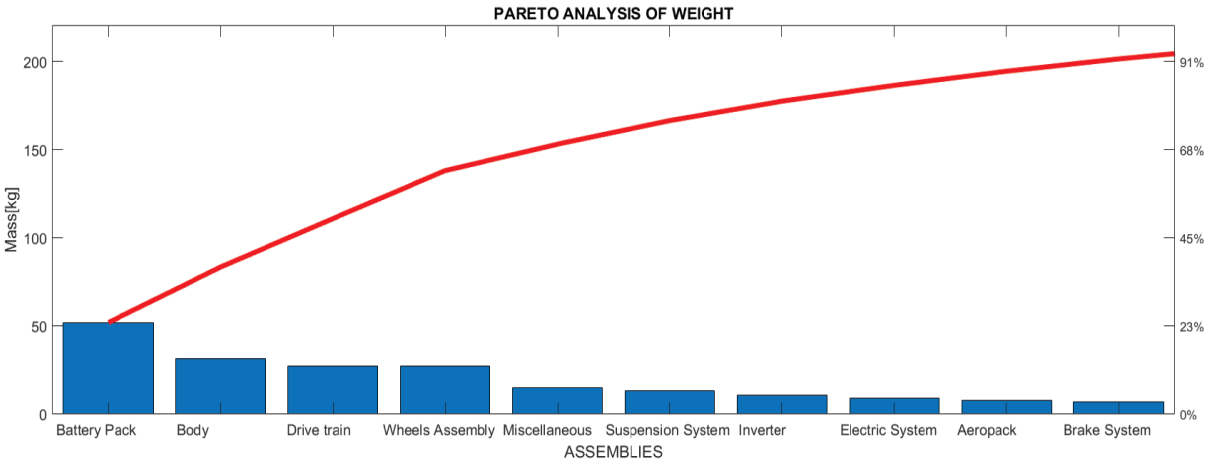

Figure 2: Pareto analysis of the weight of the main elements of the 2017 car.

Generally, in a mechanical component weight reduction is achievable through topological optimization, that is through an optimization of the component design according to its task in the overall system. However, the use of composite materials associated with recent production technologies (*i.e.* 3-D printing) can further contribute to the purpose. For battery packs, whose main weight is related to the chemistry used to stock energy, weight reduction is not so immediate, especially if it must be maintained a high specific power ratio.

1.2 Electric powertrain

The Electric powertrain comprises the main components that generate power and deliver it to the road surface, in this case the battery, the electric motors and their power inverters (Figure 5). It includes an Accumulator, which supplies power to the inverters, that take inputs from the Vehicle Control Unit to power four independent motors, each of them mounted before an epicyclic gear train inside the upright as depicted in (Figure 4).

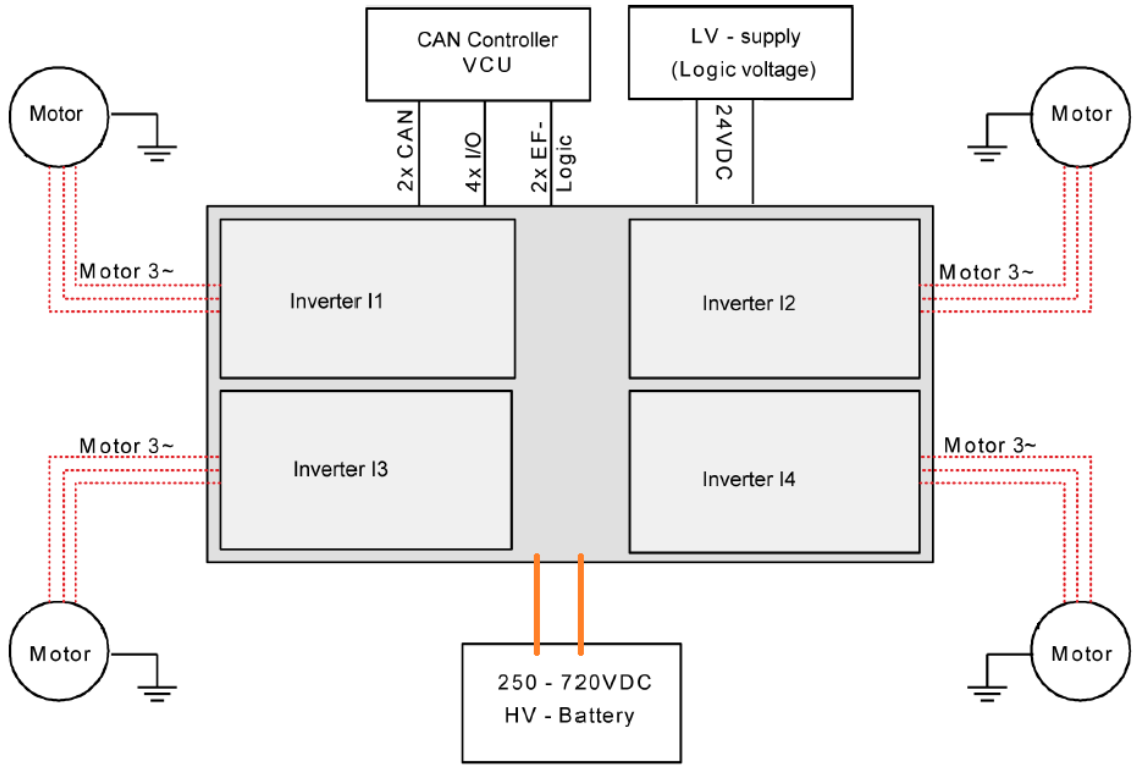

Figure 5: Overview of the electric powertrain system.

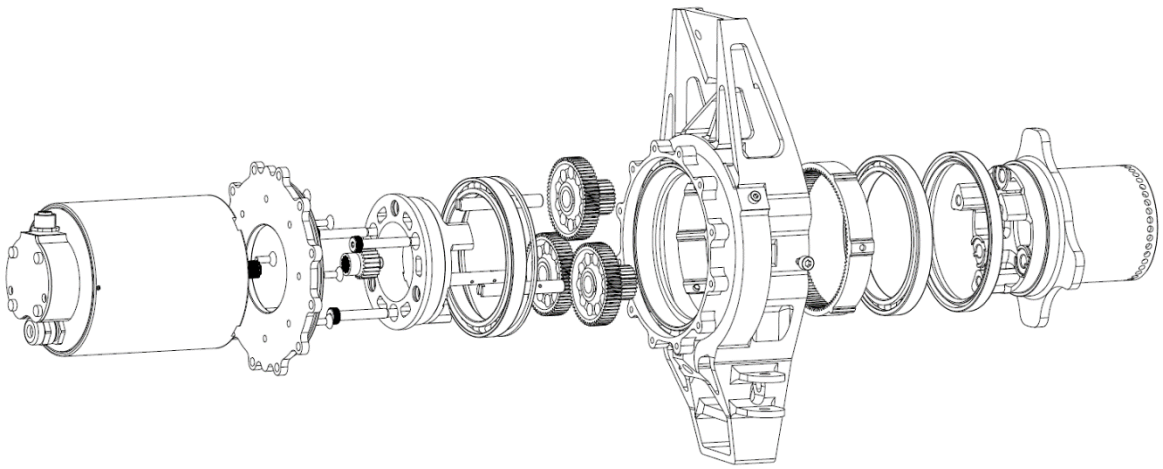

Figure 4: Exploded view of the complete in-wheel drive-train of the racing car 2018.

1.2.1 Motors and Inverters

The Formula Student Electric (FSE) Racing Kit by AMK was the only package considered to any notable degree. The FSE Racing Kit is a complete system that has been tailored to suit FSAE teams, and includes:

- An AMKASYN KW26-S5-FSE-4Q Inverter
- Four DD5-14-10-POW synchronous servo motors

The DD5-14-10-POW is a 10-pole permanent-magnet synchronous motor which has a greater power density and flatter torque profile, compared with induction motors. This result can be achieved thank to the use of the latest developments in magnet technology which allow for greater magnetic field strength and therefore greater torque and power ratings. The key specifications of the motor are listed in Table 4.

Mass	3.55 kg
Rated Torque	9.8 Nm
Rated Power	12.3 kW
Rated Speed	12,000 rpm
Maximum Speed	20,000 rpm
Rated Voltage	350 V_{rms}
Rated Current	41 A_{rms}
Maximum Current (for 1.24 s)	100 A_{rms}

Table 4: DD5-14-10-POW motor specifications.

Figure 6 is an extract from the datasheet showing the performance curves of the motor; the top graph represents the torque as a function of the speed, while the bottom one displays the power curve as a function of the speed. The continuous torque and power characteristics are represented in orange colour, whilst the blue curves represent the peak performance which are limited to protect the IGBT (Insulated Gate Bipolar Transistor) inside the power controller module. Ultimately, the dashed curves represent the performance of the motor with field-weakening, where a negative magnetisation current is spent to oppose and reduce the magnetic field strength of the Permanent Magnet rotor to have higher torque with increasing rpm. It is worth noticing that since the powertrain is supplied by the tractive pack, the voltage will reduce as the state of charge depletes, assuming no field weakening the maximum speed of the motor as well as the output power will reduce. The relatively low-speed torque range until 12000rpm of the motor is not affected by the supply voltage however and will therefore allow the same acceleration performance regardless of battery state of charge.

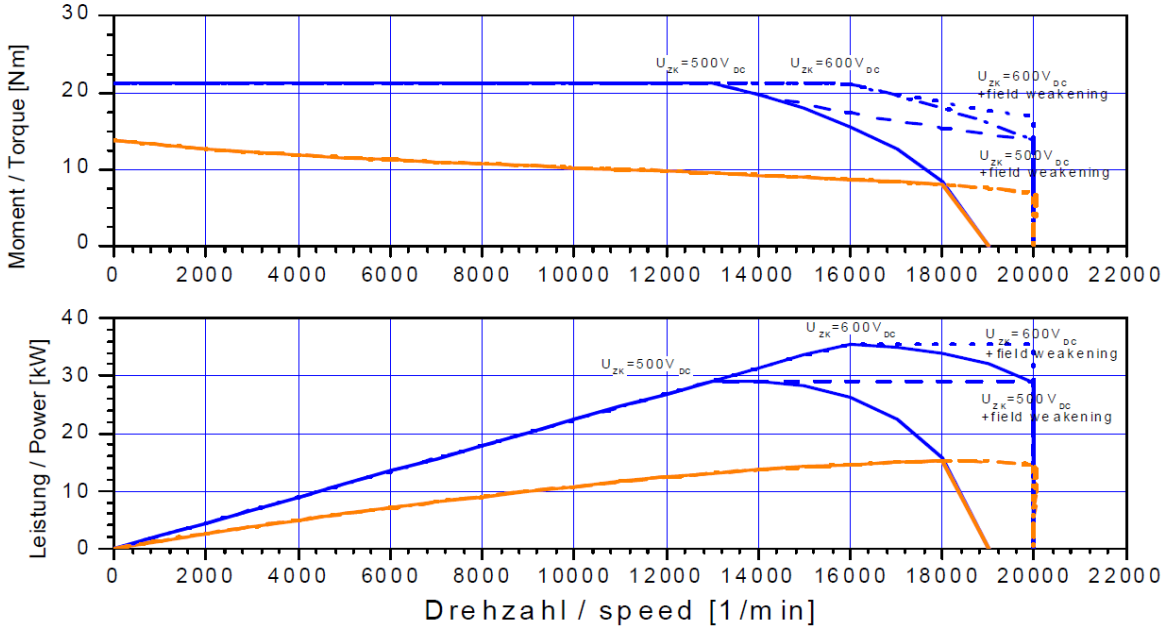

Figure 6: DD5-14-10-POW motor performance curves.

The AMKASYN KW26-S5-FSE-4Q inverter, whose characteristics are specified in , is a quad-inverter unit with integrated drive controllers, which can be assembled in modular configuration allowing to exploit different packaging design (Figure 7).

Input voltage range	250 Vdc – 720 Vdc
Input current (for HV = 540 Vdc)	48 A
Control method	PWM, Field-Oriented Control
Switching frequency	8 kHz
Output voltage range (HV = 250-720 Vdc)	160 – 490 Vac (sinusoidal output current)
Rated output current	43 A
Peak output current	105 A (for 10 s)
Efficiency	Approx. 98%

Table 5: KW26-S5-FSE-4Q inverter specifications

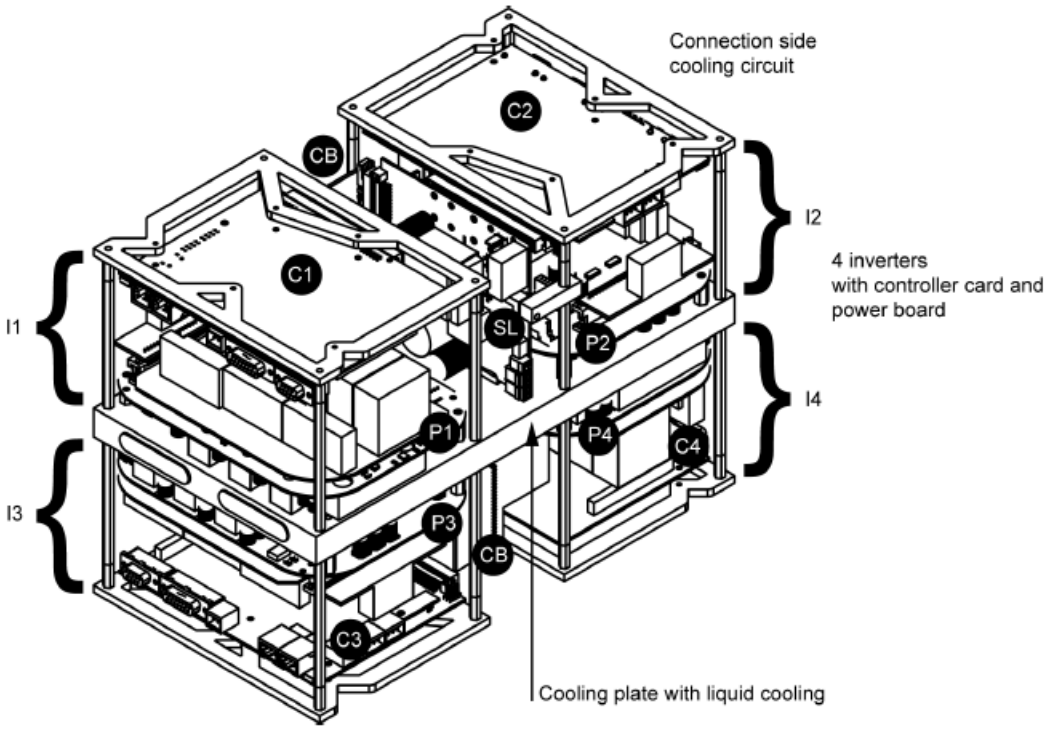

Figure 7: KW26-S5-FSE-4Q Inverter assembly view.

Where:

- I1 represents the modular inverter, which contains the power electronic and a controller card for the motor;
- P1, P2, P3, P4 are the Power Electronic for the inverter for each inverter module;
- C1, C2 C3, C4 symbolise the controller cards for each inverter module. C1 and C2 and C3 and C4 form two couples which share the same CAN network and low voltage supply;
- SL is the power supply and the logic board for the couples formed by I1 with I2 and by I3 with I4;
- CB represents the transverse board, which connects I1 with I2 and I3 with I4.

1.2.2 Tractive Battery

There are several parameters that can be used to classify battery technologies, the most important of which can be described as it follows:

- *Capacity*: the measure of the charge that can be stored by the battery. It represents the maximum current the battery can deliver under specific discharge conditions over time and it is measured in Ampère-hour (Ah);

- *Power*, calculated as the product of the current and the voltage and measured in Watts (W);
- *Energy*, the product between the battery capacity and the average discharge voltage (Wh);
- *Gravimetric power density* (or *specific power density*) and *volumetric power density*. The former is expressed as the ratio between the battery power output and its weight (W/kg), while the latter is the ratio of the power and the battery volume (W/l). They are the among the most important parameters for electric hybrid vehicles and, usually, their high values imply low electrical resistance, which results in low energy losses and high-power capability;
- *Gravimetric energy density* (also known as *specific energy density*) and *volumetric energy density*. They represent the battery capacity in weight (Wh/kg) and in volume (Wh/l) The realistic gravimetric energy density of the cell level is usually 25-50% the theoretical value, which can be calculated from the main electrochemical reaction;
- *Energy efficiency*, that is the ratio between the energy released during discharging and the energy stored during the charging event. In lithium ions batteries this is usually very high and above 95% [3][4].

Other parameters that apply to battery technologies which are – however – less important for applications with limited amount of cycles are the following:

- *Calendar lifetime*. It describes the battery lifetime until failure. The two main factors influencing this parameter are time and temperature. In standard-vehicles, many high-performance batteries might die due to calendrical ageing rather than capacity turnover.
- *Cycle lifetime*. It describes the complete charge-discharge cycles the battery can perform until failure and it is measured in full equivalent cycles. It depends on the cycle depth, current rate and average SOC .

Although capacity, power, energy and efficiency represent important parameters to characterise batteries, most of the times the power-to-energy ratio is more useful during battery design. Indeed, an increase of the total energy and power available is possible by adding more cells in a battery pack, while variation in the power-to-energy ratio allows changes in the battery pack design, which – if properly done – might result in optimized battery performance. The power-to-energy ratio mostly consists in a compromise between active materials and cell design, which can be visualised in a Ragone plot. It describes the performance of a battery technology in the power-energy plane. The Ragone plot shown in Figure 8 provides an overview of the specific power and energy densities for different battery technologies [5]. The characteristic downward-

curving shape comes from fundamental physics principles [6], which basically impose a relationship of inverse proportionality between energy production and discharge power. Clearly, lithium ion batteries represent the best technology compared to other cell chemistries. However, their specific energy and power can significantly vary changing the battery design.

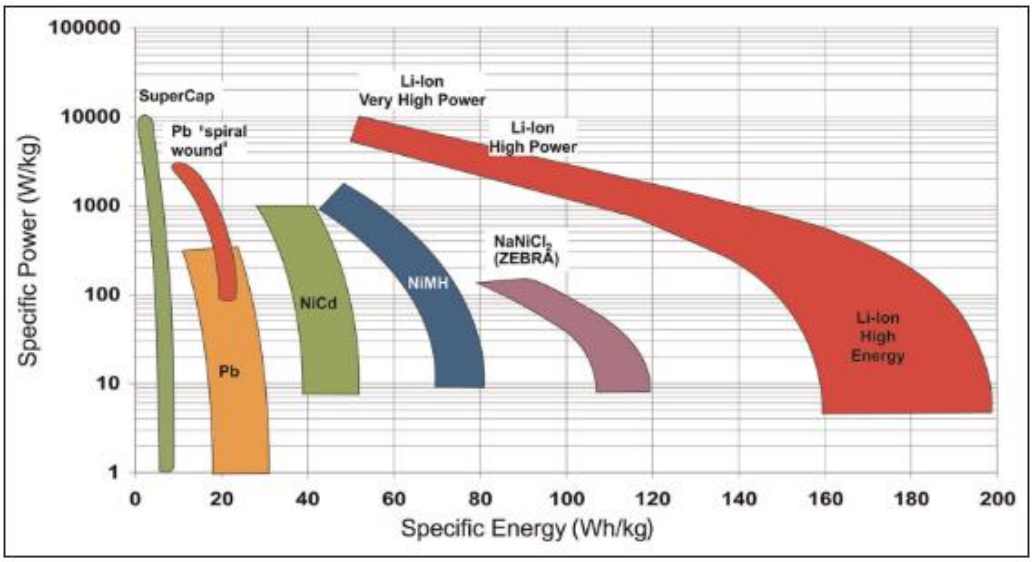

Figure 8: Ragone plot of different battery technologies [5]. SuperCap: supercapacitor; Pb: lead; Li-ion: lithium-ion; NiCd: nickel–cadmium; NiMH: nickel–metal hydride; NaNiCl2: sodium–nickel chloride; ZEBRA: Zero Emission Battery Research Activities.

The battery pack 2017 used cells with lithium-polymer technology (with specifications shown in **Table 6** and with the design depicted in Figure 9). Its characteristics are listed in Table 7, while Figure 10 provides an overall view of the pack design. For the following year it was decided to switch to a lithium-ion cell technology, with the aim of finding a better trade-off between specific power and specific density, which would have allowed a weight reduction without penalising power and efficiency. This thesis project focuses on the choices and the considerations which have been done and that brought to the design of an innovative yet high performant battery pack.

Capacity	7.0 Ah
Nominal Voltage	3.7 V
Max. Continuous charge Current	14.0 A
Max. Continuous discharge Current	56 A
Cut-off Voltage	3.0 V
AC Impedance	< 2.5 mOhm
Operating Temperature	~20°C ~60°C
Weight	134 ± 2.5 g

Table 6: Characteristics of Li-Po cells composing the Battery Pack of the racing car 2017.

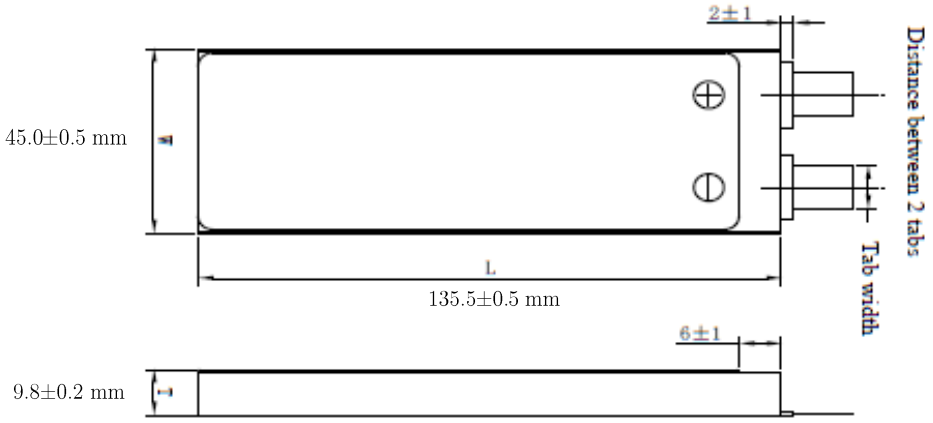

Figure 9: Dimensions of a Li-Po cell composing the 2017 battery pack.

Cell configuration	144s2p Li-Po cells
Total number of cells	288
Total number of modules	8
Max TS voltage	600 V
Energy	7.42 kWh
Peak Power	92.5 kW
Weight	53 kg
Energy density gravimetric	139.6 Wh/kg
Energy density volumetric	365.8 Wh/l

Table 7: Battery pack 2017 characteristics.

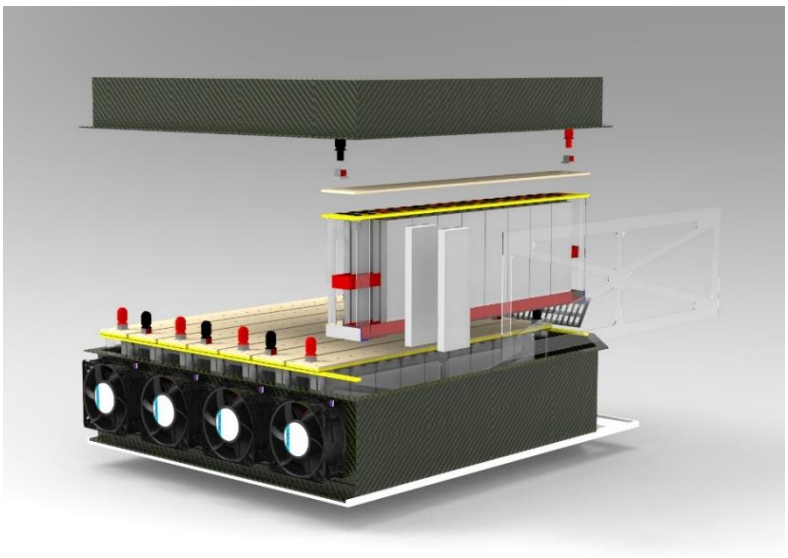

Figure 10: CAD of the battery pack of the 2017 racing car.

1.3 New Season Targets

The battery pack energy and power requirements mostly depend on the Endurance and Acceleration events respectively. During the Acceleration event the battery pack has to provide very high current levels to ensure maximum deliverable power to the motors. On the other hand, in the Endurance event the power available to the motors is limited to guarantee reasonable amount of energy considering the entire length of the course. Furthermore, part of the kinetic energy during braking can be recovered through the so called Regenerative Braking, which however would cause higher thermal stress on tractive system components.

The battery pack design represented one of the strengths of the 2017 car, due to its ability to store an adequate amount of energy. Indeed, during the three competitions the team participated to, the car has always been able to finish the Endurance event with excellent performance and a good energy management strategy. For this reason, it was decided to keep the same amount of energy and power peak performance for the racing car 2018. It is worth noticing that, by achieving an overall weight reduction, better aerodynamic efficiency and vehicle control, it might be possible to finish the Endurance events with higher mean power compared with the 2017 vehicle.

As we will see in the following chapters, the main factors influencing battery performance for electric vehicles applications are energy and power. However, there are also other relevant factors to take into account, such as cost, life, temperature, safety, rate of self-discharge (Figure 11) as well as materials availability and the need for maintenance. For EVs, designing battery packs that meet all the requirements is constrained by inherent trade-offs between the five main battery characteristics: energy, power, cost, longevity, and safety. Meeting one or two of these requirements is relatively easy, but it is very difficult to have the best performance for all five metrics. Therefore, most of the times, it becomes paramount a trade-off between the individual factors to achieve an optimal battery design.

Figure 11: Key performance parameters for electric vehicle batteries [7].

2 Cell Selection

2.1 Working principle

The working principle behind lithium ion batteries is relatively simple. During a discharging event, lithium ions (Li^+) move through a conducting electrolyte from the negative electrode (or anode) to the positive electrode (cathode). A porous membrane electrically separates the two electrodes and allows ions movement. In the meanwhile, electrons (e^-) migrate through an external circuit from the negative pole to the positive one, releasing current (Figure 12)[8]. During charging, the process occurs in the opposite direction and the battery stores the supplied electrical energy in form of chemical energy.

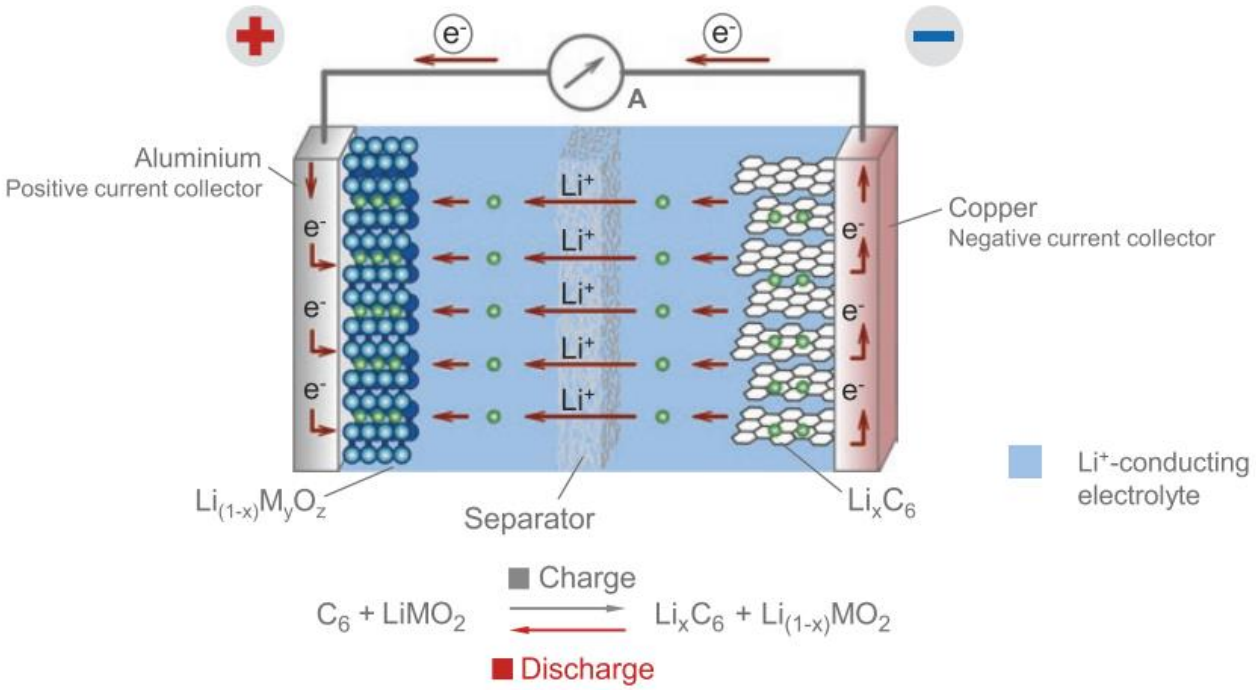

Figure 12: A lithium ion battery during discharging [7]. Lithium ions (Li^+) move from the anode, usually made of graphite (C_6 in the picture), to the cathode, a metal oxide (in the picture represented as M_yO_z). At the same time, electrons (e^-) move through an external circuit in the same direction.

Compared to other chemistries, lithium-ion cells offer several advantages. Firstly, they have high energy density, typically twice that of the standard nickel-cadmium batteries. As shown in Table 8, their higher voltage means that less cell connections in series are required to achieve the desired pack voltage. Furthermore, they show a lower self-discharge rate compared to nickel-cadmium cells, no memory effect and very good efficiency during charging and discharging [9][10]. Depending on the application, cells are produced in cylindrical, prismatic or pouch geometry; in batteries, they can be used singularly or connected in series (to increase voltage) or in parallel (to increase capacity) [8]. Finally, batteries based on lithium ion chemistries show a better cycle

life compared to other batteries, defined as the number of full charge-discharge cycles before the reach their end of life (EOL) [11].

Technology	**Nominal Voltage (V)**
Lead-acid (SLI)	2.0
Nickel-cadmium	1.2
Nickel-metal hydride	1.2
Sodium-nickel chloride	2.5
Lithium-ion ($LiCoO_2$)	3.6
Lithium polymer	3.7
Lithium-ion ($LiFePO_4$)	3.25
Supercapacitor	2.5-2.8
Lithium carbon capacitors	3.8-4
Lithium-sulphur	2.2
Rechargeable metal-air batteries	1-4 (depending on technology)

Table 8: Cell voltages of various battery technologies on a cell level. SLI: starting, lighting and ignition.

Lithium ion refers to a variety of chemistries, each of which has different characteristics and performances. The most common chemistries in use today are based on lithium iron phosphate (LFP), lithium manganese oxide (LMO), lithium titanate (LTO), lithium cobalt oxide (LCO), lithium nickel cobalt oxide (NCA) or lithium nickel manganese oxide (NMC) (Figure 13). Their performances and characteristics are summarised in Table 9 [7].

	LFP	**LMO**	**LTO**	**LCO**	**NCA**	**NMC**
Specific energy (Wh/kg)	80-130	105-120	70	120-150	80-220	140-180
Energy density (Wh/L)	220-250	250-265	130	250-450	210-600	325
Specific power (W/kg)	1400-2400	1000	750	600	1500-1900	500-3000
Power density (W/L)	4500	2000	1400	1200-3000	4000-5000	6500
Volts (per cell) (V)	3.2-3.3	3.8	2.2-2.3	3.6-3.8	3.6	3.6-3.7
Cycle life	1000-2000	>500	>4000	>700	>1000	1000-4000
Self-discharge (% per month)	<1%	5%	2-10%	1-5%	2-10%	1%

Cost per kWh in USD ($)	400-1200	400-900	600-2000	250-450	600-1000	500-900
Operating temperature range (°C)	-20 to +60	-20 to +60	-40 to +55	-20 to +60	-20 to +60	-20 to +55

Table 9: General performances and characteristics of the most common lithium ion chemistries currently in use.

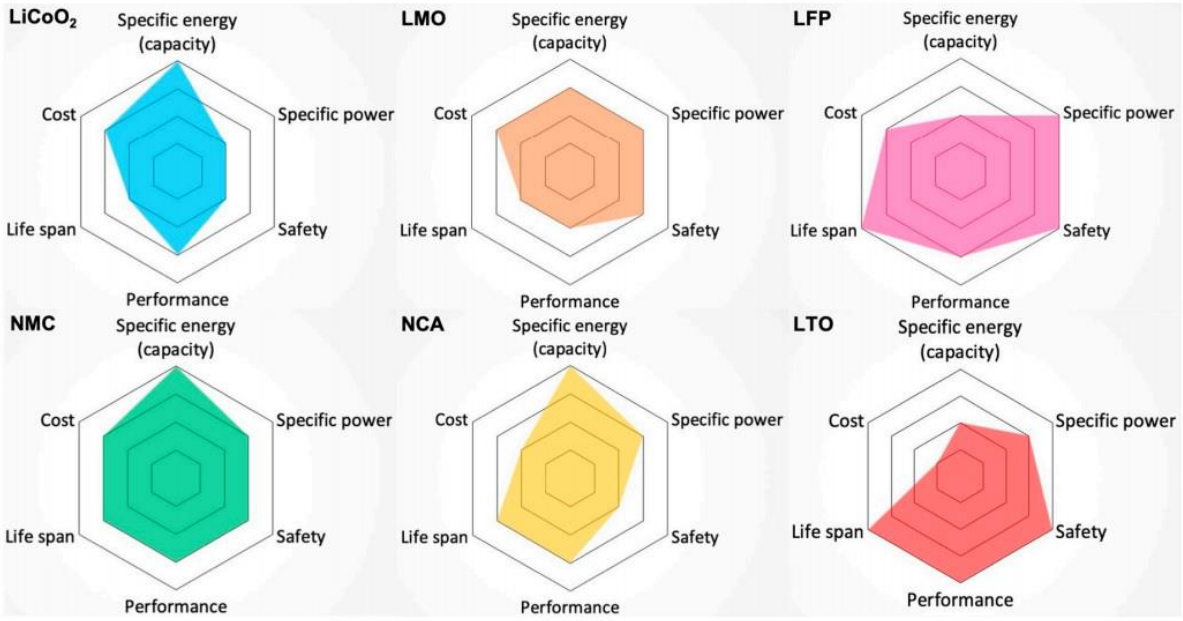

Figure 13: Strengths and weaknesses of cathode active materials for lithium-ion cells for automotive use [7].

2.2 Components

Lithium ion batteries have just few components (Figure 14), the main of which consist in the cathode, the anode, a separator material and the electrolytic liquid.

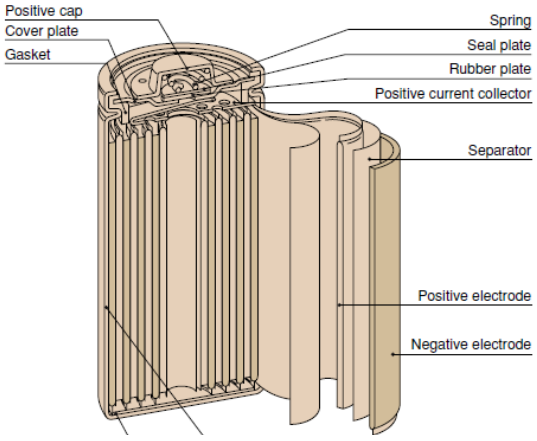

Figure 14: Components of a lithium ion battery [12].

2.2.1 Cathode

The cathode of a lithium ion battery consists of an aluminium foil coated with the active cathode material. Of the five most used chemistries, LFP is the most common in automotive applications. Indeed, LFP batteries have high power capability, meaning they can store charge during braking and release their energy very quickly during acceleration. Moreover, they better tolerate overcharging and high temperatures, being referred as "safer" compared to other chemistries. Finally, since they are composed by quite common and low cost materials, they are relatively cheap.

Due to their high energy density and voltage (Table 9), NMC chemistries have started to be used for the production of electric vehicles (EVs). LCO offers higher energy density and long cycle life, but it has lower stability and higher reactivity at high temperature compared to other chemistries. Moreover, the presence of high amount of cobalt makes it very expensive. For these reasons it is most commonly used in small customer electronics (cell phones, cameras, laptops) and it will not probably see wider or automotive applications.

NCA is frequently used in portable power applications. It is being evaluated for automotive applications due to its high power however its high cost and low safety are making this process slower.

Finally, LMO offers high energy and high power, however, suffers from shorter cycle life thus making it an appropriate chemistry to be used in portable power applications where you want long run time but not necessarily in automotive applications where you want long life.

2.2.2 Anode

It represents the negative side of the electrode and consists of a copper foil coated with the active material of the anode. Today, most anodes are made of a mixture of graphite soft or hard carbons. The quality and selection of the material play a very important roles in the performance of the cells.

Recently, LTO cell gained a lot of attention due to its ability to operate at a lower temperature compared to other chemistries and to its high power density. However, its nominal voltage is very low and the design more expensive compared to its competitors.

2.2.3 Separator and electrolyte

The separator divides the cathode and the anode; it has a key role in lithium ion cell design since, if the two electrodes come into contact, a short circuit will occur causing cell failure. It is usually made of polyethylene (PE) or polypropylene (PP) plastic or of a ceramic and it must be able to resist the high corrosive environment of the electrolytes (often hydrocarbon (HC)-based).

The separator and the two electrode foils are rolled up together to form the jellyroll, which is inserted into the container (or housing), usually made of a metal can, a plastic enclosure or a case of metal. The electrolyte is then injected into this assembly. It usually consists of a liquid- or gel-based solution into which the anode and cathode are immersed, that acts as a conductor allowing the lithium ion cells to move between the negative and positive electrodes. Usually, it is a HC-based mixture with multiple additives (typically, a combination of alkyl carbonates and lithium salts [13]) which provide different functionality within the cell.

The entire assembly is then hermetically sealed and brought to the cell manufacturing stage.

2.2.4 Safety

There are several safety issues to be taken into account when designing lithium ion cells in order to prevent early failure or unwanted energy release. One component that also carries out a safety function is represented by the separator. In PP- and PE-based separators failure (melting) occurs at a predefined temperature. Some designs opt for a three-layer PP/PE/PP cell which allows the centre layer to melt at a temperature about 20 °C lower than the PP layers. This prevents the lithium ions from flowing between anode and cathode and is intended to slow, if not prevent, a failure event. In ceramic-coated separators, melting temperature is much higher enabling for higher cell temperatures before thermal runaway onset. Moreover, ceramic separators are not affected by shrinking, as PP- and PE-based separators do.

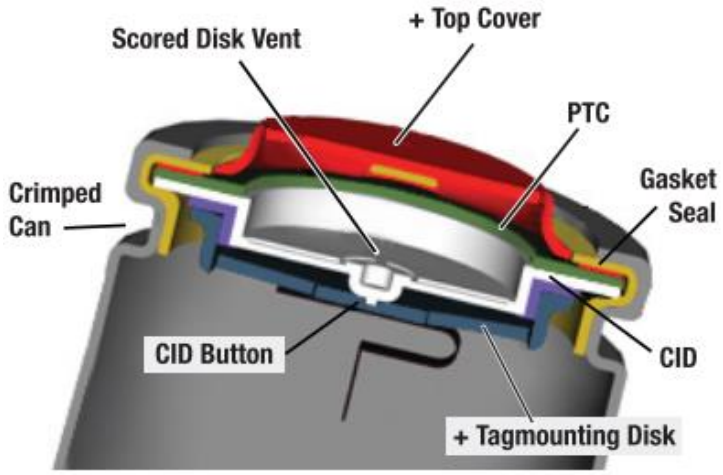

Figure 15: Structure of a resealable gas release vent [14]. In case of an internal increase of gas pressure, the vent is designed to open up and allow the gas leak.

A feature usually integrated into a wide variety of cell types is the gas release vent, which, in case of a pressure rise within the cell, opens up avoiding cell failure (Figure 15). Another safety component of most cells is the CID, a non-resettable fuse that designed to separate and break the flow of current to the terminals if the pressure builds up beyond a certain point. Some cell

designs include the PTC, a resettable thermal fuse, engineered to open and break the current flow if the cell temperature rises above a predetermined point. When and if the temperature of the cell falls back down to the normal operating temperatures, the PTC will reset, allowing the cell to start working again. Despite this convenient reset feature, PTC usually limits the maximum voltage that can flow from a cell, making its usage limited to small cells in small portable-type applications.

2.2.5 Types and manufacturers

As previously mentioned, there are three main types of lithium ion cell shapes: cylindrical, prismatic and pouch, with the 18650 cylindrical cell (nomenclature for 18mm diameter by 65mm length) being the most produced lithium cell format annually. When it comes to automotive applications, nearly all of the major manufacturers have identified small cylindrical cells suitable for hybrid electric vehicle (HEV) power applications, with the exception of Tesla who is using exclusively high-volume 18650 cells. Plug-in hybrid electric vehicle (PHEV) and battery electric vehicle (BEV) either use large prismatic, cylindrical or pouch cells (Figure 17 and Figure 16). The benefit of cylindrical cells comes from the can strength, which offers high resistance against damaging. Usually made of steel, nickel-coated steel or aluminium, it also provides stack pressure on the jellyroll. However, cylindrical cells generally have higher impedance compared to prismatic or polymer-type cells; this causes a higher heat generation rate that is although easily manageable due to the cell small dimensions. One of the challenges involved in using smaller format cells, aside from size, is in the lid assembly. Many manufacturers have transitioned to laser welding of the lids onto the cells, while some manufacturers continue to use a crimping process.

Prismatic cells are designed as a flat jelly roll enclosed in an aluminium case and are predominantly used in mobile phones, tablets and laptops. When produced in large formats they can be used in EVs and HEVs for electric powertrains, providing high capacity ratings and requiring less pack hardware to integrate into the complete Energy Storage System (ESS) compared to polymer-type cells. However, they can be more expensive to manufacture, less efficient in managing thermal heat and have short lifecycle than cylindrical cells.

Pouch cells, also known as lithium ion polymer cells (LiPo, LIP, or Li-poly), constitute the third type of lithium ion cells. Their innovative design uses conductive foil-tabs welded to the electrodes and brought outside in a fully sealed way. Compared to cylindrical and prismatic cells, pouch cells show the best packaging efficiency and lightweight, which make them the best solution for customer and portable applications. Their design is also very flexible, allowing their production in different and customizable sizes.

The main concerns of LiPo cells are related to cell venting. Due to the cell configuration, it is generally impossible to integrate CIDs or PTCs into its structure, so modules must be designed in order to manage the cell stack pressure and avoid swelling. Usually, a consistent and uniform pressure application is sufficient to ensure correct cell performances over life, as well as the correct ions movement in within the cell. When this flow is hampered, giving rise to the so called lithium plating, lithium ions get stuck and the cell impedance increases, reducing the cell's life.

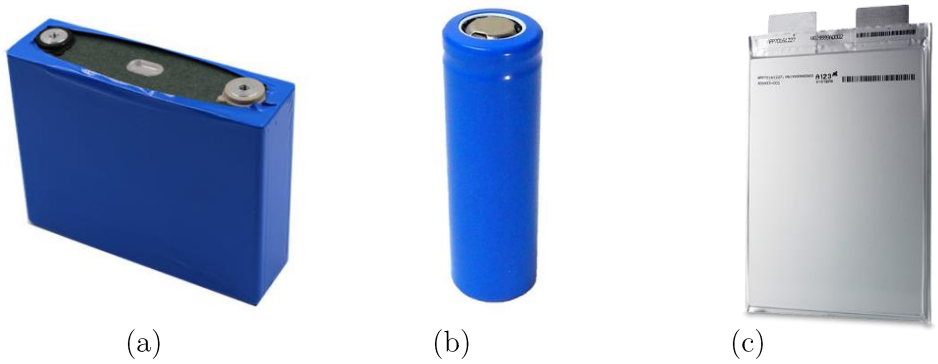

(a) (b) (c)

Figure 17: Example of (a) prismatic, (b) cylindrical and (c) pouch cells.

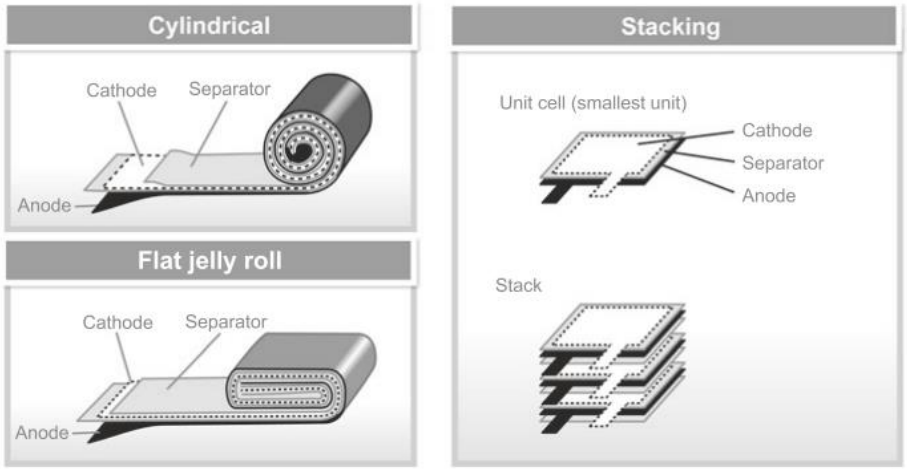

Figure 16: Internal structure of the main types of lithium cells [7].

Until today, lithium ion cells are almost exclusively manufactured in Asia [16]. Figure 18 shows the worldwide market shares of the most important lithium ion cell manufacturers.

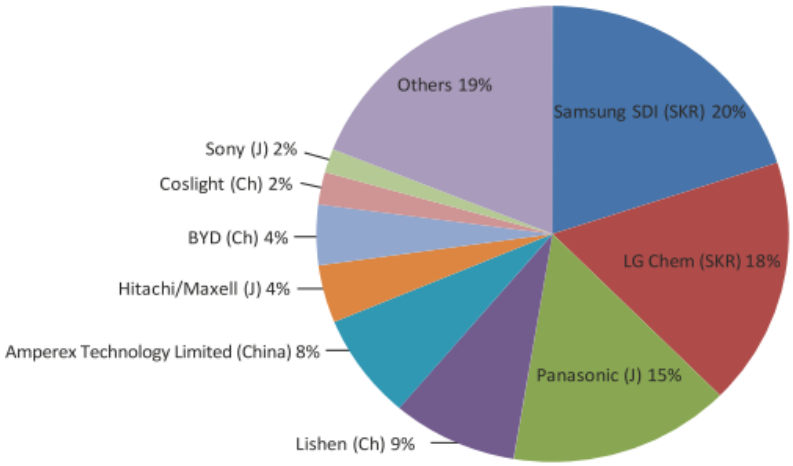

Figure 18: Worldwide market shares of rechargeable lithium ion cell manufacturers [14]. The graph includes cylindrical, prismatic, hardcase and pouch cell designs.

2.3 Initial Cell Identification

A lithium-ion cell has an inversely-proportional relationship between the specific power and the specific density. Therefore, to achieve the optimal specific energy while keeping the desired power output specification, it must be found a good trade-off between these two parameters. Several considerations have been done to identify the best cell for the battery pack 2018, which will be reported in the following paragraphs.

At 100% SOC, lithium ion cells show their maximum operating voltage of 4.2 V $\pm$ 0.05 V. Therefore, the maximum Tractive Battery voltage can be reached with a connection in series of 144 cells. The first selection stage consisted in the calculation of the number of cells to connect in parallel to reach the capacity target of 14 Ah. In the second stage the research focused on a cell that would have had a specific energy higher than the Melasta Li-Po cell used in 2017 (Table 10). In order to make the weight reduction effective, they were taken into account only cells with a specific energy much higher than the Melasta SLBPA045135, specifically in the range of 240 Wh/kg $\pm$ 5. Aside from this high specific energy, these cells would maintain a good discharge rate, which is of paramount importance for continuous power performance. The cells which satisfied these requirements were the SONY VTC6, LG HG2 and SAMSUNG 30Q (Figure 19).

Manufacturer	Model	Nominal Capacity [mAh]	Continuos Discharge [A]	Spec. En. [Wh/kg]
SONY	VTC5	2600	25	216
SONY	VTC5A	2500	25	204
SONY	VTC6	3000	20	238
SAMSUNG	24S	2400	30	202
SAMSUNG	25S	2500	25	206
SAMSUNG	30Q	3000	20	242
LG	HE2	2500	25	205
LG	HE4	2500	20	207
LG	HG2	3000	20	240
Melasta	SLBPA045135	7000	56	192

Table 10: Main parameters of the different cells used during selection. Highlighted, the specifications of the Melasta cell, used for the battery pack 2017.

To make sure these cells could effectively represent a good choice for the battery pack 2018, cells were tested according to power cycles from the racing car 2017. These data were appropriately scaled on the single cell, considering that the chosen configuration consists of 144s5p, which means an overall number of 720 cells (Figure 21).

Figure 19: SONY VTC6, LG HG2 and SAMSUNG 30Q cells.

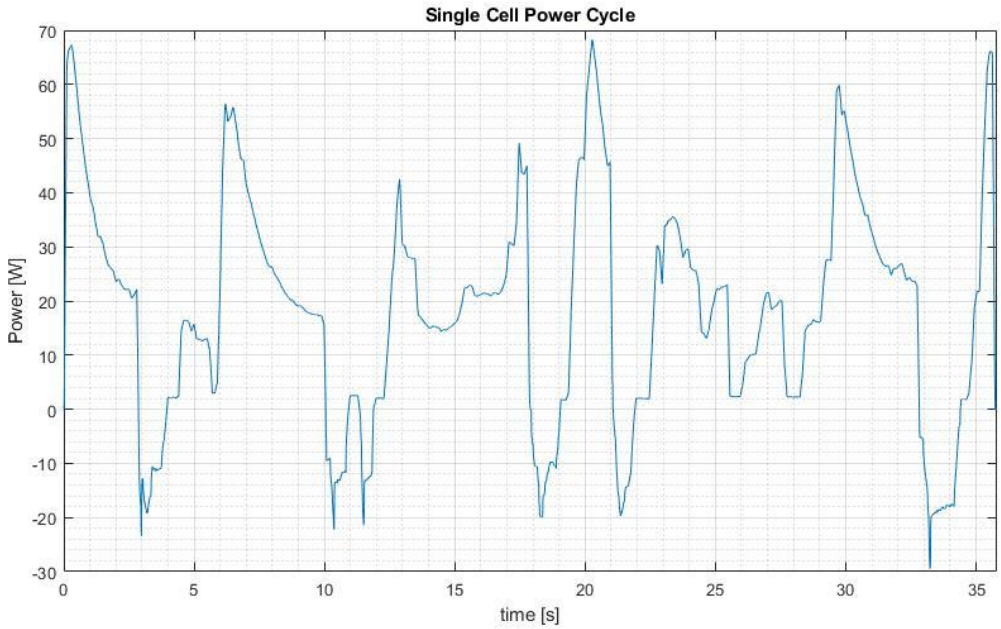

Figure 21: Single cell power cycle in time, according to the data of the car 2017.

In the tested cycles, there was a regenerative braking power of 1/3 the traction power, where regenerative braking corresponds to a negative power while traction power is associated with positive values, according to the convention. To simulate the working conditions during the real competitions, tests were performed in a thermal chamber with an ambient temperature of 35°C (Figure 20).

Figure 20: Thermal chamber that simulated the racing conditions and where tests were performed.

The test results would provide the main values characterising the cell state-of-charge (SOC) during discharging, such as voltage, current and temperature. The latter is measured with a PT100 sensor, placed close by the cell positive pole as shown in Figure 22.

Figure 22: Positioning of the PT100 sensor to measure cell temperature during discharge.

The initial OCV conditions were the same for the three samples tested (Figure 23).

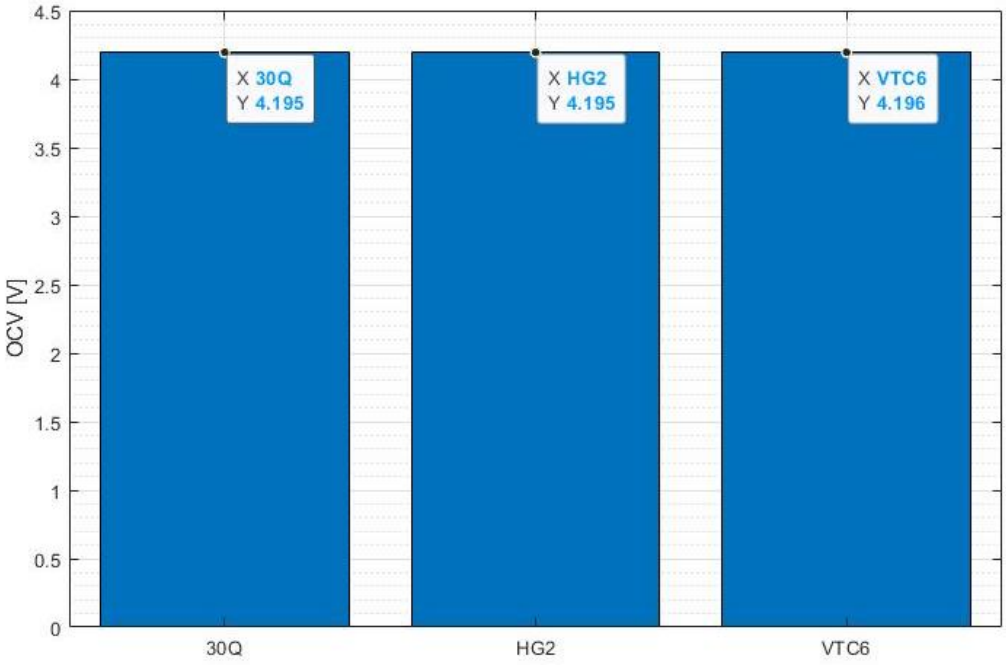

Figure 23: Initial conditions of the three cells tested.

As depicted in Figure 24, the temperature of the Sony VTC6 cells was approximately one degree higher than the other cells. However, since the test outcomes would be intended only as a rough esteem of the cells behaviour, it was decided to go further and perform the test. A correction on the results would eventually be applied to take into account later these small differences on the initial temperature.

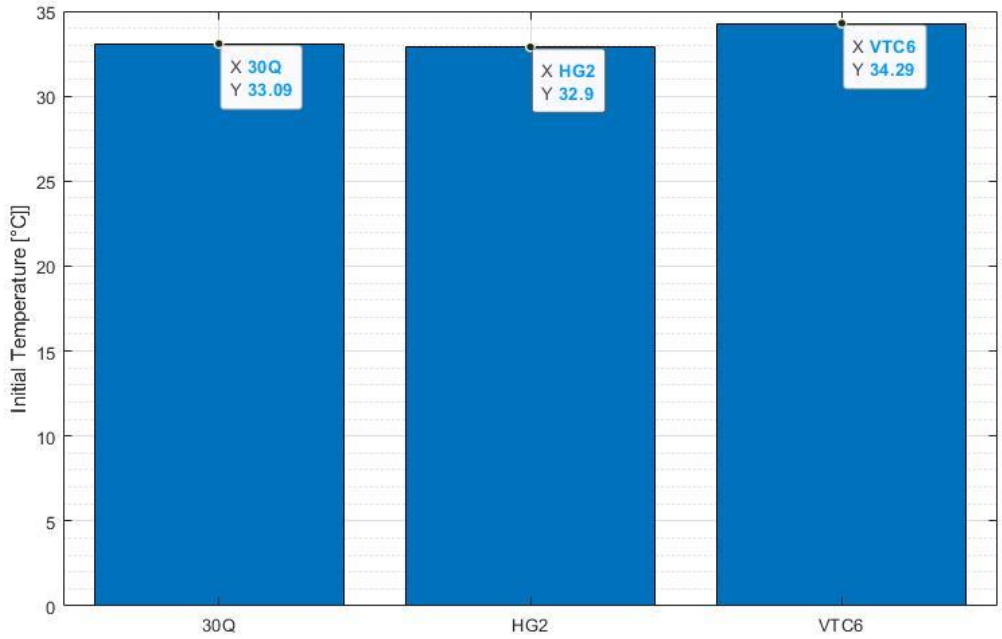

Figure 24: Initial temperature of the three tested cells.

The cycle in Figure 21 above is thus repeated n-times, until either the minimum cell tension or the maximum cell temperature of 60°C is reached. As we can see in Figure 25, the temperature threshold was reached by all the three samples before the complete discharge.

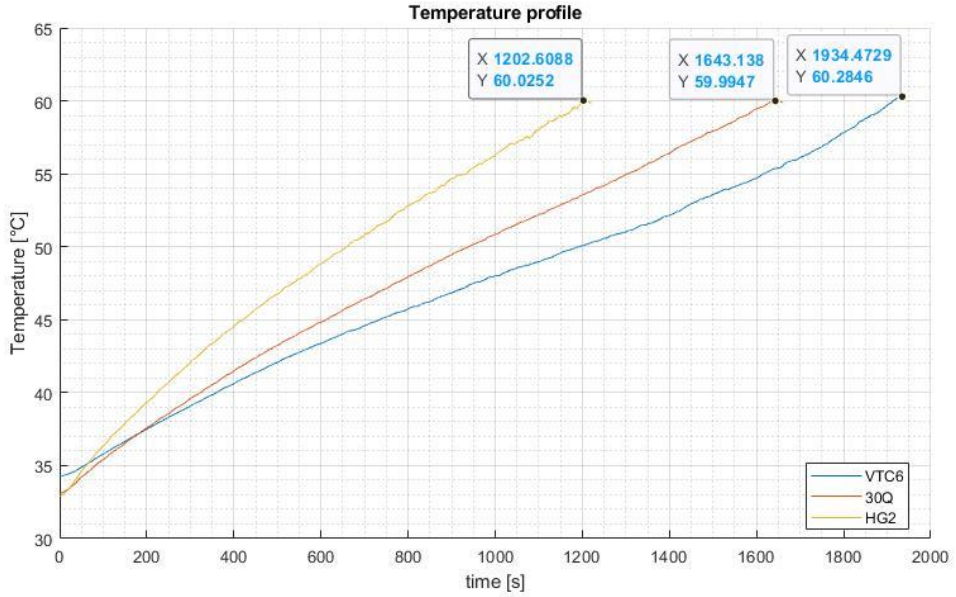

Figure 25: Temperature profile of the three cells tested over time.

As a reference, to finish an Endurance event they are required approximately 1700 seconds, therefore the two cells which can approach this target, with a power cycle similar to the tested one, are the Sony VTC6 and the Samsung 30Q. In particular, the former took more time to reach the temperature threshold, thus discharging more energy. The three trends were coherent between them, fact which is even more evident looking at the voltage drop during the current request (Figure 26).

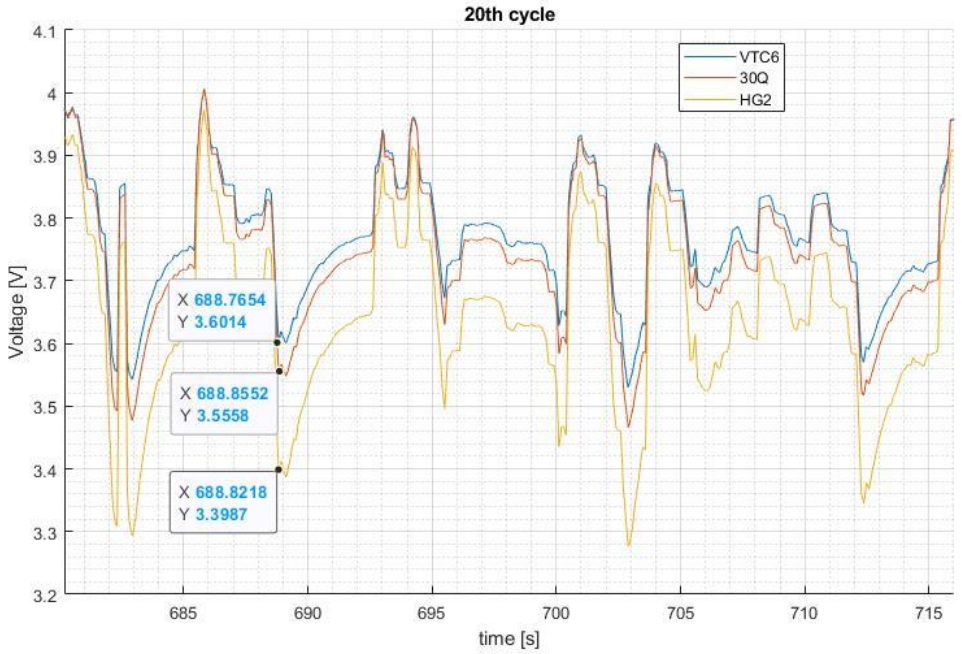

Figure 26: Voltage vs Time of the three tested cells in the 20th power cycle.

The LG HG2 has a higher voltage drop with respect to Samsung 30Q and Sony VTC6, that necessarily implies a lower cell efficiency. As first approximation, it was possible to find a rough value for the internal resistance as a function of the charge ($I > 0$) and discharge ($I < 0$) currents (Figure 27).

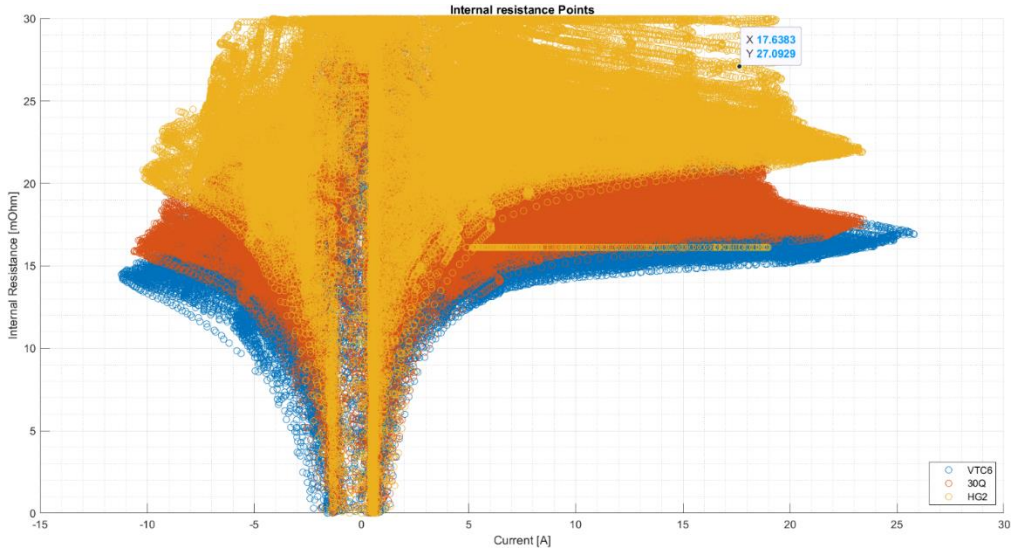

Figure 27: Internal resistance of the three samples tested.

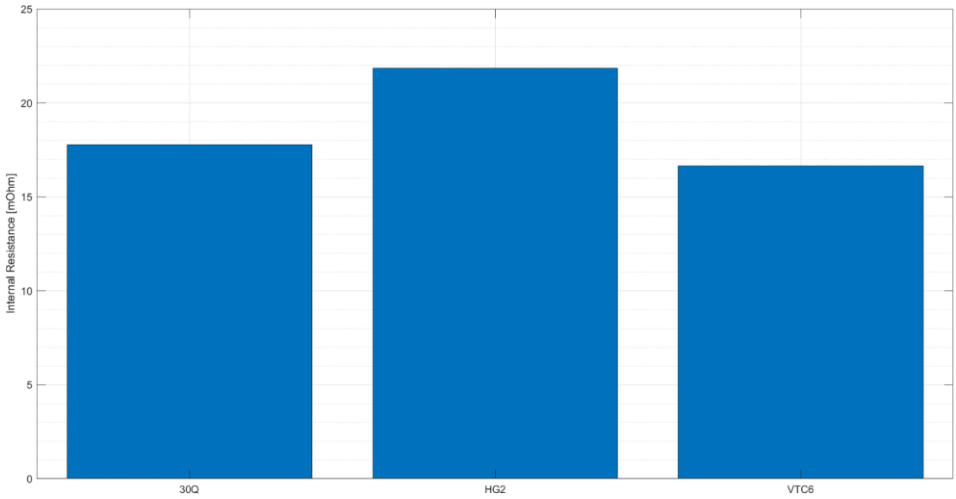

Figure 28: Mean internal resistance of the three tested cells.

The lower internal resistance showed by Sony VTC6 cells explains its behaviour during the tests compared to the other two samples tested (Figure 28). Since higher heat losses coincide with lower efficiency, the mean internal resistance could be a good parameter to esteem heat losses. The lower the mean internal resistance, the higher the cell efficiency. Although this represents only a rough estimation, it represents a key factor to create a more detailed model.

For the reasons explained until here, the Sony VTC6 represented the cell of choice for the battery pack 2018. As reference, Table 11 reports its characteristic parameters compared to the cell used for the battery pack 2017.

Cell Model	**Number of Cells**	**Configuration**	**Total Energy (kWh)**	**Continuous Discharge Power (kW)**	**Total Mass (kg)**
Sony VTC6	720	144s5p	7.78	52.3	33.1
Melasta SLBPA045135	288	144s2p	7.42	59.7	38.9

Table 11: Characteristic parameters of the chosen cells compared to the cell composing the battery pack 2017.

3 Cell Electro-thermal Model

Equivalent circuit models represent a useful tool to model lithium ion batteries behaviour and predict their performance. As opposite to electrochemical models, generally used to understand the physics and the reaction processes inside the battery [16][17] and thus to guide the manufacturing process, equivalent circuit models (ECMs) employ resistances, capacitances and voltage sources to describe the charging and discharging processes. The models are usually built in the time- or frequency-domain [18][19], where each component has a specific physical meaning, simple mathematical expressions and is easy to work with. ECMs are mainly used to estimate the state-of-charge (SOC), the state-of-health (SOH) and the state-of-function (SOF) of lithium ion batteries, which constitute the most critical information to simulate, optimize and maximize batteries performance [21][22].

The first-order RC (resistor-capacitor) model (Figure 29a) and second-order RC model (Figure 29b) are the two ECMs mostly used in literature. They provide a good picture of the dynamic and static characteristics of lithium ion batteries, while still remaining mathematically accessible and easy to implement. Characteristic parameters of the two circuits in Figure 29 are:

- Current flowing through the load, I. It can be directly measured from a current sensor.
- Terminal voltage of the battery, U. It can be directly measured from a voltage sensor.
- Open circuit voltage (OCV), V_{OC}. It is the stable voltage of the battery when this is left in the open circuit condition [23]. In practice, it coincides with the electromotive force of the battery, parameter generally used to calculate the energy inside the battery [24].
- Ohmic resistance, R_0. It describes the electrolyte resistance and connection resistance of the battery. In battery management system, it is widely used to size the energy storage system and its cooling sub-system as well as to determine the SOC, SOH and state of power (SOP) [21].
- RC networks, R_1 and C_1 and R_2 and C_2. They are used to determine the transient response of the terminal voltage U. In the second-order equivalent model, the prime RC network

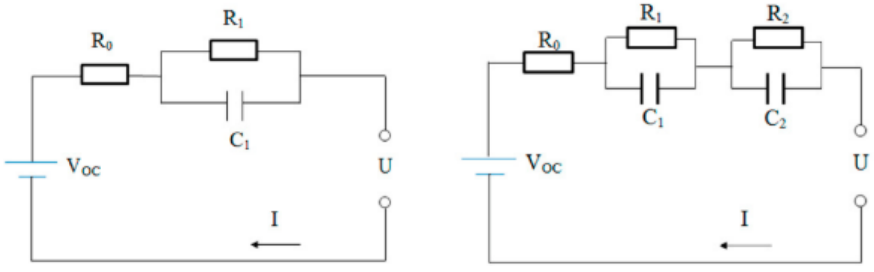

Figure 29: Schematic representation of the first-order RC (a) and second-order RC (b) equivalent circuit models.

(R_1 and C_1) represents the small-time constant of the battery cell feedback and models the charge transfer procedures. On the other hand, the secondary RC network (R_2 and C_2), describes the lengthy-time constant of the battery cell feedback and exemplifies the diffusion processes.

The comparative study led by Zhang and colleagues [25] demonstrated that, under constant current conditions, the maximum relative errors of the first-order RC and second-order RC models are less than 2%, with the latter model slightly improving the output error compared to the former in both simple and discharging conditions. For these reasons, it has been opted for a first-order RC model approach, as a trade-off between modelling, complexity, precision and computational costs.

3.1 Hybrid Pulse Power Characterization (HPPC) Test

The Hybrid Pulse Power Characterization (HPPC) test is a parametrization method used to determine the power capability of a lithium ion battery and to describe its dynamic behaviour. It is mostly used to compare the battery, or the pack performance based on a set of performance goals. The HPPC test profile includes a short period of discharge, followed by a rest period and a subsequent short period of charging (that coincides with the regenerative braking), under controlled conditions (Figure 30Figure 30). During the test, the terminal voltage, current and temperature are monitored.

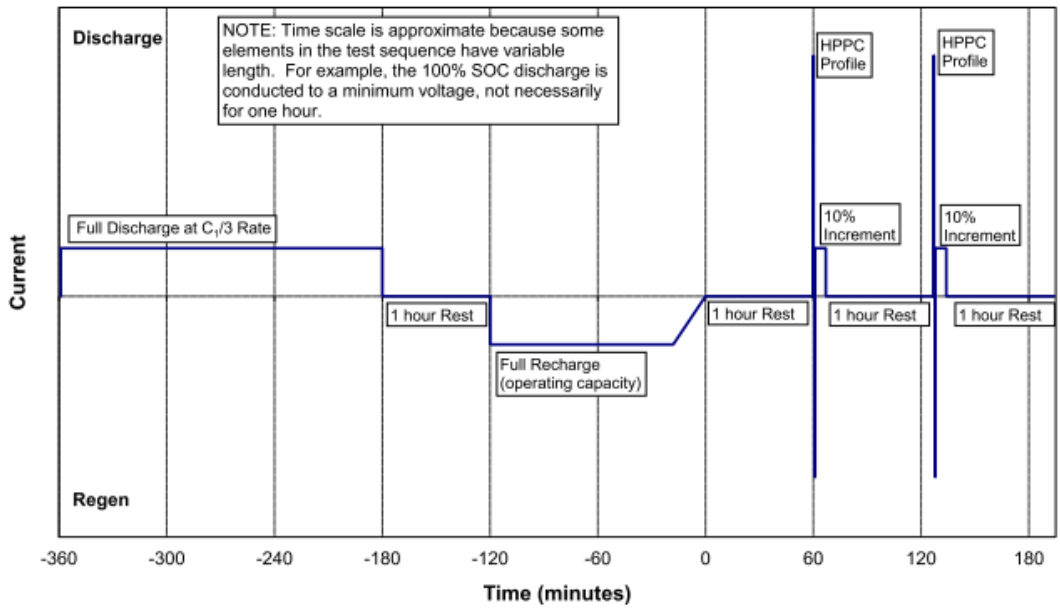

Figure 30: Start of the HPPC test sequence

The test aims to establish, as a function of the removed capacity [26]:

1) The device minimum voltage (discharge power capability) in the operating voltage range at the end of a 30 seconds discharge current pulse;
2) The device maximum voltage (charge power capability) at the end of a 10 seconds regen current pulse.

The thus obtained discharge and charge power capabilities are used to derive other performance characteristics: the resistance as a function of the depth of discharge, the pulse power capability, the amount of energy and power available at different depth of discharges, the power and energy decay the battery will experience over its life, the maximum and minimum depth of discharge values the battery can achieve while meeting the performance requirements, and the amount of heat generated during operation. These data can be used to evaluate resistance degradation and to develop hybrid battery performance models for vehicle systems analysis [26].

As described by Christopherson "*the objective of the HPPC test is to determine the 30-second discharge-pulse and the 10-second regen-pulse power capabilities at each 10% increment relative to the beginning-of-life (BOL) operating capacity. Between each pair of discharge and regen pulses, the device is discharged to the next 10% increment based on operating capacity using the C/3 rate.*" [26] The pulse profile is shown in Table 12.

Time Increment (s)	**Cumulative Time (s)**	**Charge-Discharge Rate**
30	30	1.00
40	70	0
10	80	-0.75

Table 12: Hybrid Pulse Power Characterisation test profile. Positive values are used to define discharge current and power, whilst negative values refer to charge or regen values.

3.1.1 Description of the HPPC Test procedure

In this paragraph, it is reported the description of the HPPC test as suggested by Christopherson, which ultimately represented the guideline followed during our experiments [26].

> *The HPPC Test is made up of single repetitions of the HPPC test profile, followed by discharge to the next 10% increment based on operating capacity point using the C/3 rate, each time followed by a default rest period to allow the cell to return to an electrochemical and thermal equilibrium condition before applying the next profile. The HPPC test begins with a charged device up to* $Vmax_{op}$ *using the manufacturer recommended procedure. Following a default rest period (nominally a 1-hour rest), an HPPC profile is performed immediately followed by a discharge*

to the next 10% increment of the rated capacity at the C/3 rate (based on the established operating capacity at BOL) and a default rest. This sequence is repeated until the final profile at or near 90% of the operating capacity removed (or the maximum discharge specified by the manufacturer). The test terminates with a discharge of the device at the C/3 rate to $Vmin_0$ *and a final default rest.*

If at any point $Vmin_0$ *is reached during an HPPC pulse then taper the current to finish the pulse. If* $Vmin_0$ *is reached in the C/3 discharge portion, stop the test. The voltages during each rest period are recorded to establish the cell's OCV (open-circuit voltage) behaviour. The sequence of rest periods, pulse profiles, and discharge segments is illustrated in* Figure 30 *and* Figure 31.

The HPPC Test may be performed at the low-current level, the high-current level, or both. Generally, the low current HPPC test results in a more conservative estimate of the pulse resistance. Each HPPC Test sequence is performed using peak currents scaled to one of the levels. Scaling of the levels is determined by the following criteria.

- *LOW CURRENT HPPC TEST—The pulse profile discharge current is at least a C/1 rate.*
- *HIGH CURRENT HPPC TEST—The pulse profile discharge current is selected as 75% of* I_{max} *(the manufacturer's absolute maximum allowable pulse discharge current for 30-s at some state-of-charge, which needs not be specified).*

The Available Energy is then verified by direct measurement during the HPPC Available Energy verification test. If the test article is a cell-level device, the manufacturer must specify the C/3 available energy level based on their end-of-life criteria (alternatively, the manufacturer can specify a beginning of life margin from which the energy level can be determined based on a C/3 static capacity test). The HPPC Available Energy Verification test is performed in three steps.

1. *Starting at manufacturer's specified* $Vmax_{op}$*, remove the Available Energy from Table 1 (45 kWh at the system level or as specified by the manufacturer for the cell-level) at the C/3 rate.*
2. *Rest for 1 hour at open circuit voltage conditions.*
3. *Perform a 30s discharge pulse at the appropriate power levels. If the pulse is performed without violating the minimum voltage requirements (i.e.,* $Vmin_{pulse}$*), the test article has passed the energy verification test. If*

the discharge pulse cannot be completed without violating the minimum voltage requirements, this should be reported and the technical program manager will determine whether or not this constitutes an EOL criterion.

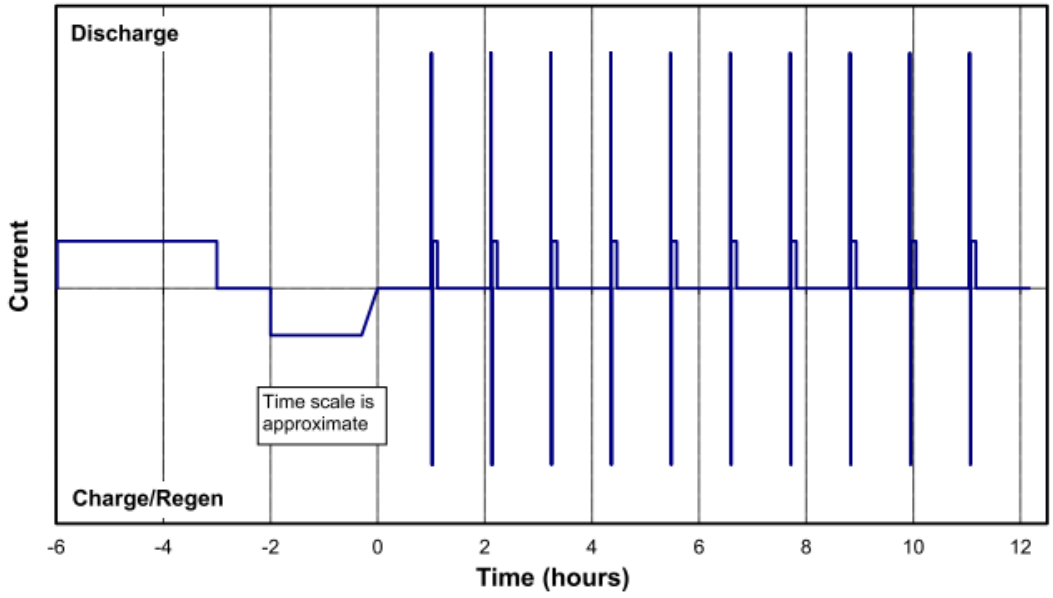

Figure 31: Complete HPPC test sequence.

3.2 Thermal model

Performance of lithium ion cells greatly depends on temperature. Indeed, according to the specific thermal characteristics of each battery, charging and discharging in the proper temperature environment can contribute to the electrochemical reaction. Operating at low temperatures may lead to an increase in the cell internal resistance, reducing output power and performance. Temperatures below 0°C initiate severe aging mechanisms which can result in irreversible cell damage. Lithium plating represents the most important of these mechanisms; as introduced in Section 2.2.5, it refers to the deposition of pure lithium on the anode during the charging process. This event reduces the cell capacity and will eventually result in an internal short circuit. Since lithium plating only occurs when temperature drops below zero, it can be prevented provided good operational strategy and thermal management.

On the other hand, excessively high temperatures may provoke unproper thermal distribution, resulting in capacity variability between cells and, ultimately, speeding up the aging process. As a rule of thumb, a 10K raise in the operating temperature leads to a decrease of 50% in the battery life. Moreover, high temperature encourages the cycle performance loss, that is the capacity of abatement of a cell during charging and discharging cycles [27]. Additionally, when the cell temperature exceeds a certain threshold, it would induce the occurrence of exothermic

reactions that will lead to a further increase in the temperature, until the so called thermal runaway. Thermal runaway starts at about 90°C when the solid electrolyte interface (SEI) – the protection between the negative electrode and liquid electrolyte – decomposes. When SEI gets damaged and the temperature reaches 100°C, the electrolyte and electrode start reacting. This reaction is highly exothermic and will lead to further increase in temperature. At 130°C, the separator between anode and cathode melts down and results in an internal short circuit. If temperature keeps rising to 200°C, a chain reaction might start, causing the lithium metal oxide and the electrolyte to react with oxygen, leading to fire and explosion [28].

For lithium ion batteries the optimal working temperature is set between 20 and 40°C (Figure 32) [7]. In this range, they exhibit peak performance rates and acceptable aging. If a longer service life is required, since aging rises following temperature increases, cooling should be configured closer to the low temperature limit.

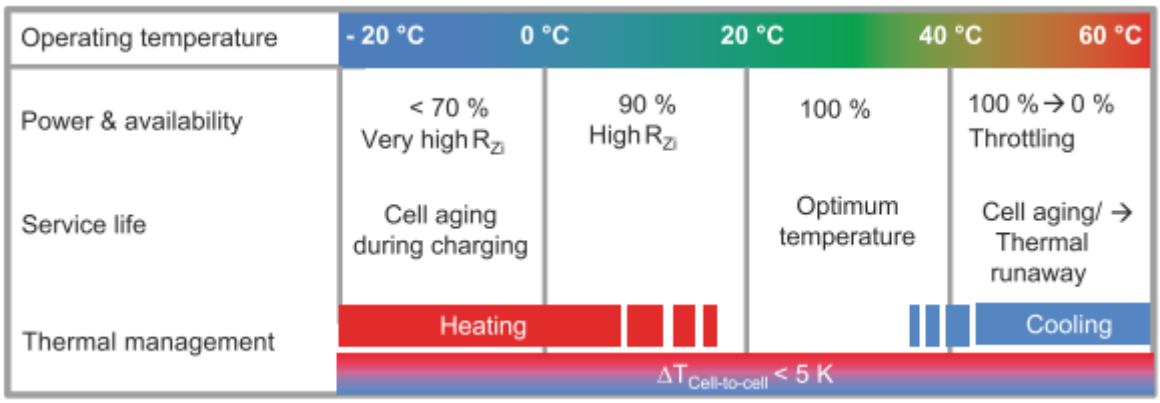

Figure 32: Relation between operating temperature, thermal management and service life in a lithium ion cell [7].

4 Module Design Development

4.1 Battery Thermal Management System (BTMS)

As discussed in Section 3.2, high temperatures will have a negative impact on batteries affecting their performance, lifetime and safety. Therefore, every battery pack needs a battery thermal management system (BTMS) to keep cells in the optimum temperature range and maintain a uniform temperature distribution inside the battery pack. Indeed, heterogeneous cell temperature can cause the cells to age differently and a reduction in the battery available energy content. Subsequently, based on the application, other factors such as weight, size, reliability and costs must be taken into account.

4.1.1 Air cooling

Despite its low thermal conductivity and heat capacity, air still represents the most popular cooling technique, mainly due to its simplicity and low cost (Figure 33) [28]. Cooling can be achieved through natural convection or passive cooling, only suitable for low-density batteries, and forced convection, or active cooling. Generally, passive cooling makes use of blowers and fans to increase the convection coefficient [29].

In case of battery packs with cells arranged in series, the low heat capacity of the configuration leads to an increase in temperature and a heterogeneous temperature distribution. To guarantee homogeneity, usually the cooling medium speed is increased which creates turbulence in the flow and optimizes the cell positioning. Wang and colleagues [30] analysed different cylindrical cell arrangements and positionings of the fan. They found that the best cooling performance was

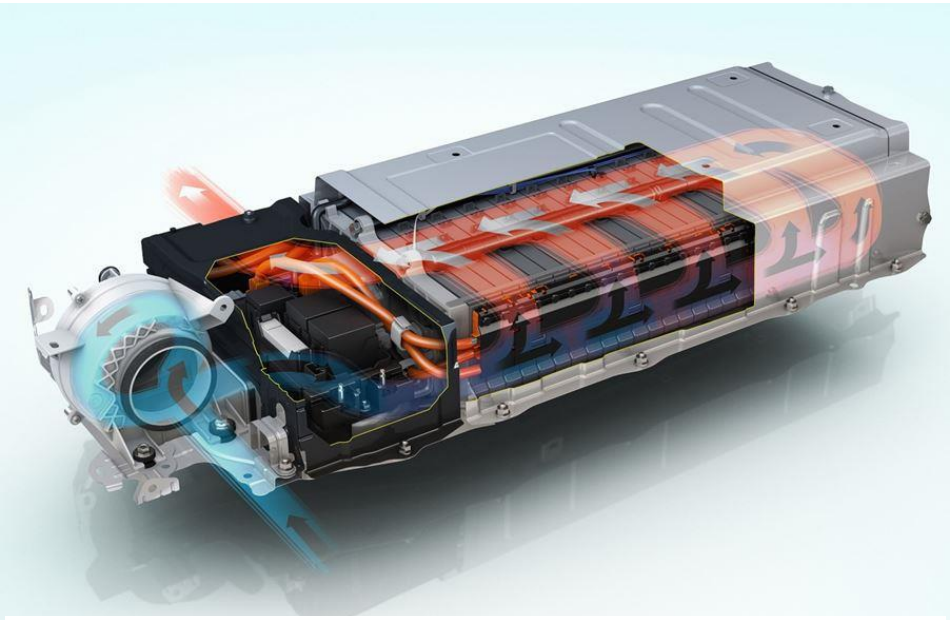

Figure 33: Air cooler battery thermal management system (BTMS) used by Toyota

achieved when the fan is placed on top of the module and the most desired arrangement, considering cooling effect and costs, was obtained through a square pattern arrangement of cells.

4.1.2 Liquid cooling

Compared to air, liquid cooling is generally more efficient, more compact, less noisy and can save up to 40% of parasitic power. However, it is more expensive, complex and can present leakage issues. Liquid cooling can be direct and indirect.

Direct or immersion cooling provides uniform cooling of the cells, improving their performance by decreasing the presence of hot and cold spots (Figure 34). It uses dielectric coolants with low viscosity, high thermal conductivity and capacity. Due to high cost and safety issues, direct

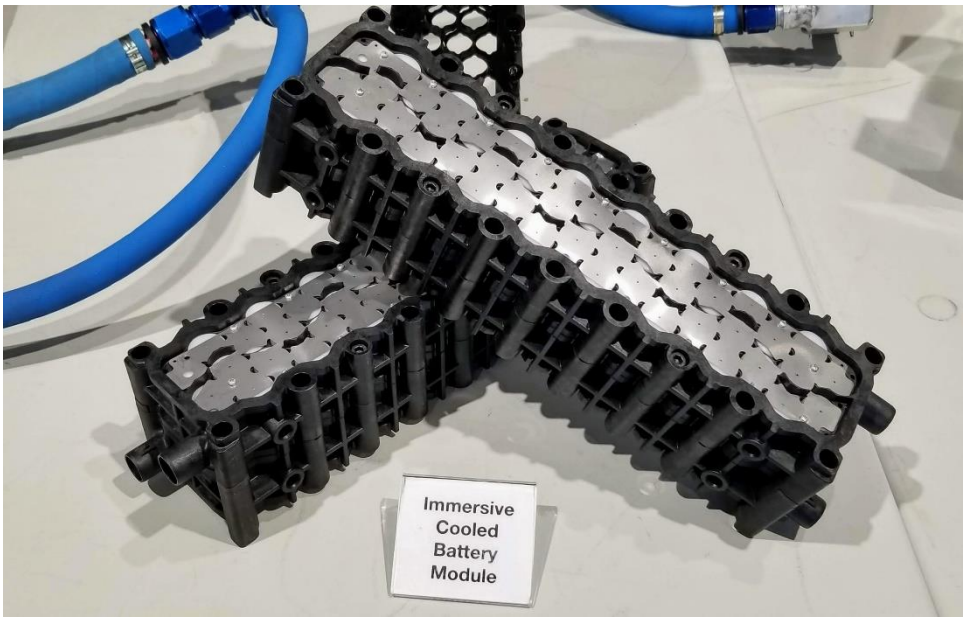

Figure 34: Direct liquid cooling battery module by Xing Mobility with 3M Novec Dielectric Fluid.

cooling is avoided in mass-produced EV market. As of today, immersion cooling has been used only for high performing EVs, due to their high-power requirement which can only be covered by this type of cooling. The mass market will only be reached following improvements in leakage proofing of the battery pack and a reduction in the cost of the dielectric liquids.

Indirect cooling is the preferred method when water is employed as coolant. It can guarantee high thermal conductivity while preventing the risk of short circuit with the cells. Adding an electrical resistance will also add extra thermal resistance, but if it is controlled it barely affects the cooling.

Tesla represents an example of manufacturer that adopted wavy tubes running between cylindrical cells as indirect cooling method in its cars (Figure 35) [31]. To fill the space between cells and cooling channels, it employed a thermally conductive and electrically insulating material. Despite having a small heat transfer contact area, the wavy tubes offer safety to the system under both the mechanical and electrical points of view. Moreover, since the coolant connections are made outside of the battery enclosure, it eliminates leakage points.

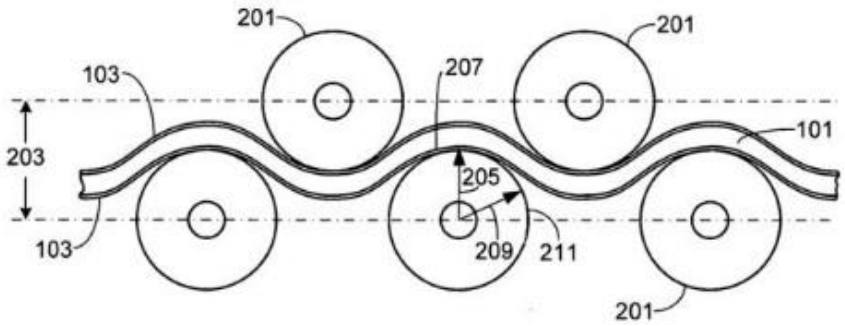

Figure 35: Schematic representation of the Tesla indirect liquid cooling system [31].

4.1.3 Phase change material (PCM)

The phase change material (PCM) provides high latent heat and acts as a heat sink during battery discharge (Figure 36). When the cells are on standby, the PCM releases heat to the cells and the environment. For lithium ion cells applications, the PCM melting point is in the optimum performing range, which guarantees operation in the optimal cell range for a long time. However, when batteries operate for a long time or if the temperature of the environment is too high, the PCM might completely melt and act as thermal barrier, due to its low thermal

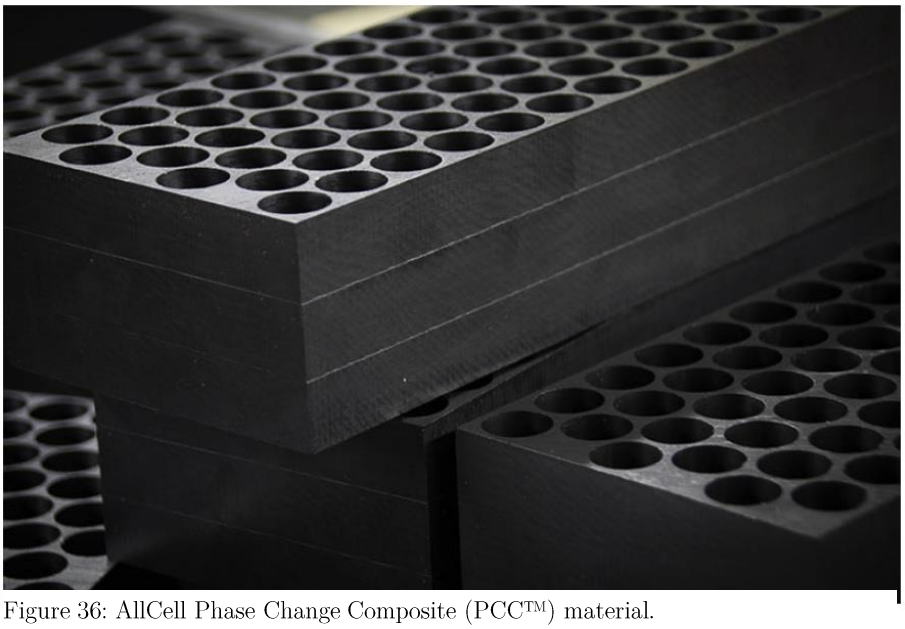

Figure 36: AllCell Phase Change Composite (PCC™) material.

conductivity. If the environment is too cold, the PCM will add thermal mass to the modules, making more difficult for the cells to reach the right temperature [28].

Overall, PCM can be considered the best passive solution for modules with a low operating rate. For higher operating rates and extreme ambient temperatures, it can be used in combination with active cooling.

4.2 Cells connection

Large battery assemblies, like the ones integrated in electric vehicles (EVs), are made up of several hundreds or thousands of single lithium ion cells connected together in order to provide the desired power and capacity. In these systems, proper cell connection acquires a crucial importance to prevent premature cell degradation, power capability and efficiency reduction, and unexpected failure [32] (Figure 37). Materials are usually joined through welding, a technique which can be further classified in resistance welding, laser welding and ultrasonic welding. Each of these techniques is associated with advantages and limitations that come from the materials to weld, from the contact geometry or from the cell casing.

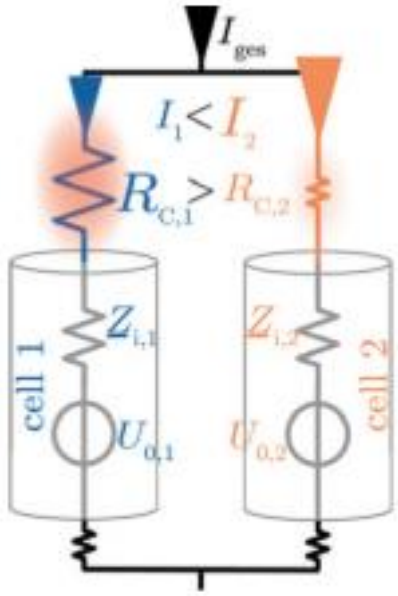

Figure 37: Parallel connection of two batteries with different electrical resistances. The higher resistance $R_{C,1}$ generates thermal and electrical overloads at the terminal of cell 1 and an uneven splitting of the current I_{ges} [32].

4.2.1 Joining classification

Resistance welding

Resistance welding is a thermo-electric process where welding is generated through the application of a welding current (I_{weld}), which flows through the contact resistance (R_{weld}) that arises at the interface between the electrodes and the pieces to join (Figure 38a) . The process generates localized heating and leads to fusion of small pieces of the materials; moreover, it is

very fast and can be easily automated, characteristics which make it suitable especially for automotive and electronics industries.

When determining the electric power to provide to the process, it should be considered the possible rise of a stray welding current, which might flow through elements of the welding equipment that act as undesired conductors [33]. Therefore, the welding power supplies a current ($I_{electrode}$) usually higher than the welding current, which can however lead to electrodes sticking and voids inside the weld nuggets, compromising the strength of the joining [33]. To avoid sticking, the resistance beneath the electrode $R_{electrode}$ should be minimized. On the other hand, a high contact resistance, R_{weld}, contributes to the formation of a good weld.

The characteristics of the joining materials, such as the melting point and thermal conductivity, represent other factors that contribute to the determination of the power source. Indeed, when the workpieces are very thick or have high conductivities the power required can become very high [33], making difficult to focus the current flow on a spot and to minimize stray currents. A feasible approach can be projection welding, which increases the current density and focus the heat, enabling welding of thicker tabs and production of repeatable welds with fixed resistance [34].

Resistance welding of lithium ion batteries, where the thermal and electrical conductivities of the electrodes (generally made of aluminium and copper) are high, is usually very challenging. Nickel plating can constitute a solution to this issue, due to its electrical and thermal resistance and ease of welding [35]. By applying a nickel coating to the workpieces, weldability of high conductive materials can be enhanced.

Laser welding

Laser welding is a non-contact process that uses a laser beam to join materials together (Figure 38b). The electromagnetic waves produced by the beam generate a concentrated source of heat which creates a weld with the smallest heat affected zone, compared to the other welding techniques. The high power density of the laser beam allows high welding velocities, but the high thermal conductivity and reflectivity of electrode materials limit the use of laser welding, since it might cause damaging of the surrounding material. Nevertheless, laser welding provides narrow and deep welds, and allows the joining of arbitrary geometry and multiple sheets, all desirable characteristics for applications involving lithium ion batteries [36]. However, welding of different materials may affect the mechanical properties of the system, which can in turn lead to weld defects, such as brittle phases, crack sensitivity [37]. Coating of the workpieces can again represent a solution to improve the mechanical characteristics of the joints, as well as the application a proper beam offset [37].

Ultrasonic welding

In ultrasonic welding, high-frequency ultrasonic vibrations applied locally are transferred from the knurl patter of a sonotrode to the workpieces, creating solid-state bonds between two sheets of material, that are held together under pressure (Figure 38c) [38]. The most important parameters which concur to determine the weld quality are the sonotrode pressure, the amplitude of the vibrations and the welding time. Usually, high pressure translates in high power input, which provides more heat to the system and, thus, favours the atomic diffusion involved in the bonding mechanisms [39]. However, extremely high pressures may lead to decreased mechanical strength and to higher contact resistance, which might damage the workpieces [32].

Since it is a solid-state welding technique, ultrasonic welding is independent of the melting temperature of the working materials. Moreover, it provides good welding of different materials and multiple sheets designs [36]. In addition, it is an environment-friendly process due to the absence of filler metals or gases. On the other hand, it is dependent on hardness and surface roughness of the joining materials, which are two parameters to consider before applying this technique.

Summary

When it comes to connect cells in large battery assembly, it is important to consider advantages and drawbacks of each of the previously analysed techniques to determine the most suitable for each case.

Resistance welding is generally not recommended to connect battery cells with parallel electrodes, due to the employment of high currents. Moreover, stray current may damage other welds made in the vicinity and voids inside the weld nugget could cause a decrease in the mechanical strength. Nonetheless, this technique is preferable when the materials to weld have low conductivity.

Laser and ultrasonic welding offer more flexibility in terms of thickness, geometry and materials of the workpieces, making these techniques preferable for battery cell connection. However, surface reflection may compromise laser beam welds and the absence of clamping in ultrasonic welding can cause damage to the cell and cracks in the external conductor.

Finally, the electrochemically active materials of the cell, in direct contact with the cell casing, impose careful evaluation of the welding temperature. Melting occurs in both resistance and laser beam welding, while ultrasonic welding uses temperatures below the material melting points, which may however vary consistently for different welding parameters and materials. A general rule consists in keeping the heat input very localised to avoid damaging of the cells.

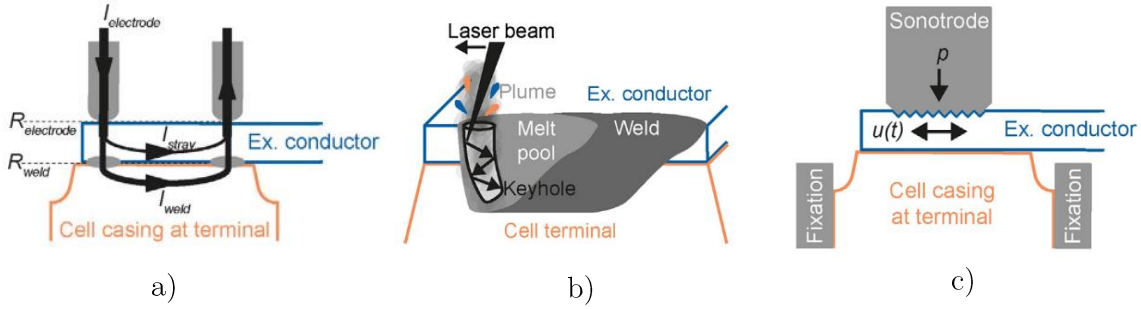

a) b) c)

Figure 38: Resistance, laser and ultrasonic welding of cell terminal. Adapted from [32]. a) Resistance welding of a battery cell with parallel electrodes. b) Keyhole laser welding of a cell terminal. c) Ultrasonic welding of a battery cell through ultrasonic vibration.

4.2.2 Ultrasonic Heavy Wire Bonding

Wire bonding is a type of ultrasonic welding that uses wire bonds to connect battery cells and conductors in parallel. In particular, heavy wire bonding is used to join together wires with a diameter larger than 100µm. The major advantage of this technique is that, in case of a single cell failure due to overcurrent condition, the wire acts the as fuse which melt down isolating the cell from the pack, whose function will not be compromised. It also does not require high temperature to create the bond, since welding occurs through the synergic use of pressure and ultrasonic vibration, which constitutes a great advantage in heat sensitive cells or integrated circuits. Moreover, wire bonding machines are able to bond pieces of different heights and at different distances, allowing for many configurations as well as for cost and time savings. During wire bonding, several electrical and mechanical signals are captured in real-time, enabling the immediate evaluation of the bond conditions and quality.

The ultrasonic energy employed can cause harmonics that create resonance with the substrate surface, which may lead to weak or no-stick bonds. The manufacturing process must, therefore, provide a stable bond surface to ensure the highest success for the bonding process. Furthermore, accurate bond placing typically requires each cell to be located at a known location. Usually, this task is accomplished through machine vision to locate reference marks on the product while each battery cell is placed relative to that reference mark. However, as product dimensions grow, tolerances accumulate in the battery module assembly process which can negatively affect cell location accuracy. A more precise assembly process can improve cell location accuracy, leading to a significant increase of the product cost. Another approach is to introduce more reference marks throughout the product to lessen the effect of stack-up tolerances across a large area by sub-dividing the area into small sections. Locating additional reference marks, however, requires additional find time prior to the wire bonding process, thereby increasing the overall cycle time. One more strategy would be to locate each cell before the product enters the bonder with the drawback of having to transfer and synchronize a large amount of data between various systems.

In summary, the solution to accurate cell placement comes at a significant cost and technical complexity.

The materials used for bonding wires must fulfil the mechanical and electrical criteria required for EV application. Firstly, they must be durable, capable of withstand the high vibration of the battery pack and they must provide rigidity to the battery module assembly to guarantee its integrity in the harsh EV environment. Moreover, they should be manufactured such that they ensure high performance under high current and voltage levels. This mostly depends on the materials used to construct the busbars, which usually are gold, copper and aluminium. Gold wires provide good electrical conductivity, high resistance to corrosion, homogeneous chemical composition and stable mechanical properties. Copper has the best electrical and thermal conductivity and the lowest thermal expansion. Moreover, it is less expensive than gold, has stable mechanical properties and the bonding joints offer high reliability. However, it oxidizes very fast following air exposure. Aluminium provides high conductivity and good resistance to oxidation, excellent bonding properties and low weight. Moreover, it is the least expensive amongst gold and copper, thus usually the preferred choice.

One important parameter to consider following material selection is the wire fusing current. Fusing current is dependent on the material, the diameter and the length of the wire. For heavy ($\Phi > 100\mu m$) aluminium wires, Figure 39 below shows the fusing current for different diameters:

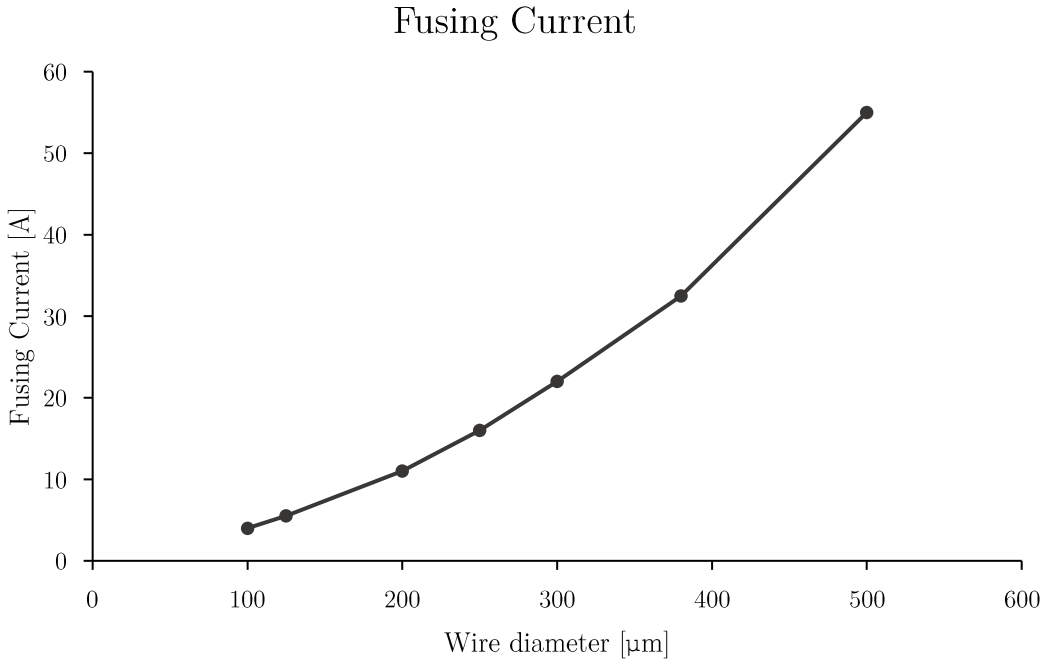

Figure 39: Fusing current for heavy aluminium wires.

4.3 Cooling design

4.3.1 Cells off-set on Z axis

The best cooling technique both in terms of weight impact on the battery pack and simplicity resulted to be air cooling, although it does not represent the most efficient approach. However, performance can be optimised by studying the pack fluid-dynamic behaviour following variation of some geometrical parameters.

Figure 40 reports the initial configuration of the 120 cells of the battery pack, arranged in columns of 5 parallels to form 24 series. Since cells account for the majority of the pack weight, it's worth noticing that by raising or lowering their positioning on the Z-axis, the centre of gravity (COG) of the entire vehicle will necessarily vary, directly affecting the vehicle dynamic. However, air flow is also influenced by cell spacing, therefore a CFD analysis was carried out to determine the best compromise between the COG height and cooling performance.

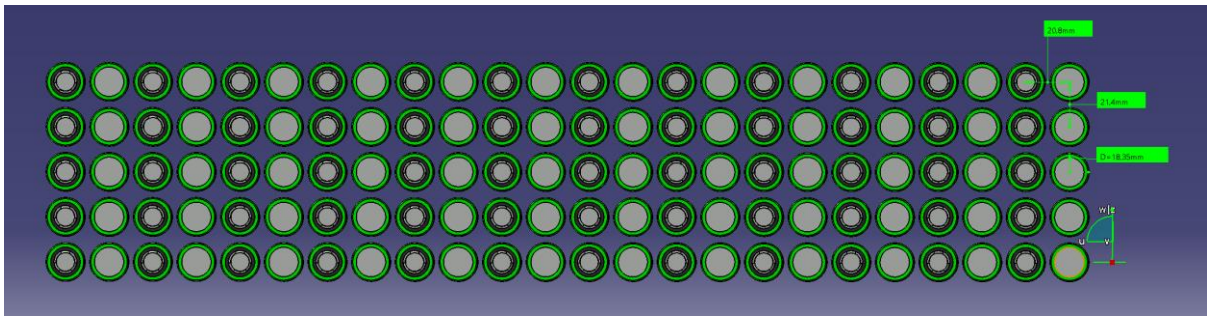

Figure 40: Configuration of the 120 cells composing the battery pack.

Three different configurations were examined: starting from a 19.4mm Z-interaxle distance between cells, the axial distance was increased of 2mm each time to reach the final offsets of 21.4mm and 23.4mm (Figure 41).

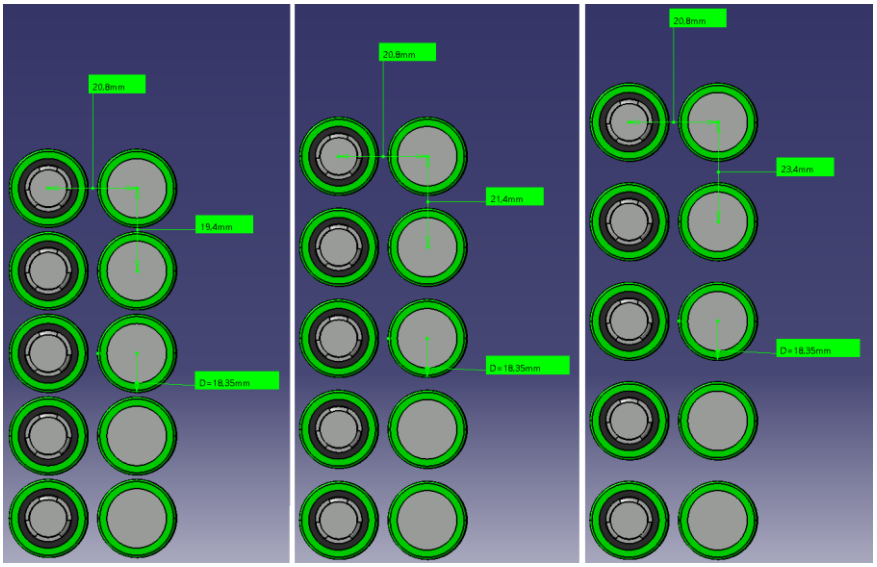

Figure 41: Three different cell configurations on the Z-axis analysed during the CFD analysis.

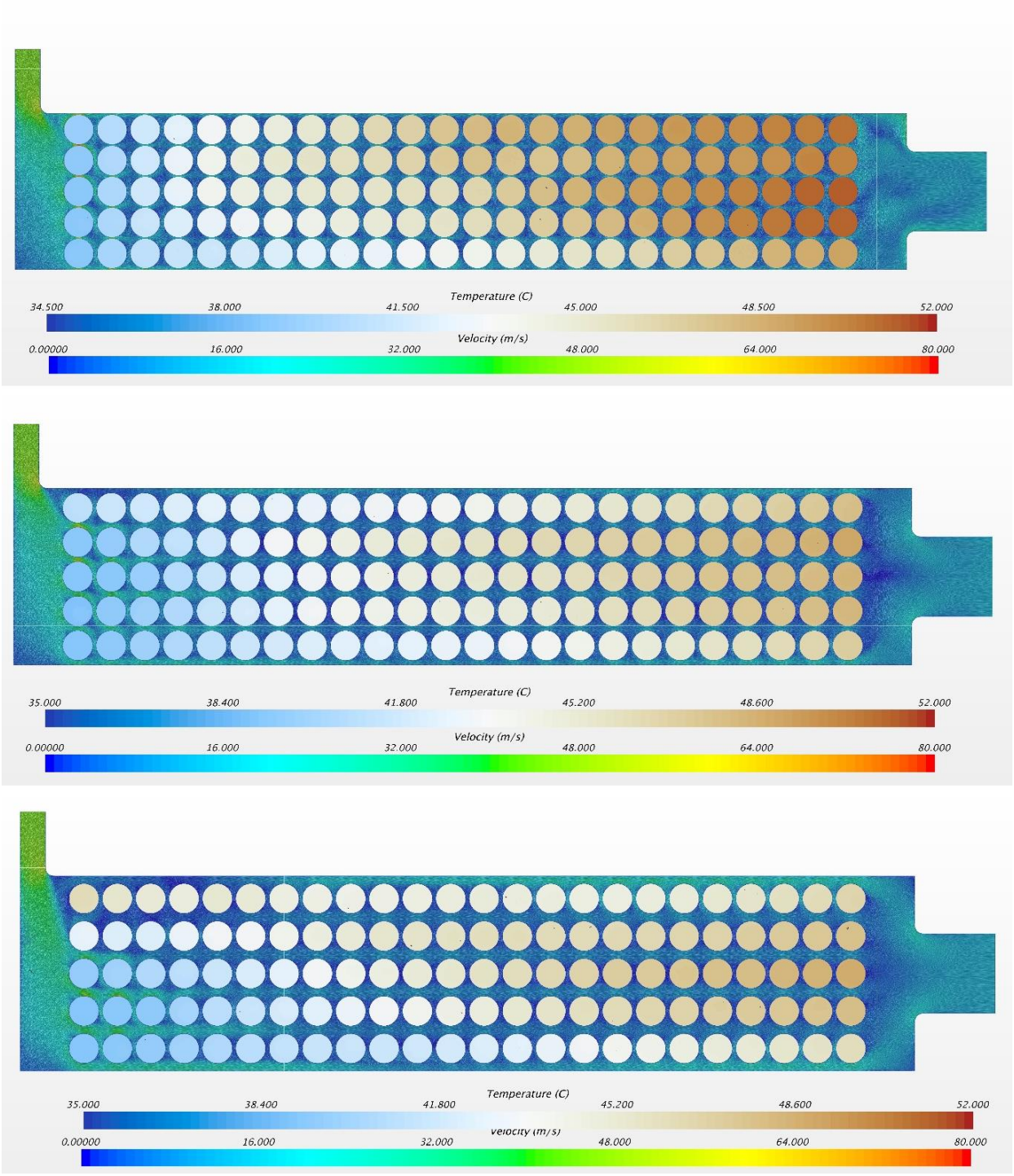

Figure 42: Air velocity and cells temperature varying the cells off-set on Z axis.

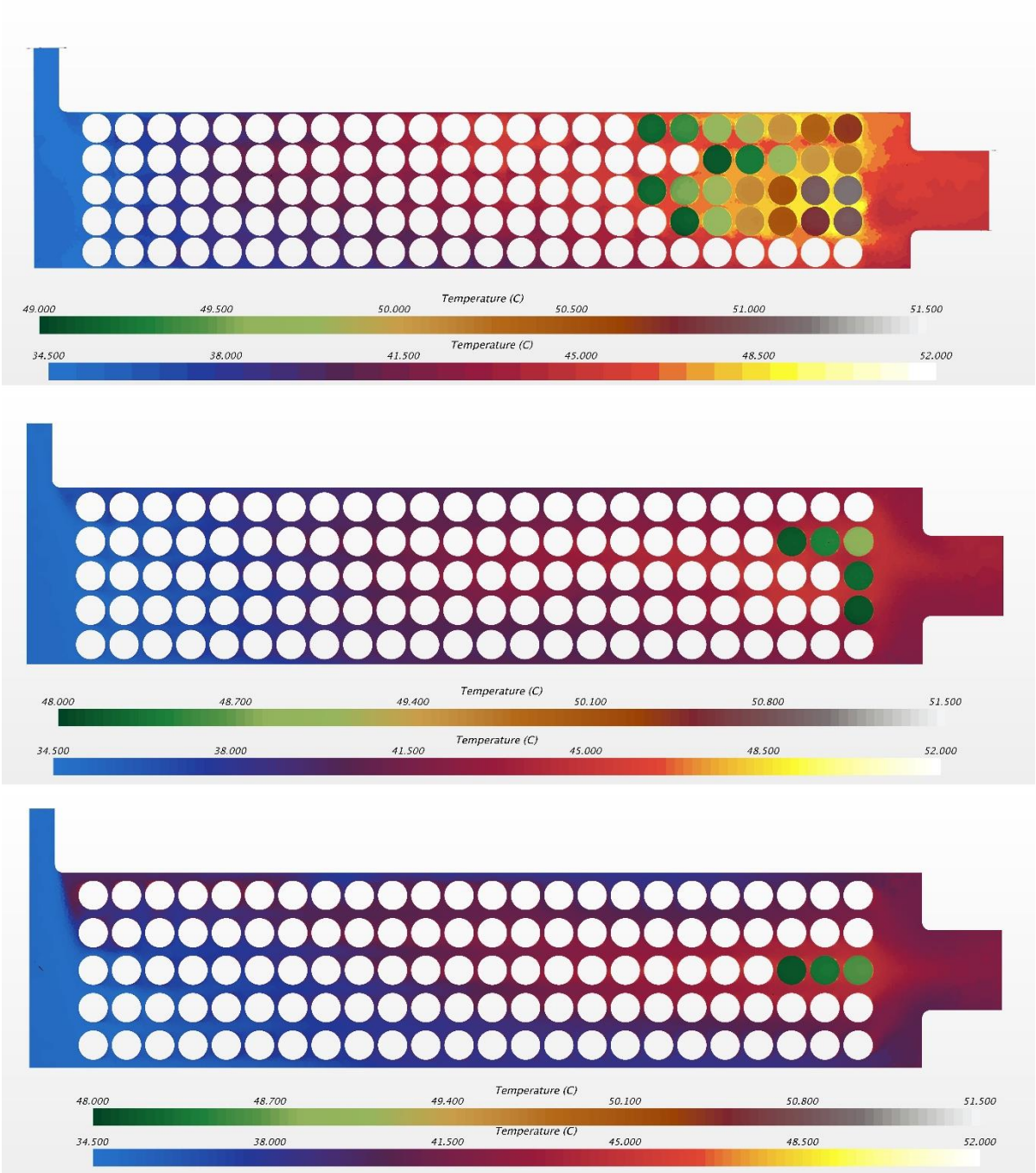

Figure 43: Air temperature and cells temperature above the threshold on the first scale varying the cells off-set on Z axis.

Following a CFD analyses of the air speed and cell temperature and the air temperature and cells temperature varying the cells offset on the Z-axis (Figure 42 and Figure 43), the best compromise resulted to be the 3mm offset (Figure 44). Increasing the offset to 5mm would not have significantly affected the cooling performance compared to the 3mm and it would have penalised the COG Z-positioning. A 1mm offset would not have brought to relevant advantages.

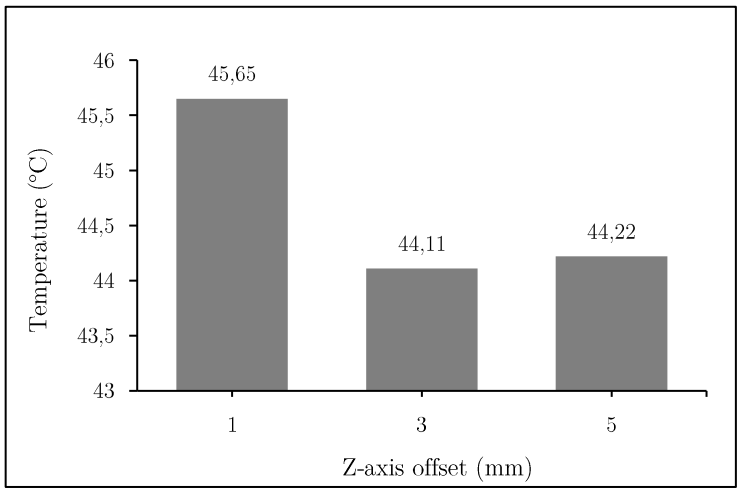

Figure 44: Temperature vs offset in between cells in Z-axis.

4.3.2 Fan positioning

Following determination of the best Z-offset, another crucial parameter was represented by the fan positioning along the Z-axis. Indeed, an optimal fan location would improve the air flux from the module inlet. Starting from the module midplane (Figure 45), which represented our 0-offset configuration, two different fan configurations were tried: 12mm up to the midplane (referred as +12mm) and 12mm down the midplane (named -12mm).

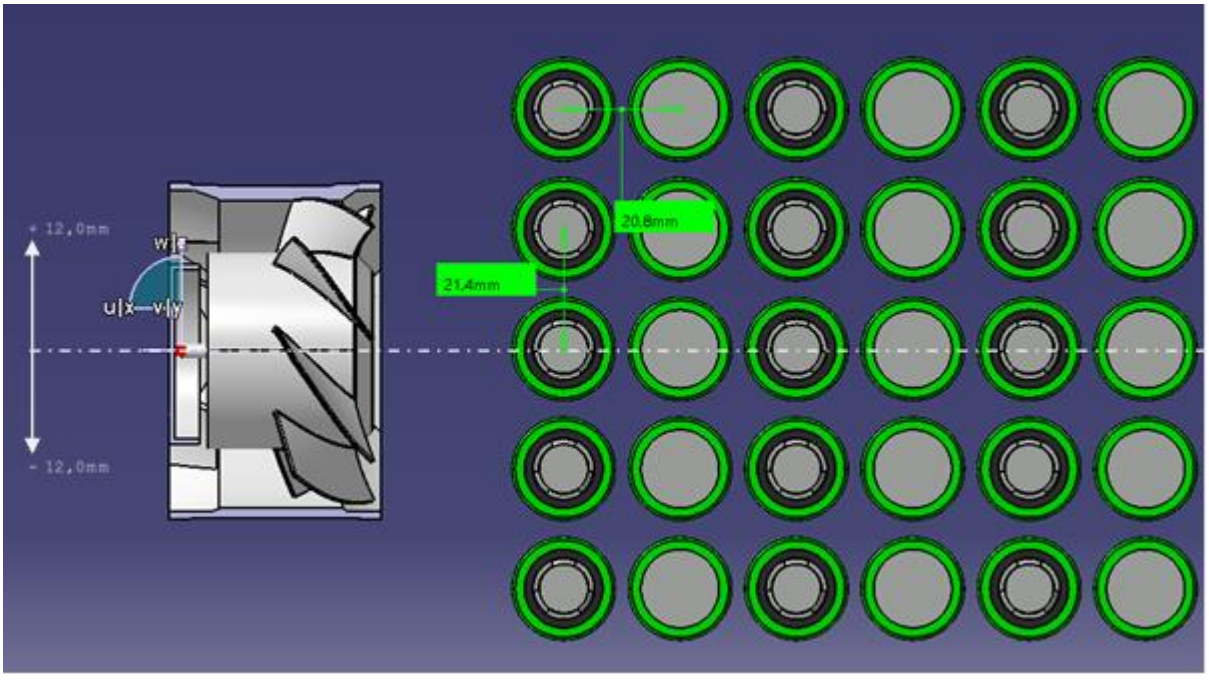

Figure 45: Midplane (0-offset) fan configuration.

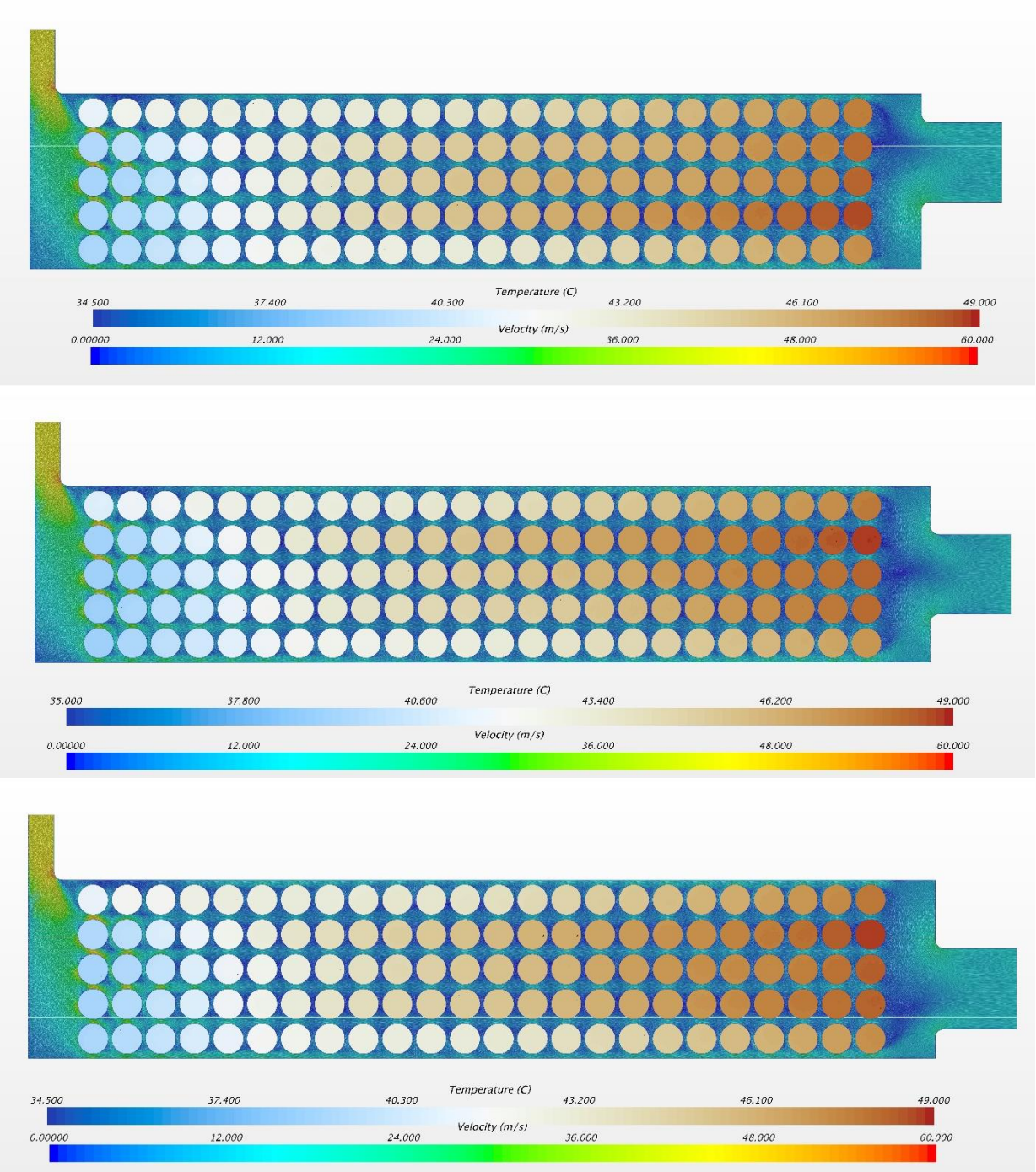

Figure 46: Air velocity and cells temperature varying the fan positioning on Z axis.

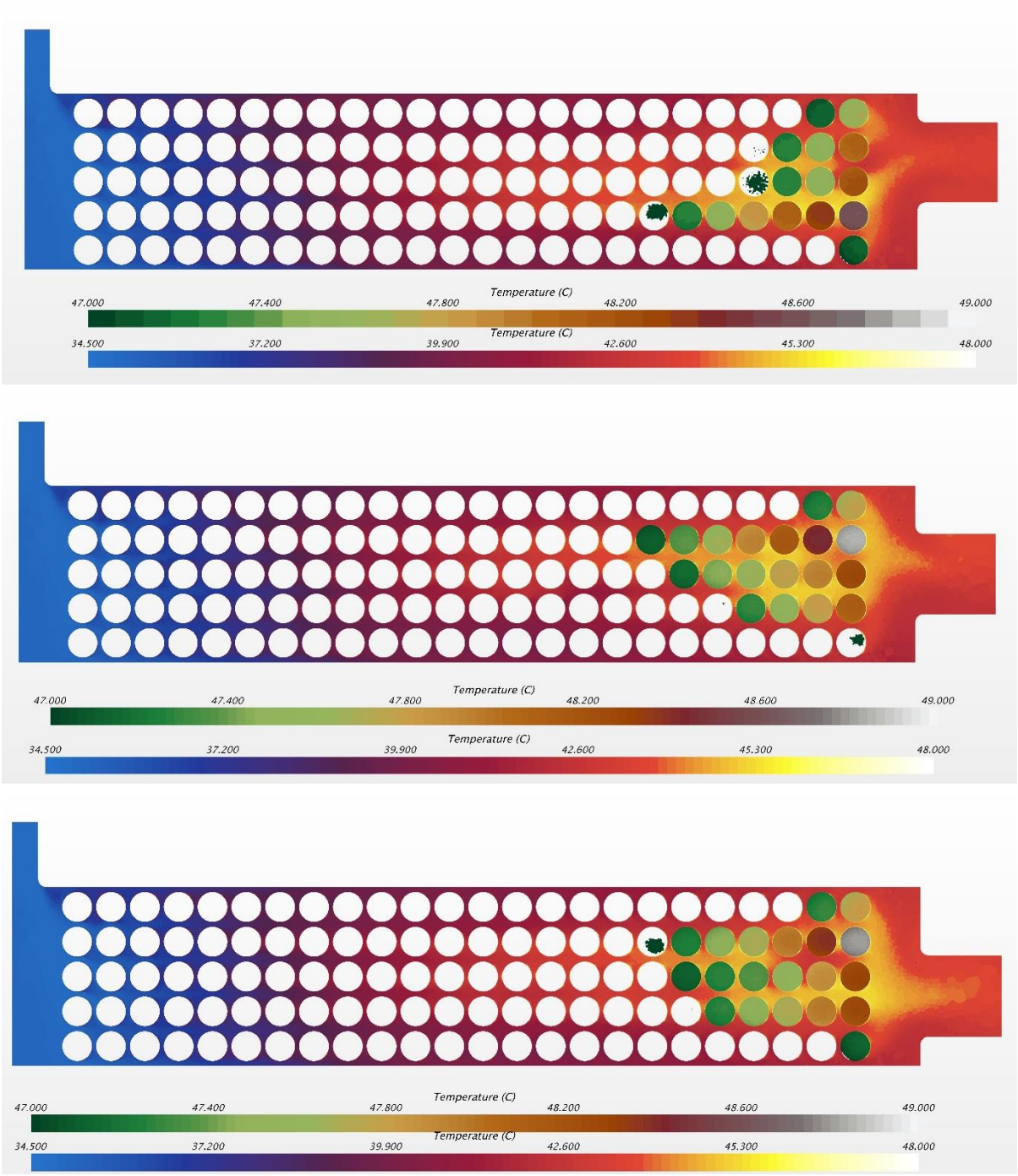

Figure 47: Air temperature and cells temperature varying the fan positioning on Z axis.

Following CFD analyses of the air speed and cell temperature and the air temperature and cells temperature varying the fan positioning along the Z-axis (Figure 46 and Figure 47), there is not an appreciable difference between the three configurations, probably due to inaccuracies of the CFD simulation (Figure 48). Therefore, the fan positioning can be determined according to packaging and spacing constraints rather than based on the fluid-dynamic analysis.

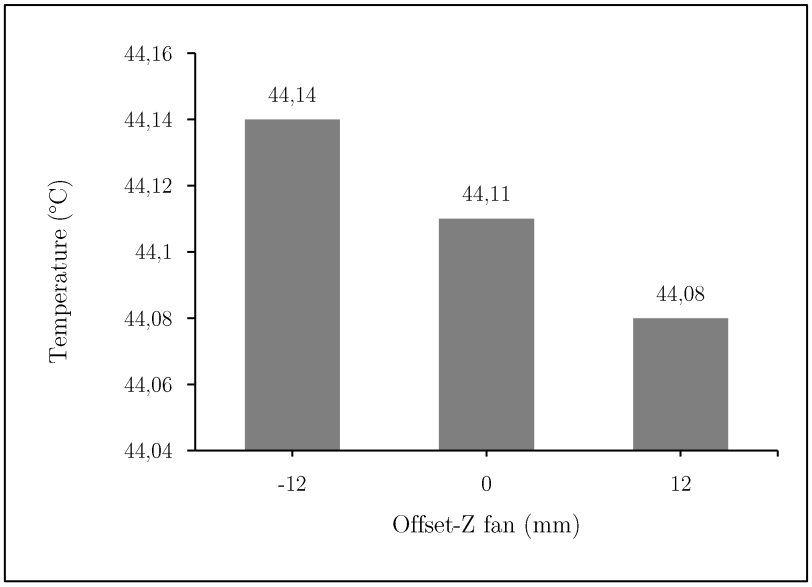

Figure 48: Temperature vs fan positioning from the Z-axis midplane.

4.3.3 Inlet dimensioning

With the previous results available, it was evaluated the dimension of the module inlet opening. This unusual inlet configuration is determined by two FSAE regulatory constraints, which force modules to be separated from each other and impose a frontal wall between the modules and the other battery pack components. The evaluation was carried out by simulating, through two different CFD analyses, the air velocity and the cells temperature and the air temperature and cells temperature following variations in the inlet dimensions (Figure 49 and Figure 51).

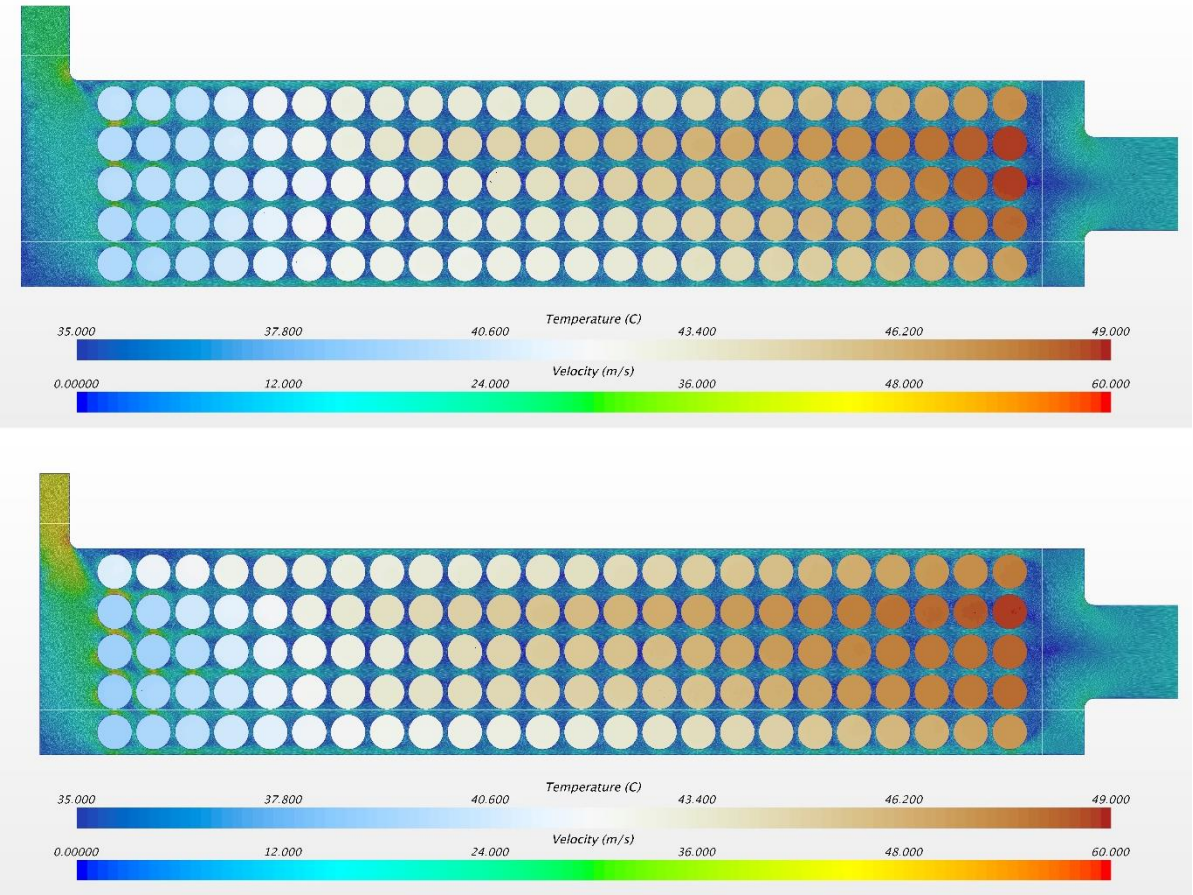

Figure 49: Air velocity and cells temperature following variation in the inlet position.

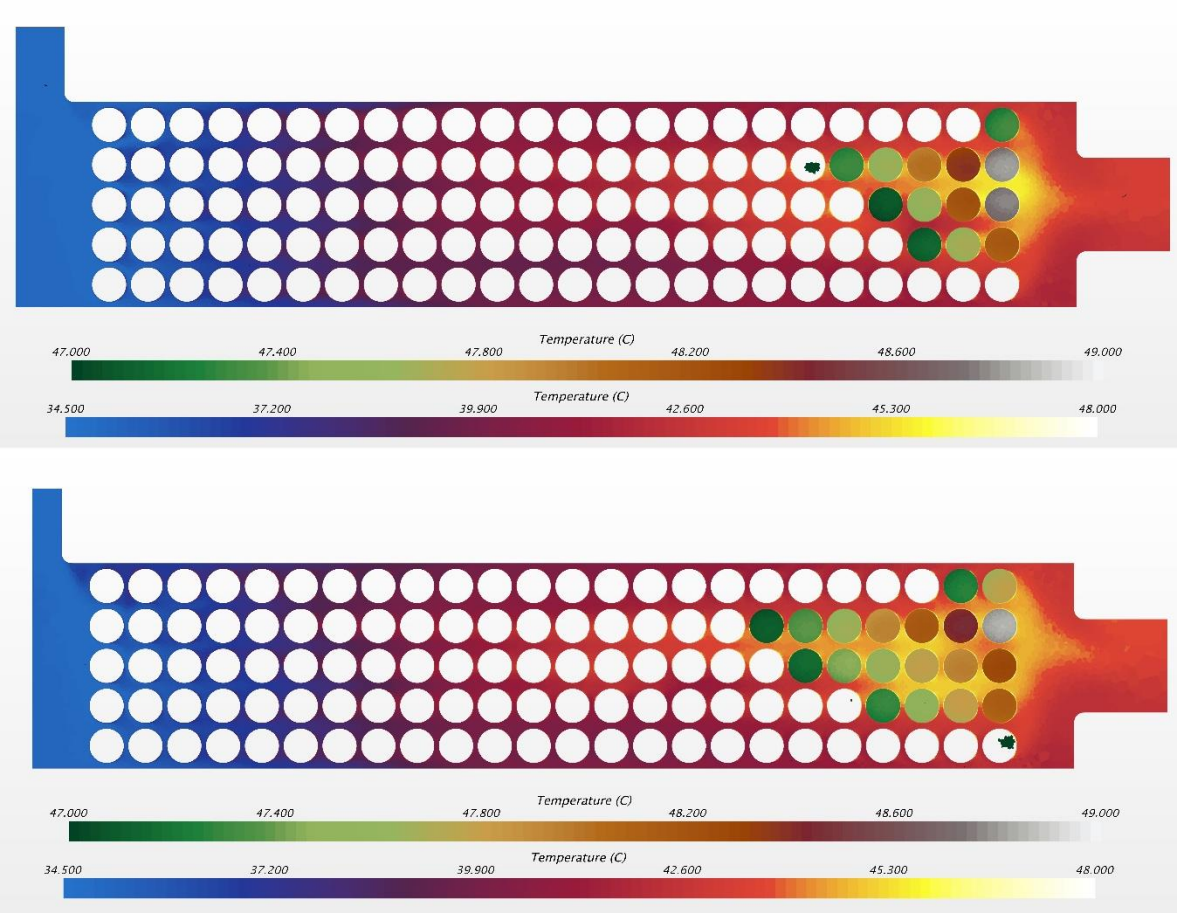

Figure 51: Air temperature and cells temperature following variation in the inlet position.

Increasing the inlet cross section, the average cell temperature decreases substantially (Figure 50). However, this would inevitably worsen the case dimension, affecting negatively the overall volumetric energy density.

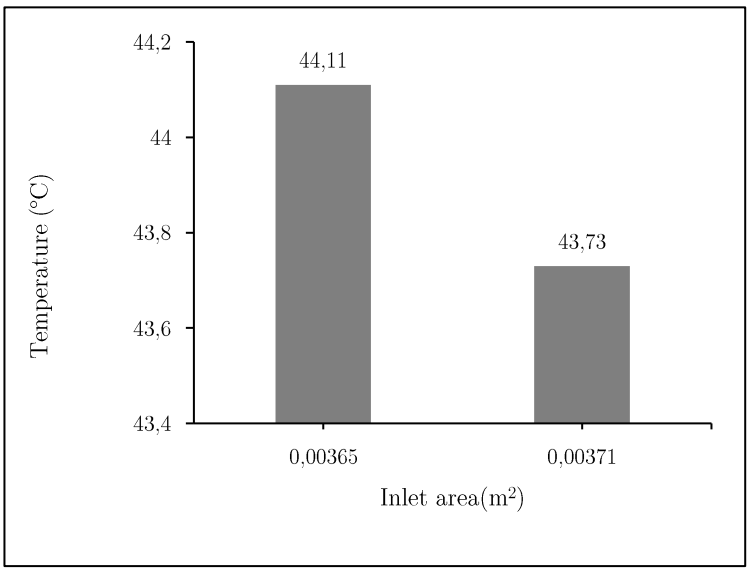

Figure 50: Temperature vs inlet area.

4.3.4 Fan configuration in push- or pull-mode

Finally, it was analysed the effects of different fan configurations, that is in the push- or pull-mode (Figure 52 and Figure 53). In the first configuration, cooling is achieved by pushing the air into the battery pack, while in the second arrangement the pack is cooled by pulling the air from the inside to the external environment.

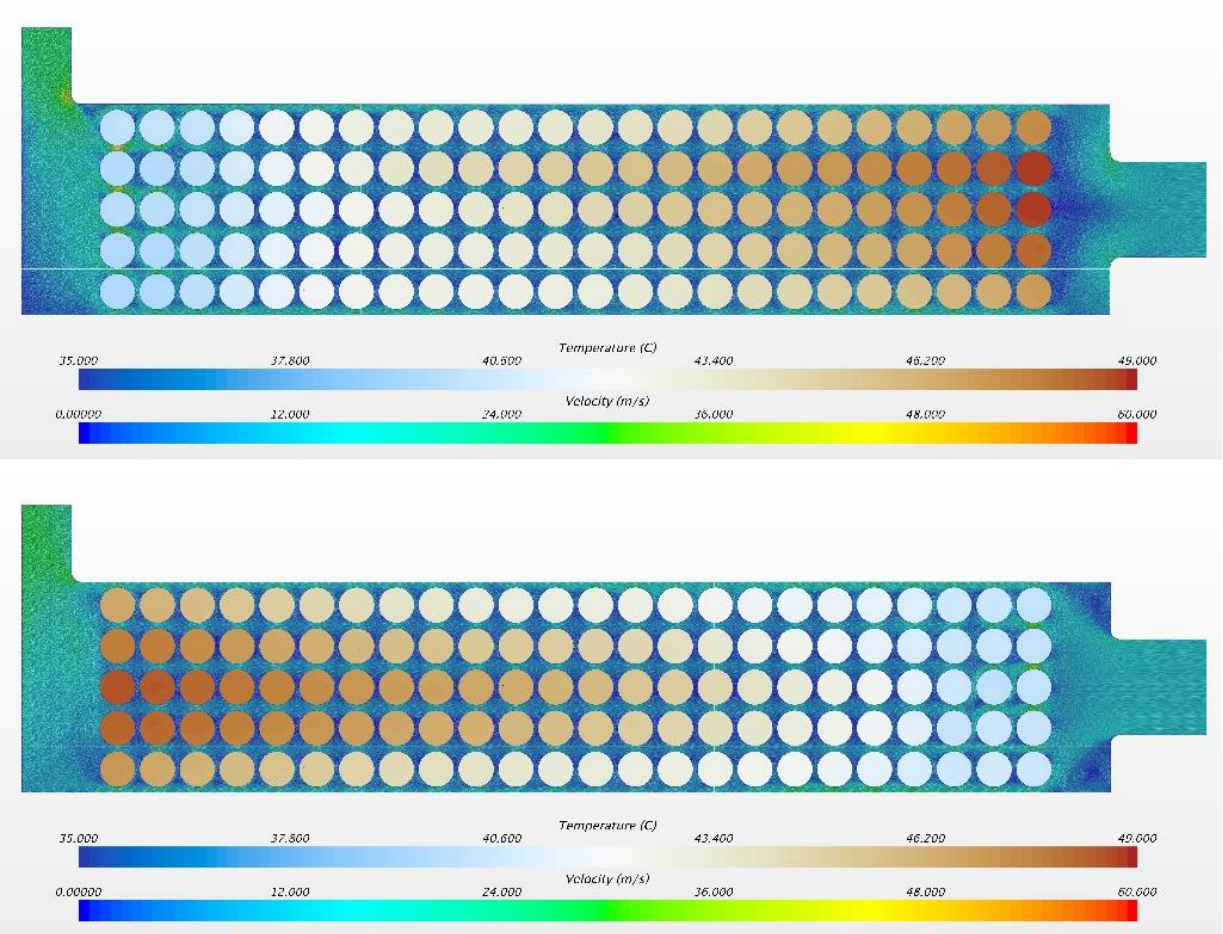

Figure 52: Air speed and cells temperature following variations in the fan configuration.

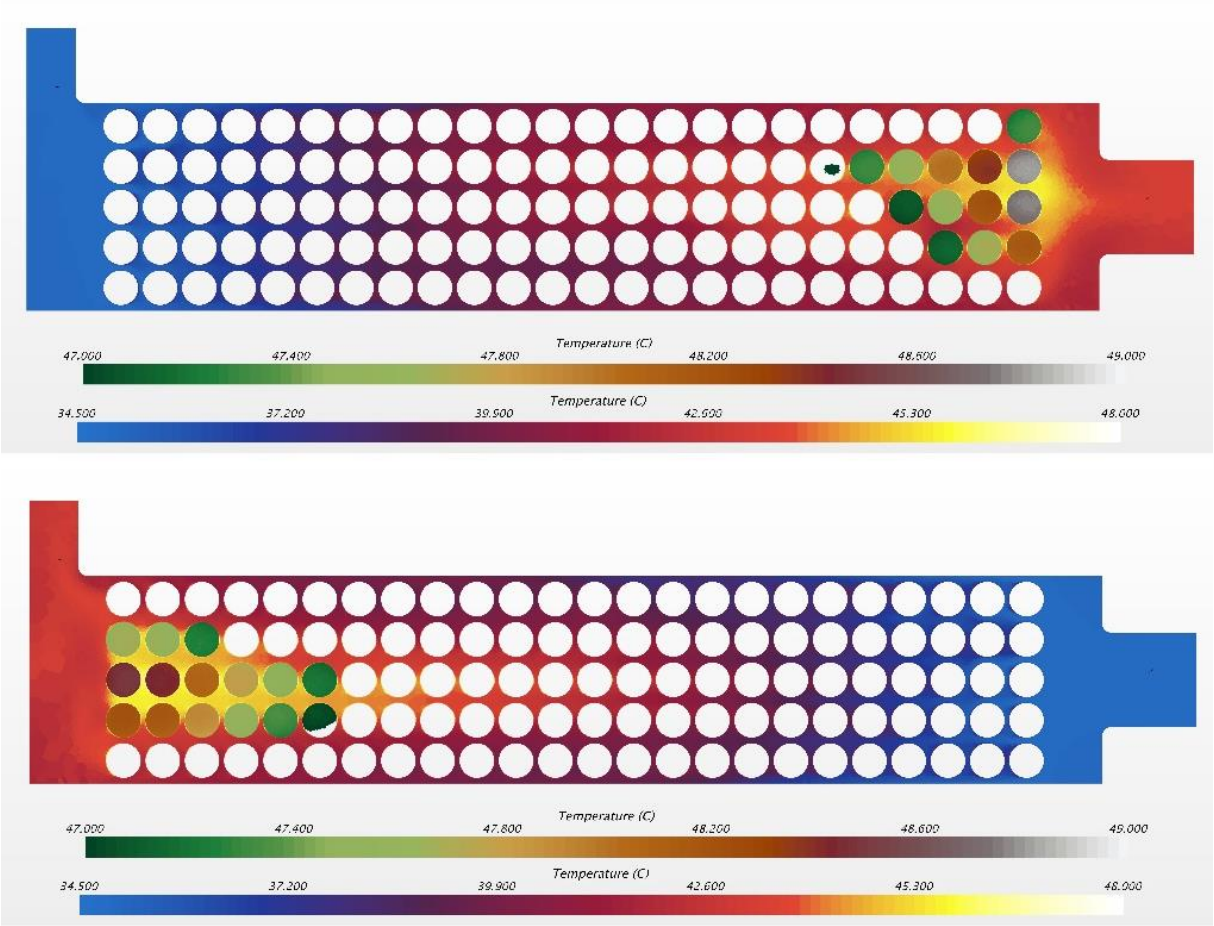

Figure 53: Air temperature and cells temperature following variations in the fan configuration.

Variation of the fan axial flow direction didn't bring to substantial changes (Figure 54). Therefore, we opted for a Pull configuration, where the fan ejected the air outside the chassis.

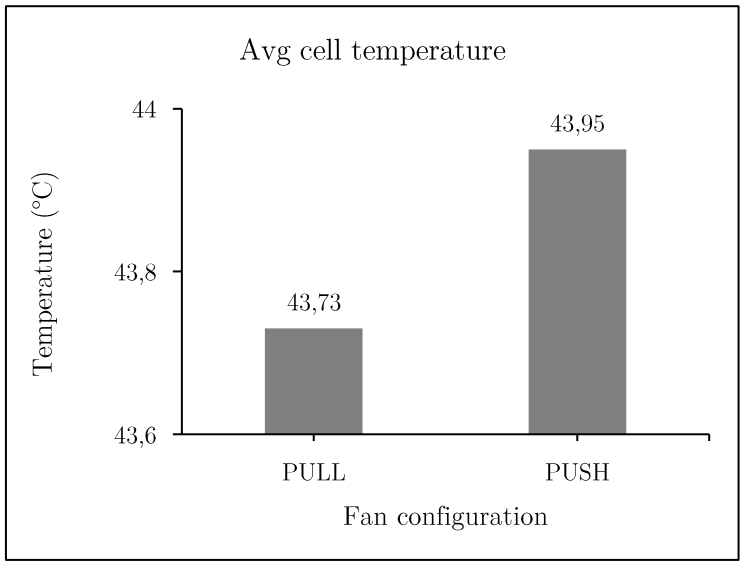

Figure 54: Temperature vs fan configuration.

5 Battery Pack Design

5.1 Battery Management System

The Battery Management System (BMS) represents the fundamental control unit of the battery pack. In short, it manages the amount of power and energy inside the battery pack to safeguard its lifetime and safety, protecting against failure, monitoring the state of battery and cells, communicating with the internal pack and the external system and ensuring optimization of the performance [40]. In addition, the software inside the BMS provides an esteem of the key battery parameters (state-of-health (SOH), state-of-charge (SOC), maximum voltage, etc.) to the external controllers [40].

The BMS is composed of a master control unit, several secondary control boards, sensors and software. The master controller comprises a hardware controller board and several software algorithms, which ensure the performance and safety of the entire system. In particular, it is in charge of (Figure 55):

1. Monitoring the cells and pack temperature;
2. Managing the heating and cooling based on the temperature read-out;
3. Monitoring the battery pack voltage and cell control boards;
4. Managing the state and the safety of the system, based on the values of voltage, temperature, SOH, SOC, etc.;
5. Communicating with the vehicle (or other master system).

The BMS can be arranged in the centralised and distributed configuration. In the centralised BMS, the master control board and the cell-monitoring control boards are located in one unit which is then connected to all the cells in the battery pack. In the distributed configuration, the master control board is centrally located and the “slave” boards are mounted directly onto the cells and interconnected in a daisy chain manner. This configuration minimizes the wiring but is usually more expensive, due to the amount of hardware required. However, the distributed BMS is generally preferred because of the greater functionality and control offered compared to the centralised distribution.

The BMS hardware is usually made up of one or more printed circuit boards (PCBs), that integrate all the communication components of the controller board, capacitors, resistors, current sensors and the application-specific integrated circuit (ASIC). The slave boards comprehend a

balancing circuit and the boards waste-heat management, which should minimize the impact of the heat on the other components of the board and on the cells.

An important factor to consider in the hardware design are the electromagnetic interference and electromagnetic compatibility of the system components. In case the control board is close to a high-voltage equipment, such as a charger, inverter or converter, it must be provided adequate shielding of the hardware and the cabling which connects them.

Aside from the hardware, the BMS also comprehends a series of algorithms which compose the BMS software. The algorithms consist of mathematical formulas and calculations designed from software engineers to understand the battery SOC, the instantaneous energy and power available. These parameters are crucial to accurately predict the performance and the health of the cells under most working conditions.

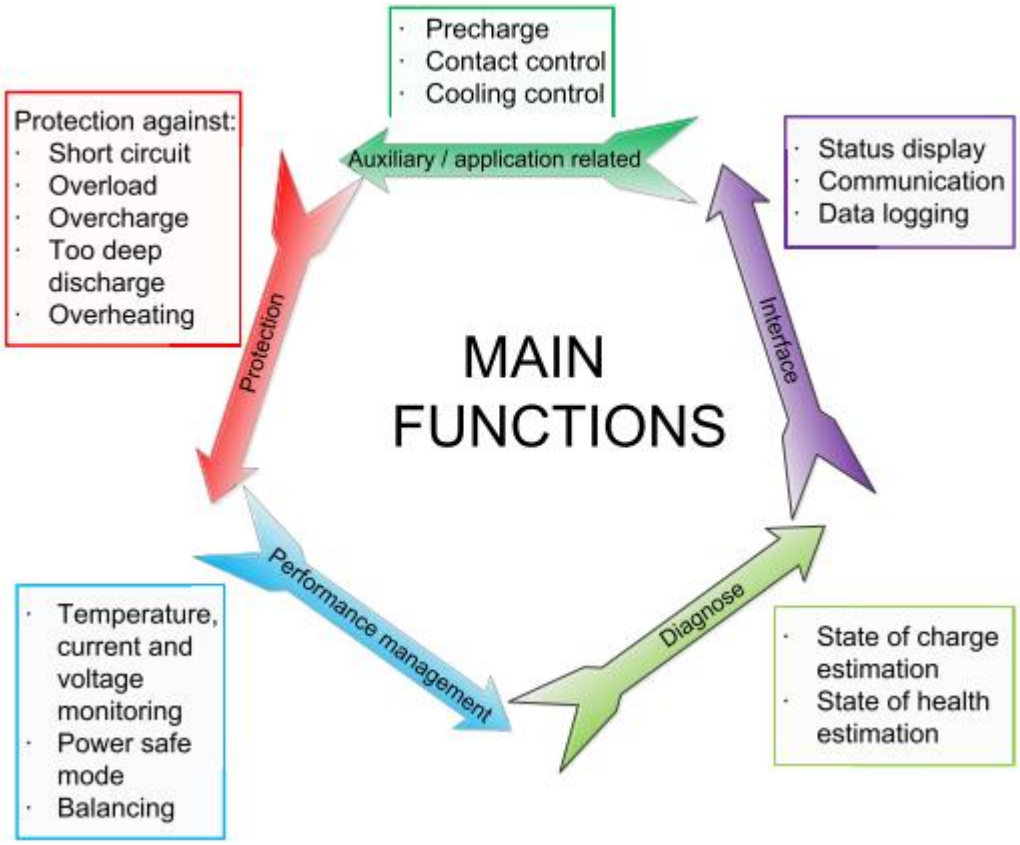

Figure 55: Main functions of the Battery Management System (BMS) [40].

5.1.1 Current, voltage and temperature monitoring

As manager of the battery pack, the BMS is in charge of constant monitoring of the battery pack current and of the cells and battery voltages and temperatures.

Monitoring of the pack current is needed to determine the power availability in discharging and charging modes. Data of the cells and pack voltages can direct the system in the starting and ending of the charge or discharge event. Finally, temperature analysis directs cells cooling and heating, functions requested to avoid continued operation outside the temperature limits, which can cause life reduction and thermal runaway.

5.1.2 Pre-charge

One switching function integrated in all electric vehicles is the precharge relay. Its function is essential to limit the magnitude of the inrush current into capacitive loads during power-up. Indeed, the power inverters usually have large capacitors at the tractive input stage to filter the high frequency switching noise. Initially, they are not charged, which could lead to very high inrush currents that, if not properly limited, can cause contact welding and component failure. Precharge relays are, thus, used to limit the charging current to a sufficient small value.

Figure 56 shows the inclusion of a precharge circuit in parallel to the positive DC. When the vehicle is precharging, the precharge relay and negative AIR are closed, such that the series resistance is predominantly that of the precharge resistor. Once the intermediate capacitor has been charged to a threshold near 95% of the accumulator voltage the precharge relay opens and the positive AIR closes. As the voltage difference between the battery and the inverter is less than 30V in the case of a fully charged battery, the resulting peak current is at an appropriately low value.

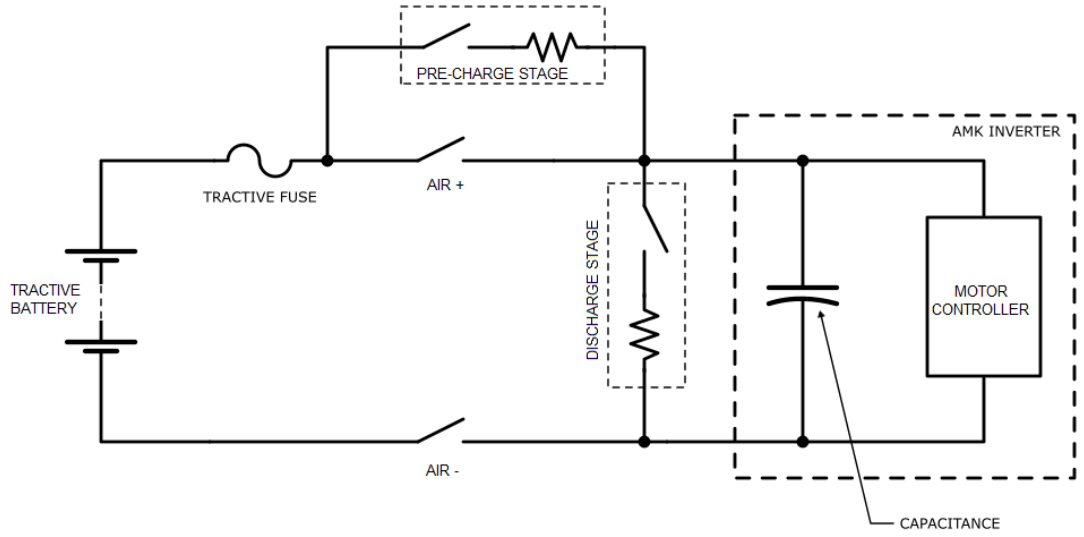

Figure 56: Tractive System Stages Diagram

The size of this precharge resistor, once is set the battery voltage, is presented as a compromise between the maximum peak current, power dissipated and time. The capacity of each inverter is 75µF, so the total capacity of load is 0.3 mF being 4 parallel connection. Assuming acceptable

a precharge time of almost 4s, a dissipated power of 12W and an RMS current of 50mA, with an iterative process a resistance value of 4.7kΩ has been chosen, indeed:

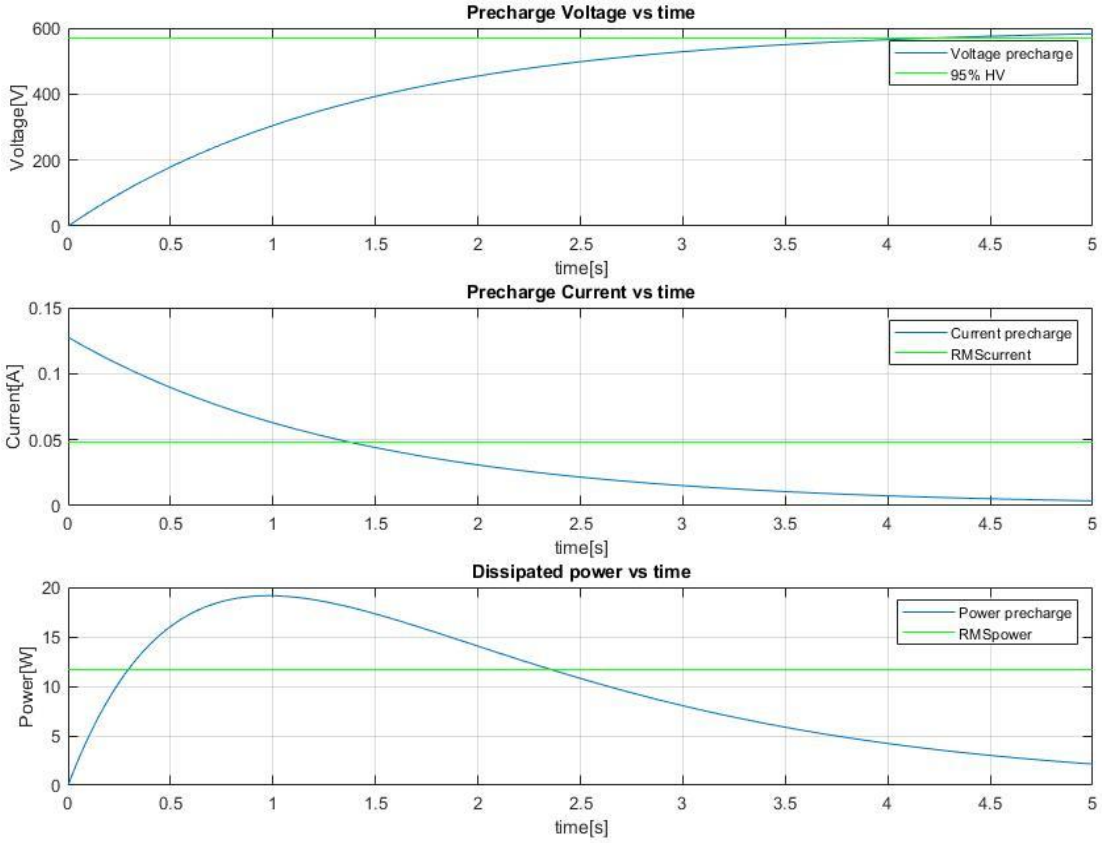

Figure 57: Tractive System Stages Diagram

The resistor of choice has been a TE connectivity THS50 (

Table **13**), rated for 50W, so there is no problem for power dissipation.

Resistor type	TE connectivity THS50
Resistance	4k7
Continuous power rating	20W (without heatsink)
Overload power rating	100W for 5s without heatsink
Voltage rating	1250V
Cross-section area of the wire used	AWG24

Table 13: Precharge resistor specifications

5.1.3 Balancing

One of the most important function the BMS has to carry out is cells balancing, which consists in making all the cells inside a battery pack at the same state-of-charge (SOC). Indeed, when there is an imbalance of SOC in the cells composing the battery pack, the overall SOC depends on the cell with the lowest SOC. This leads to incomplete discharge and eventually premature failure and aging of the entire system.

There are two main methods through which the BMS can balance a large lithium-ion battery pack: passive and active balancing. In passive balancing, the excess energy of the cells with the highest SOC is converted into heat and dissipated through resistors integrated into the slave boards that monitors the cells. Although this balancing method causes dissipation of part of the energy, it is less expensive than active balancing. Indeed, in an active balancing system, the excess energy coming from the cells with higher SOC is transferred to the lower SOC cells until all cells reach the same SOC level. In this way, the energy is not wasted but the system requires more space within the battery pack, increasing the costs.

Currently, passive balancing is the preferred balancing method since the benefits offered by the active balancing system are not worth more than the added costs of this technology. Of importance, when cells are assembled into parallel configurations, they will automatically balance to each other.

5.2 Component design

5.2.1 Accumulator Isolation Relays (AIRs)

As specified from the article EV3.5.1 of the Formula SAE regulation [1], each accumulator must have at least two accumulator isolation relays (AIRs) for each pole. An AIR is a normally-open contactor powered by the vehicle's shutdown circuit that, in case of a break of its loop, interrupts the power supply to the contactors, causing their opening. Its opening and closing logics are part of the BMS authority.

The main contactor is selected upon its rated voltage, continuous current rating and interruption capability rating, that is the maximum current flow it can interrupt without fusing its inner contacts. Life of a contactor depends on the fault current but also on its opening and closing currents. Indeed, a large number of open-close cycles at high current can cause the contactor degradation and early failure.

The contactors of choice were two LEV100H5CNG from Tyco Electronics®, are able to sustain safely all the designed mission profiles.

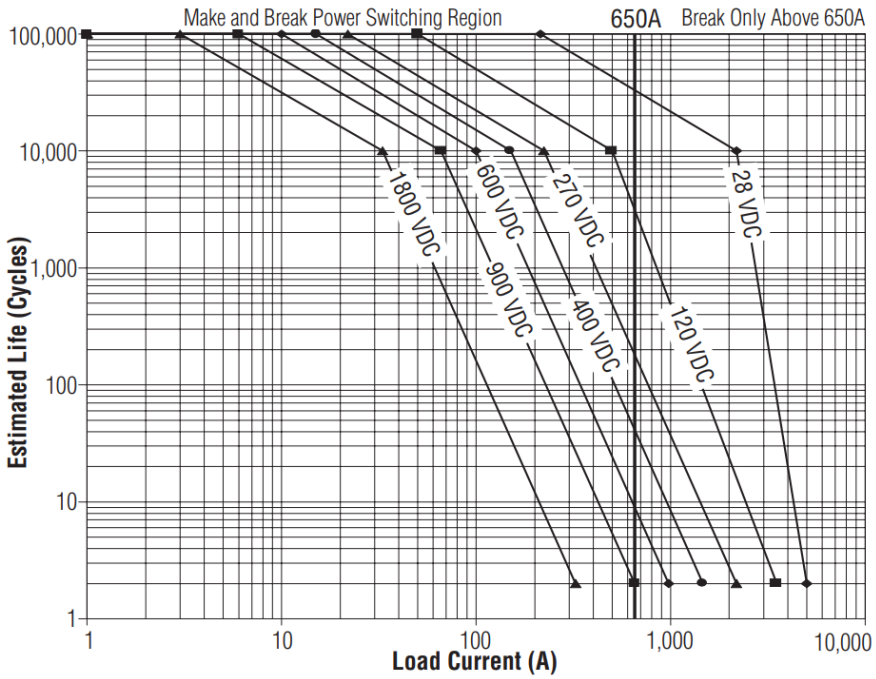

Figure 58: Estimated Make & Break Power switching ratings.

Table 14 summarizes their characteristics:

Relay type	**Tyco Lev100H5CNG**
Contact arrangement	SPST-NO
Continuous DC current rating	100A
Overload DC current rating	200A for 3 minutes
Maximum operating voltage	1000VDC
Nominal coil voltage	24VDC
Normal load switching	Make and break up to 50A @ 1000VDC
Maximum load switching	10 times at 600A @ 1000VDC

Table 14: Specifications and characteristics of the LEV100H5CNG Tyco Electronics ® contactor.

5.2.2 Cable sizing

Lithium-ion battery wiring usually consists of a low-voltage and high-voltage wiring. The former connects the sensor technology with the control unit, while the latter connects the modules and provides power for the electric loads. FSAE regulation has specific requirements on high-voltage wiring. As specified in the article EV.6.5.7: *"All Tractive System wiring that runs outside of electrical enclosures must either be enclosed in separate orange non-conductive conduit or use an orange shielded cable."* In addition, high-voltage cables must be:

- designed for voltages of max. 600 V;
- suitable for transmission of high amperages;
- transmit short-term current peaks while preventing overheating;
- highly flexible;
- suitable for small bending radii.

All vehicle wirings were chosen and dimensioned by computing the RMS currents from a data log taken from a real autocross event (Figure 59), the most demanding in terms of mean power.

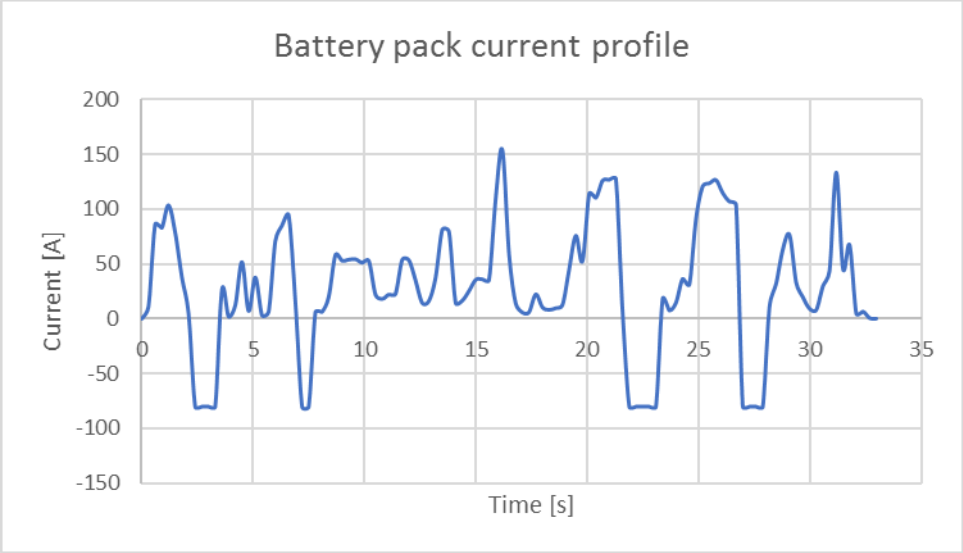

Figure 59: Battery pack RMS current profile from a real autocross event.

High-voltage cables must also be electromagnetically shielded to protect other vehicle components from electromagnetic radiation and reduce electrical noise. A typical shielded cable cross section is shown in Figure 60.

To ensure high reliability and provide the structure with lightweight components, the battery pack was connected to the vehicle through connectors for aerospace application, which meet the strict military standards.

The electrical separation of the modules has been guaranteed through maintenance plugs. According to the FSAE requirements (EV.3.3.4) they:

- *Must not be possible to connect in any way other than the design intended configuration;*
- *Must not require tools to install or remove;*
- *Must include a positive locking feature which prevents the plug from unintentionally becoming loose;*
- *Must be nonconductive on surfaces that do not provide any electrical connection.*

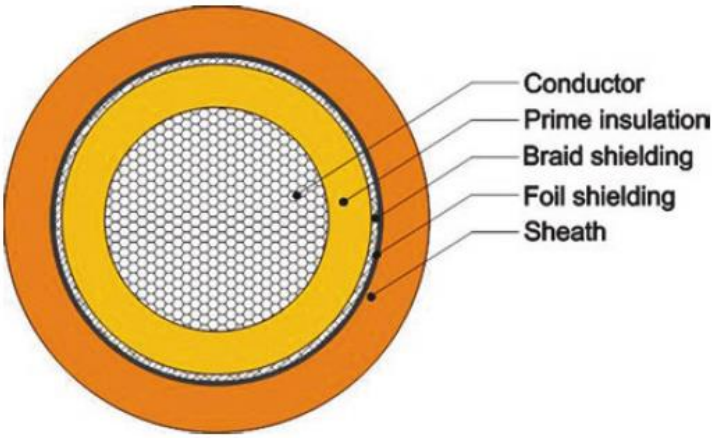

Figure 60: Composition of a shielded high-voltage cable cross-section [41].

The technical datasheet of the RADLOK™ maintenance plugs of choice is represented in Figure 61. To ensure their configuration was the only one possible, two pillars were added to the configuration, as depicted in Figure 62.

RADLOK™ Connector

RADLOK™ Connector Parameter (Tubular Version)

RADSOK® Size(mm)	RADSOK® Size (mm)					
	W	N	H	h	D	P
3.6	15.5	38.0	18.3	7.3	Φ 8.1	27.0
5.7	18.5	47.7	22.9	9.4	Φ 11.2	33.0
8.0	21.6	56.0	27.7	11.8	Φ 14.6	38.8
10.0	31.0	61.0	35.3	15.9	Φ 17.5	37.0
10.3	31.0	61.0	35.3	15.9	Φ 17.5	37.0
12.0	33.0	70.5	35.9	15.0	Φ 20.0	44.5

RADLOK™ Connector Parameter (Stamped Version)

RADSOK® Size(mm)	RADSOK® Size (mm)					
	W	N	H	h	D	P
5.7	18.5	46.0	21.9	9.2	Φ 11.2	30.0
8.0	21.7	54.4	27.7	12.5	Φ 14.6	34.3
10.0	25.7	65.0	33.3	16.1	Φ 17.5	35.7

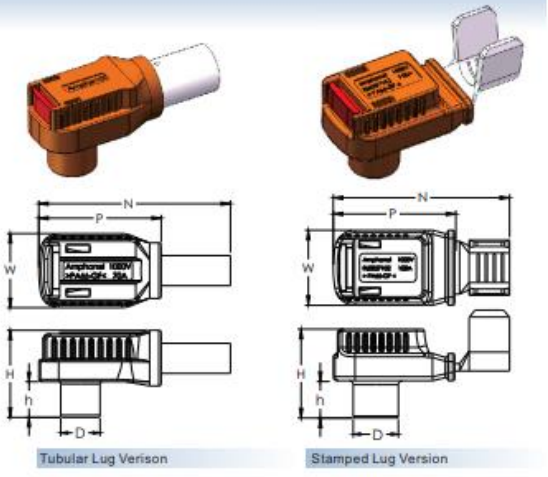

Figure 61 Radlok datasheet

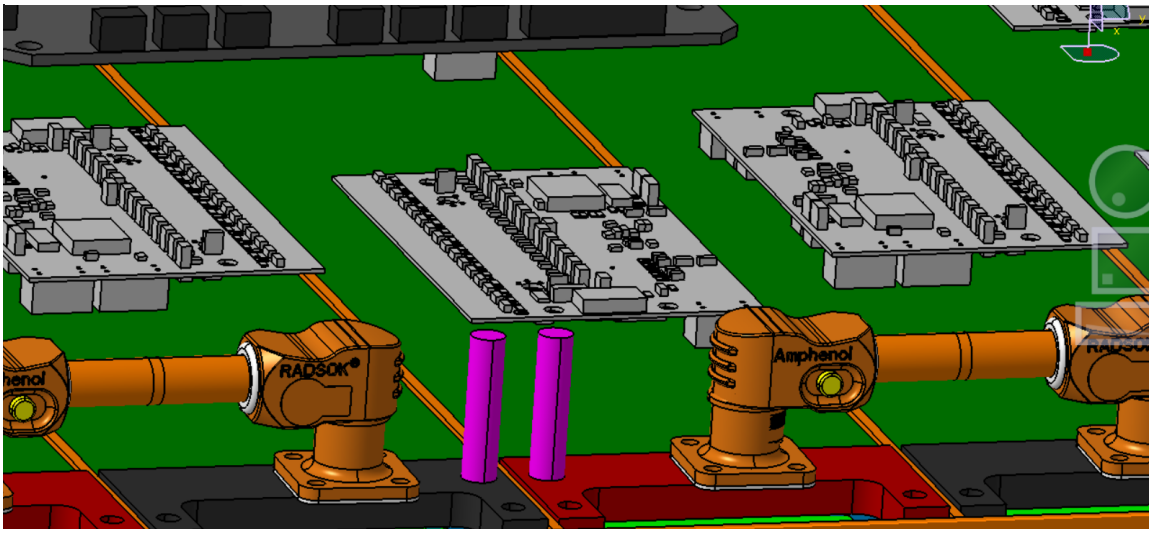

Figure 62: Configuration of the maintenance plugs with the pillars.

5.2.3 Fuse

The function of a fuse is to interrupt an uncontrolled fault current or an overcurrent before serious damage occurs. The main characteristic parameters, which must be considered before selection, are:

- Current rating: the maximum current a fuse can carry continuously at the rated temperature. As fuses characteristics are dependent on temperature, changes in ambient temperature affect their behaviour, usually worsening their performance in the most common applications where working conditions are more severe than the rating ones. The current rating should be therefore corrected according to the expected ambient temperature.

- Voltage rating: the maximum voltage the fuse can withstand before it is physically damaged. In a circuit where the voltage is equal or less than its rated voltage, the fuse can withstand safely its rated short circuit current break. An excess in the rated voltage creates the risk of arcing across a ruptured fuse, which maintains circuit continuity. Voltage ratings are specified for AC or DC circuits, whereby the former is generally higher than the latter.
- Interrupt rating: the maximum overload current a fuse can break at its rated voltage. A fuse can be expected to receive a fault current many times greater than its rated current in the event of a short circuit. Provided the fault current is less than the interrupt rating of the fuse, the fault will be interrupted without external damage to the fuse (for example the fuse body exploding).
- Fuse characteristics: they can be classified into three general categories: very fast-acting, fast-acting, or Slo-Blo®Fuse (Figure 63), which refer to how rapidly the fuse responds to various current overloads.

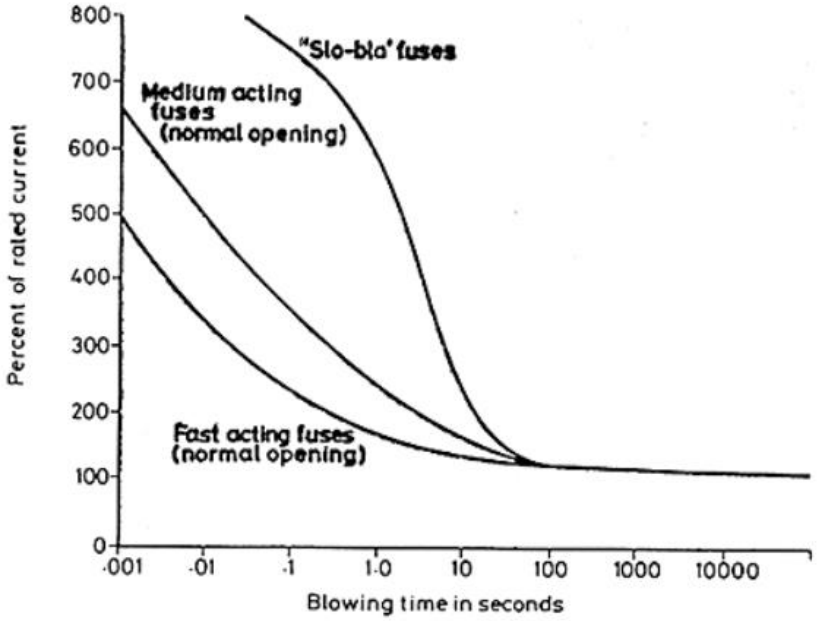

Figure 63: Relation of percent of rated current to blowing time [42].

The primary purpose of the tractive fuse is to disconnect the accumulator from the vehicle's tractive system in case of a fault. In case of overload, the wire forming the fuse will heat up and melt, interrupting the current flow and preventing damage to the rest of the circuit. According to the Formula SAE rules that apply to the fuse selection process:

- *The continuous current rating of a fuse must not be greater than the continuous current rating of any electrical component it protects (EV6.1.1).*

- *A fuse must be rated for the highest voltage expected. DC rated fuses must be used to protect dc circuits (EV6.1.2).*
- *A fuse must have an interrupt rating greater than the theoretical short circuit current of the system it protects (EV6.1.3).*

Starting from on overview of continuous current ratings of the main components in the tractive system (Table 15), the fuse must be rated for 90A or a lower value.

Component	Current Rating
Radlok busbar	120A
Cable 16mm^2	130A
AIRs	100A
Cable 10mm^2	90A

Table 15: Continuous current ratings of the main tractive system components

According to the De-rating temperature curve (Figure 65), in case of a temperature of 50°C – selected as the worst-case scenario – one should expect a decrease of the performance of approximately 10%.

To calculate the short circuit current, the system has been considered with one resistance, sum of the contribution of each cell connected in series or in parallel (Figure 64). However, this simplification implies that the cell internal resistance is constant, which is far from the real situation where it is dynamic and depends on several factors. To take into account this assumption, the fuse was chosen with a higher rating compared to the calculated one.

The internal resistance of a single cell, as in the datasheet, is around 13mOhm. With a configuration 144s5p the total resistance is:

$$R = 144 * \frac{1}{\frac{1}{0.013} * 5} = 0.374\ [Ohm] \tag{1}$$

The short circuit current, at the maximum battery voltage, is:

$$I = \frac{600[V]}{0.374[Ohm]} = 1604.3[A] \tag{2}$$

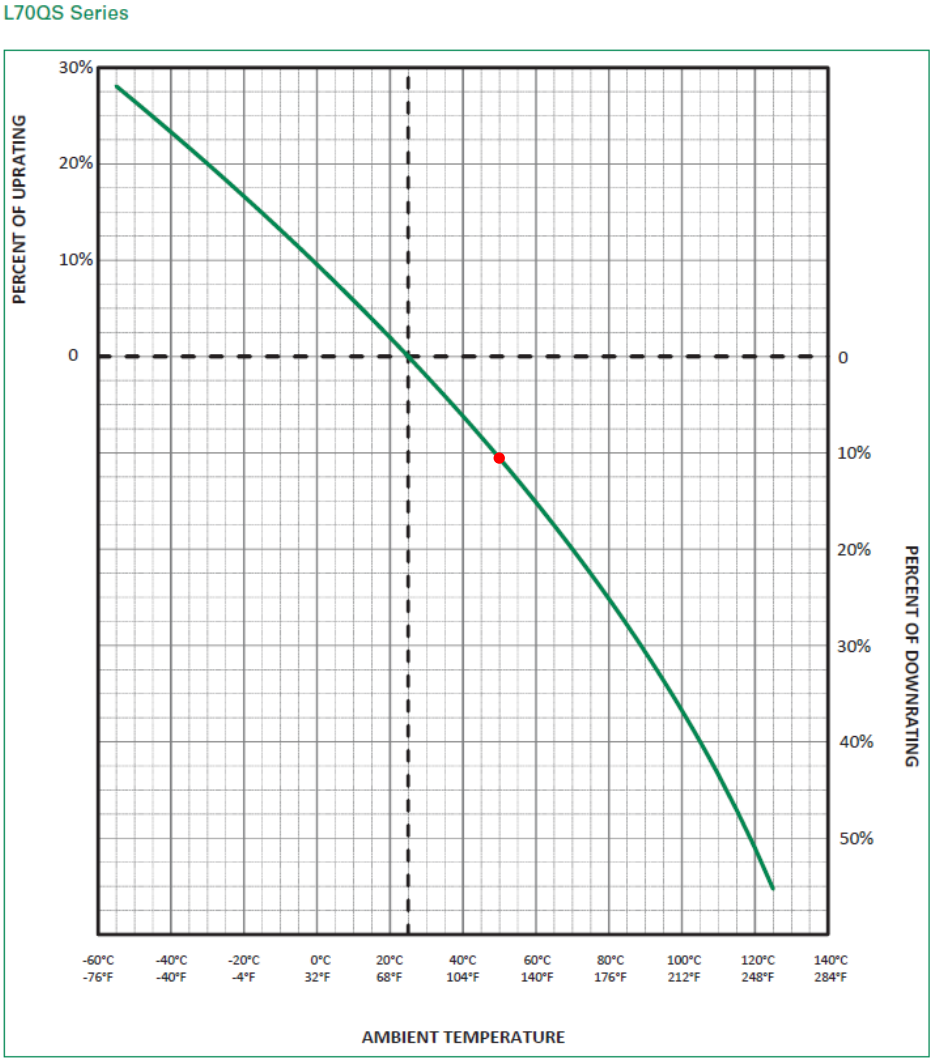

Figure 65: Temperature De-rating curve

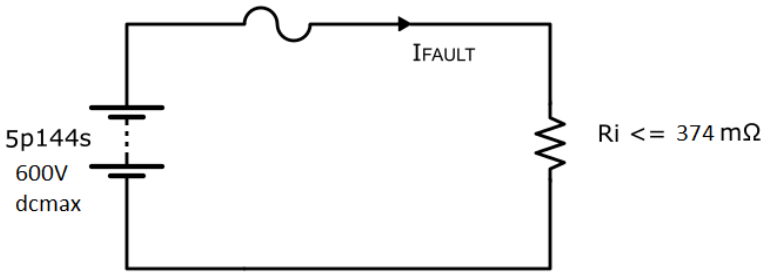

Figure 64: Simplified scheme of battery under short circuit conditions

Two final aspects to consider before fuse selection are the RMS current and the current peaks the fuse can withstand for a short amount of time without melting. If maintained within the accepted temperature range, the fuse can sustain the RMS current for an infinite amount time. Considering an arbitrary current peak of 200A, the fuse would perform in this condition for a maximum time of 40 seconds (Figure 66).

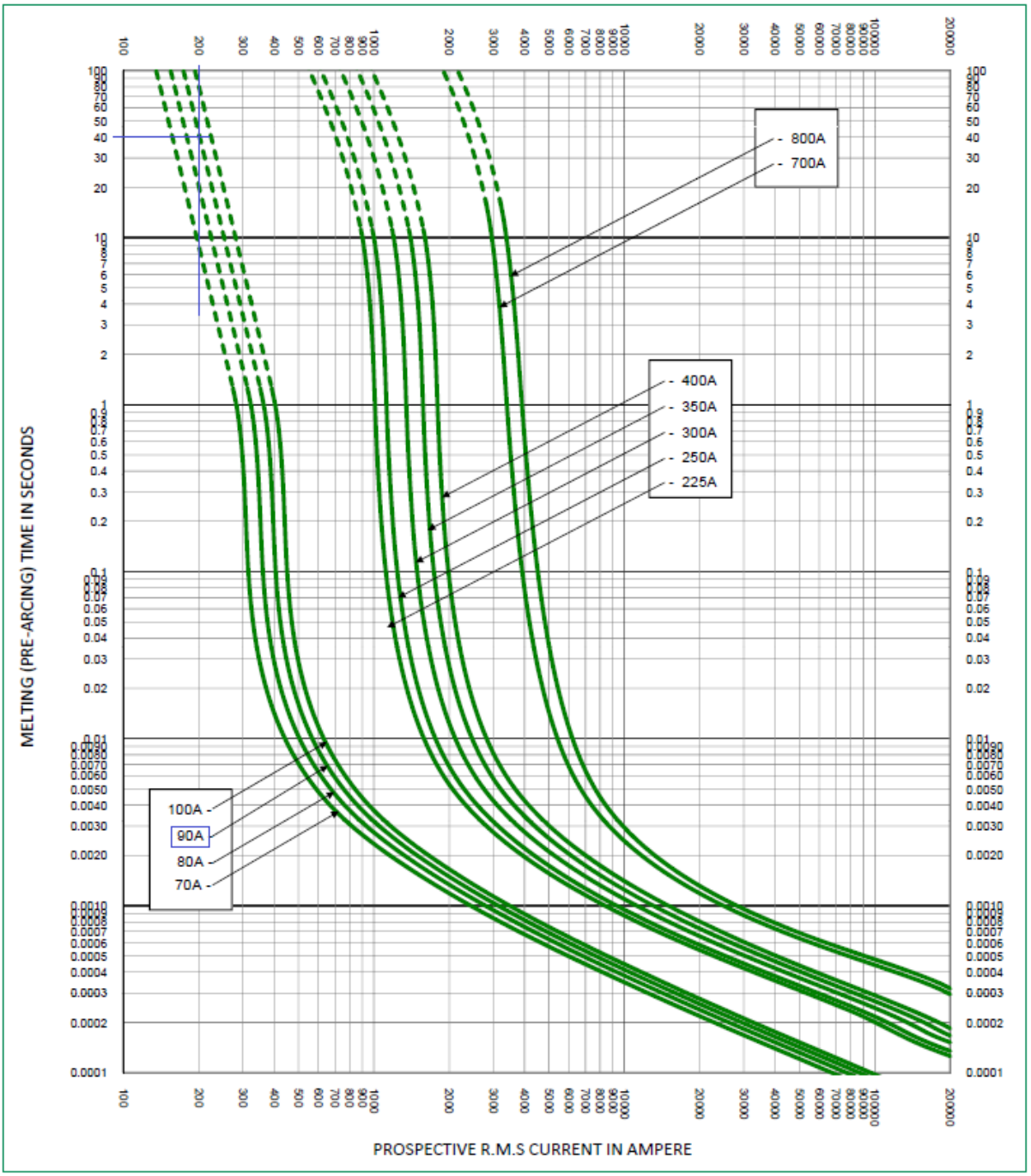

Figure 66: Time-RMS current curve

The fuse L70QS90 Littlefuse® fulfilled all the requirements, thus it was the preferred choice.

5.3 Structural design

The battery enclosure was designed according to the functional requirements suggested by the FSAE rules (EV.4.2 “Accumulator Container - Design” [1]). Specifically, the enclosure must be able to secure the modules when subject to the following accelerations:

- 40 g[1] longitudinally;
- 40 g laterally;
- 20 g vertically;

which are intended to be representative of a crash scenario. The applied load will thus be calculated as the product of 40g acceleration and the mass of the modules, and it will be applied at the centre of mass of the modules. To achieve these targets, the FSAE regulation provides the following design guidelines regarding both material and thickness:

- *The floor or bottom of the accumulator container must be constructed of steel 1.25 mm minimum thickness or aluminium 3.2 mm minimum thickness;*
- *The external vertical walls must be constructed of steel 0.9mm minimum thickness or aluminium 2.3 mm minimum thickness;*
- *Internal vertical walls separating cells and/or segments must be constructed of steel 0.9 mm minimum thickness or aluminium 2.3 mm minimum thickness;*
- *Covers and lids must be constructed of steel 0.9 mm minimum thickness or aluminium 2.3 mm minimum thickness.*

In addition, the battery enclosure needs to be sealed against dust and water and, most importantly, it must be isolated from the High Voltage sources. When the material used are highly conductive – as it happens with the metals suggested by the FSAE guidelines – the enclosure's inner wall must be carefully insulated with an electrically non-conductive material, which however leads to an increase in the design volume, weight and complexity.

The choice fell on a composite material made of a non-flammable resin, rated for UL-94V0 standard as requested by the FSAE rules, and a Kevlar® aramid fibre in two different thicknesses to meet the structural equivalences of the FSAE rules.

To reduce the weight impact and, at the same time, satisfy the structural requirements, the two composite laminates were tested with a three-point bending test and a perimeter shear test. The three-point bending test (Figure 67) is a structural test performed to determine the Young's modulus of a sample and determine its mechanical behaviour under flexural deformation (*i.e.* stress-strain behaviour, ultimate flexural load, failure limit). The perimeter shear test constitutes another major structural test useful to determine the sample shear strength, that is the maximum shear stress that the material can withstand before failure occurs (Figure 68)

[1] g represents the gravitational acceleration, g = 9.81 m/s^2

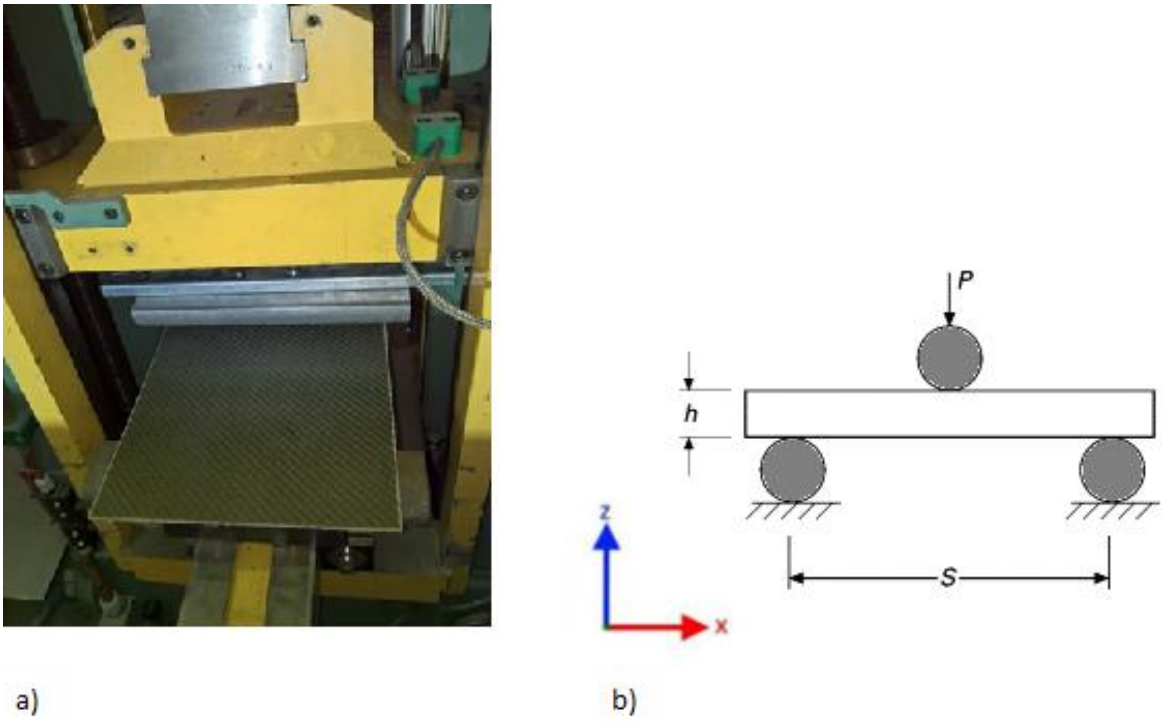

Figure 67: a) Setup for three-point bending test. b) Test schematic front view.

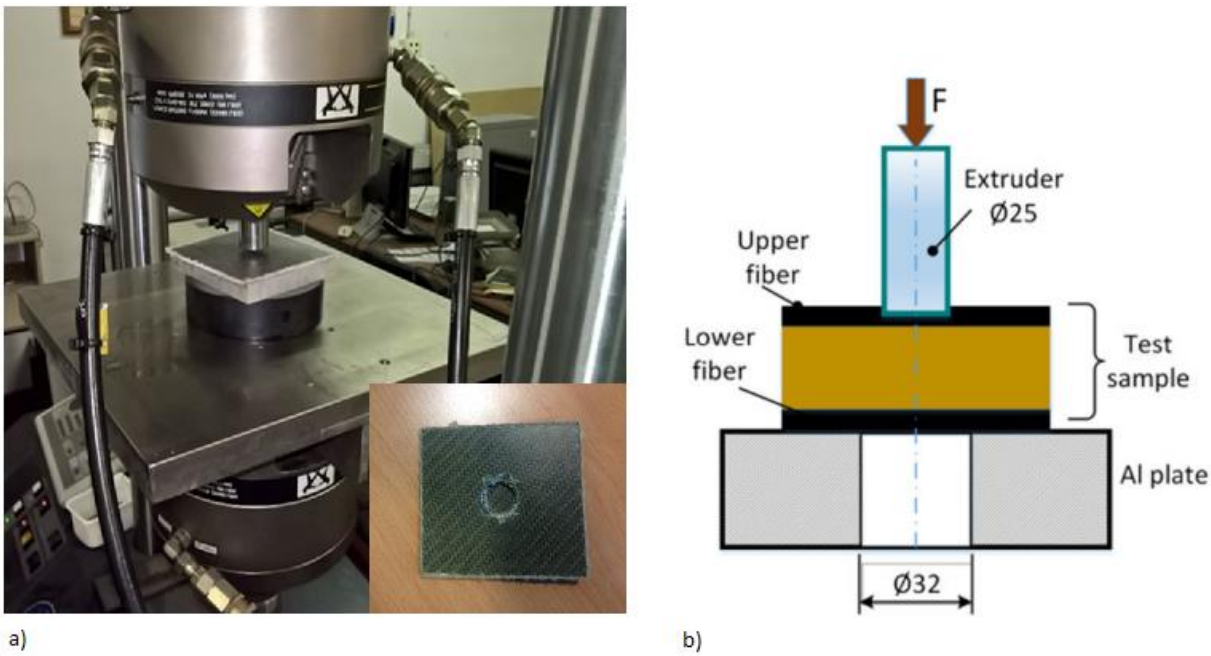

Figure 68: a) Setup of perimeter shear test. b) Schematization of the setup parts. Adapted from [43].

6 Design Implementation and Testing

6.1 Module Assembly

Several production technologies were used to manufacture the module components, such as a CNC machining for the module supports; a laser cutting which provided high precision and at the same time high production volumes with lower cost; a 3D printer with an anti-flammability material to fulfill the FSAE requirements. Once all the components were manufactured and ready to use, segment assembly was conducted by a group composed of myself and four team members, which helped during the entire work. It took over 100 hours to complete the entire assembly. Figure 69 shows the module during the cells Heavy Wire Bonding, which represented one of the main stages of assemblies.

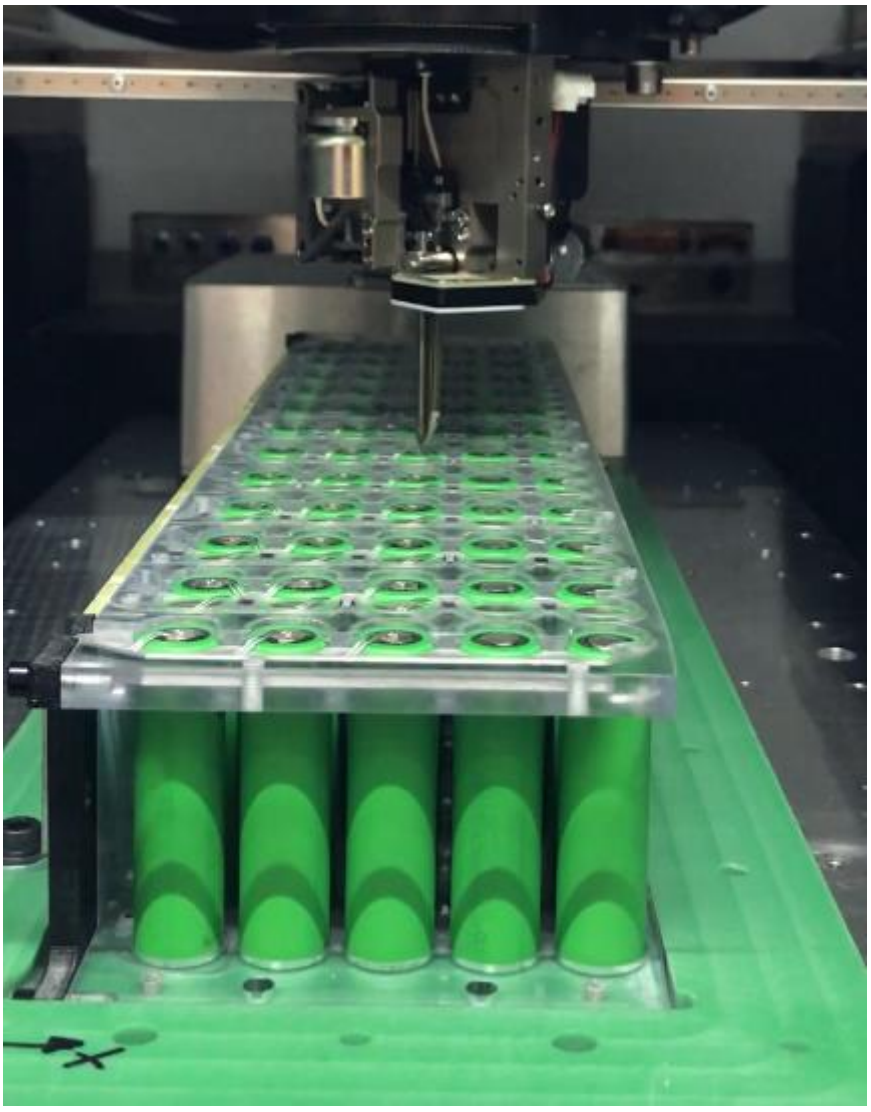

Figure 69: Heavy Wire Bonding machine and module.

The result was almost unexpected since the Heavy Wire Bonding machine worked automatically after the bonding path was implemented in the code, showing a good mechanical assembly between the cells and their supports. Figure 70 shows a detailed view of the bonded wires.

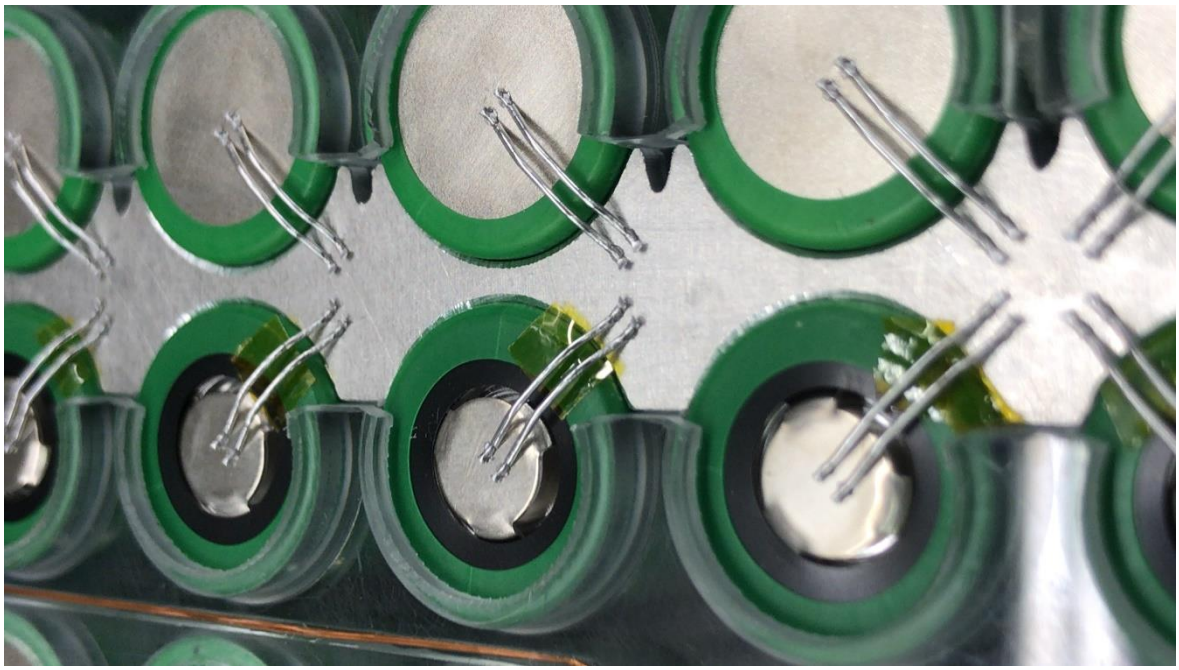

Figure 70: Heavy Wire Bonding detail.

6.2 Module Testing

Together with cells bonding, each module was tested to verify if one or more wires were not corrected welded. As explained a bad connection between cells leads to a higher contact resistance, that is easily detectable when the voltage is measured and a current flows through the connection.

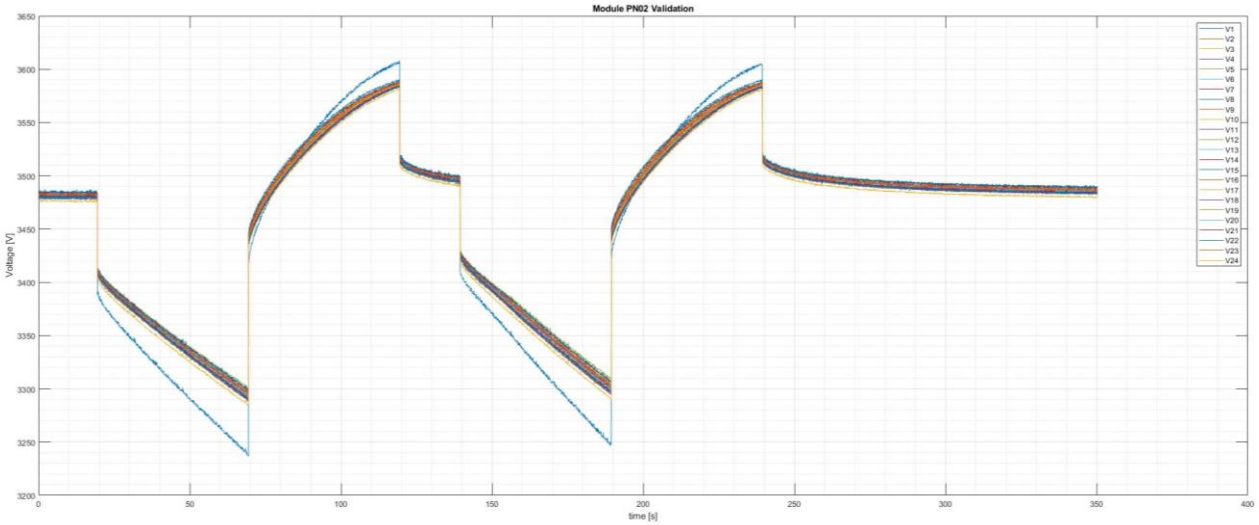

Figure 71: Module Heavy Wire Bonding validation.

In Figure 71 the series number 08 has a failed bonding. The grater voltage drop during the discharge means a fault connection between the wire bonding and the cell. Once the faulty bonded series has been identified, a new bonding procedure is needed.

The module cooling effectiveness was also tested in a climatic chamber to make a correlation between the CFD simulation and a real working condition. A complete module discharge was made with an ambient temperature of 35°C and the cooling fan was powered at the maximum rotational speed to have the maximum achievable airflow. In Figure 73 the module is placed inside the climatic chamber where a thermal camera was placed to constantly acquire thermal images during the module discharging (Figure 72).

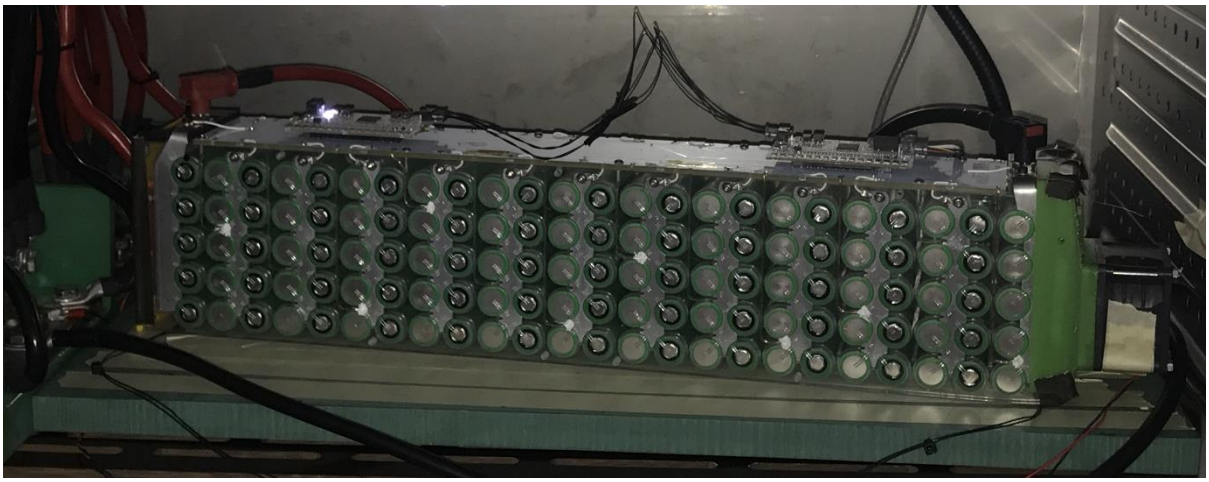

Figure 73 Module experimental set-up for thermal analysis.

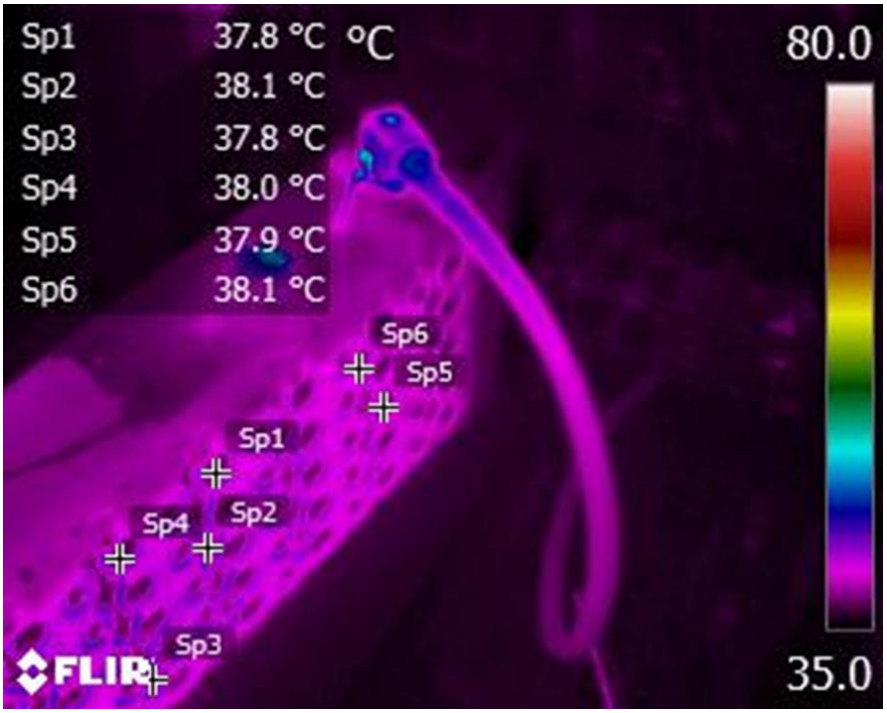

Figure 72 Module thermal image during discharging.

After the discharge cycle, the highest temperatures reached were below the limit of 60°C (Figure 74).

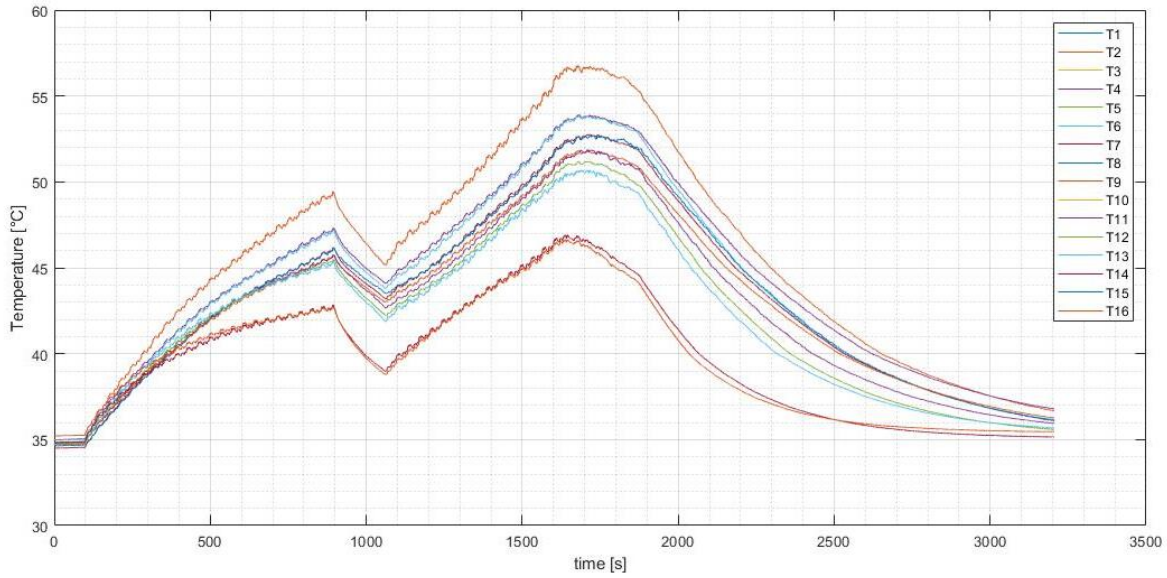

Figure 74 Module temperature distribution during Endurance discharge cycle.

A 3D plot helps to visualize the distribution along the length of the module, in which the temperature sensor in 0 position is the farthest from the inlet side of the module. In turn, the inlet side results to be the coolest part, as it can be seen from the temperature sensor in position 16 (Figure 75).

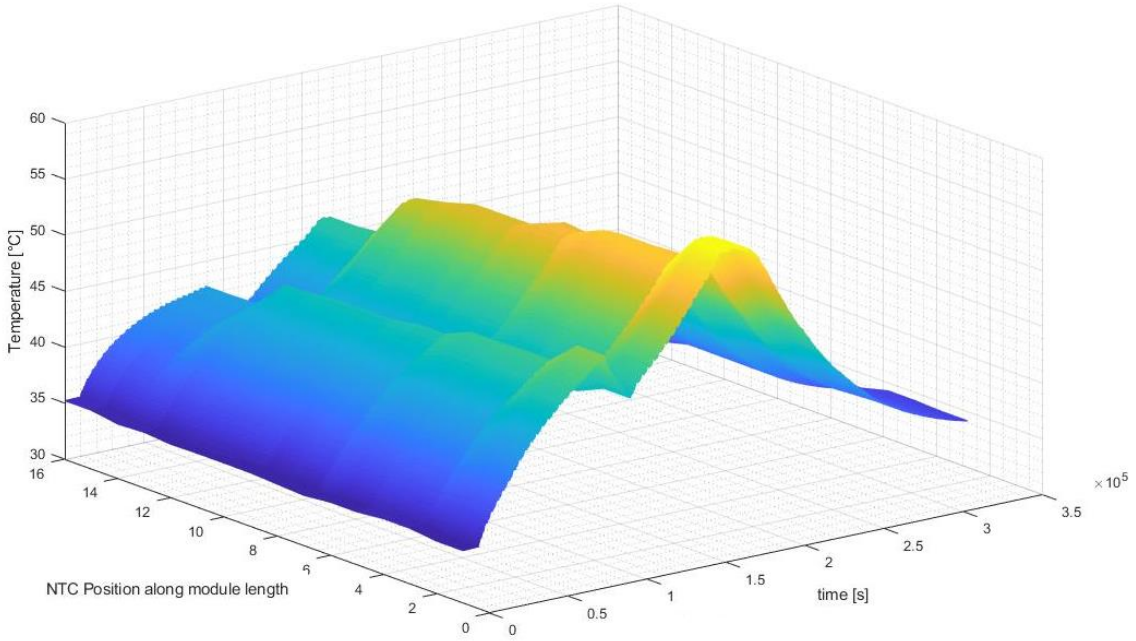

Figure 75 Temperature sensor monitoring along the module length.

6.3 Final Assembly

Figure 76 shows the overall assembly of the accumulator. During the assembly no major issues were discovered since the CAD model lacked enough manufacturing tolerance. A weak point has been the cable managing since HV cables have small bending radius and most of the connectors weren't available at the moment of purchase. Therefore, we were obliged to use the 2017 ones which were heavily used.

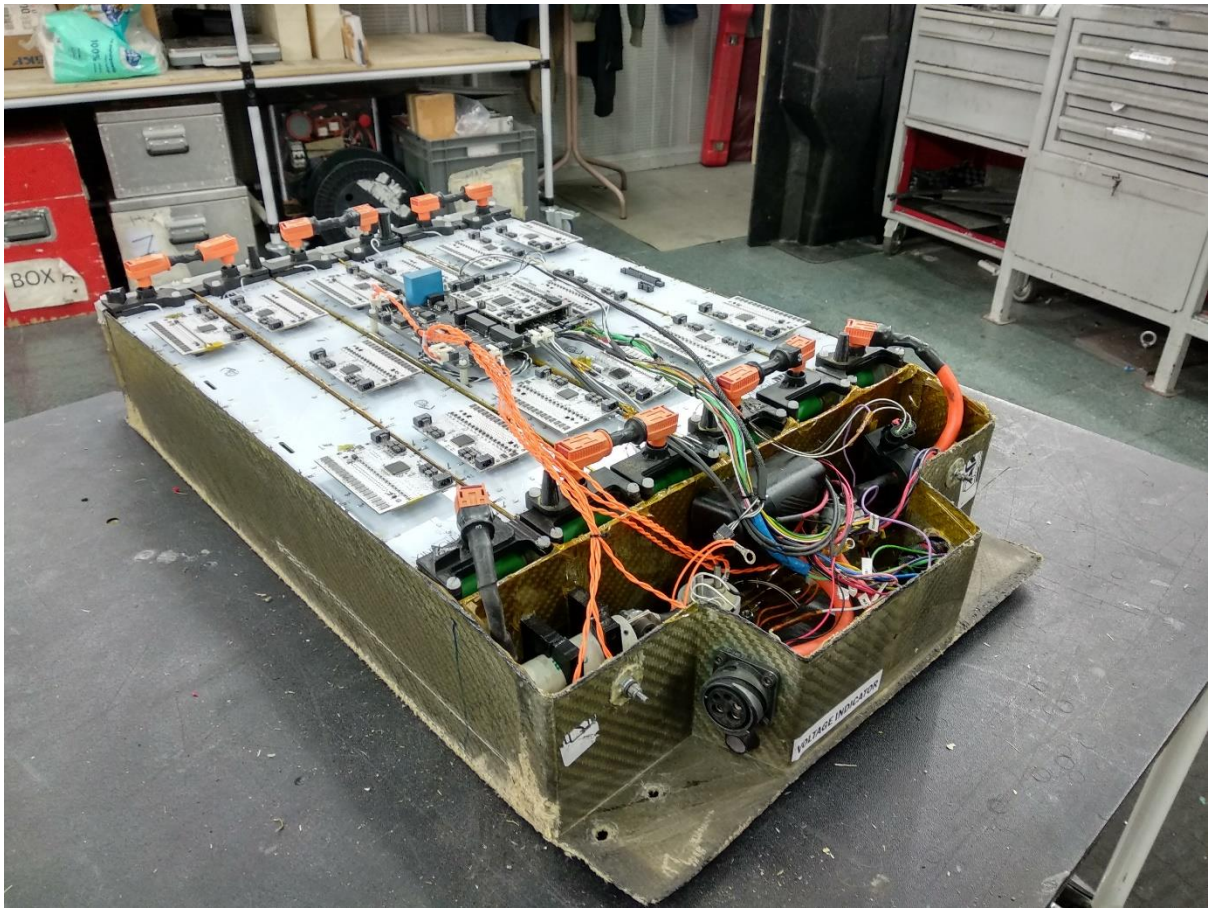

Figure 76 Accumulator fully assembled prior to cable managing.

An overall weight reduction of 17% was achieved with respect to the 2017 Accumulator. During the entire 2018 season, the battery fulfilled its mission profile while sometimes the cooling system was not as effective as simulated and tested in a single module case. Further investigations on conjugate heat transfer between all modules inside the assembly are thus needed.

7 Conclusions

The battery pack represents one of the most important components of a racing electric vehicle. Its complete design, starting from conception to manufacturing, and its final testing during the three different competitions the team participated into, took over ten months.

The starting point of the project has been the achievement of a weight reduction to decrease the battery pack impact on the overall vehicle weight, to align our design with the top world competitors while improving our performance during the races. Following an analysis of the battery pack adopted during the season 2017 and an extensive literature study, it was opted for a completely new design of the pack. A new cell chemistry based on lithium ion cells has been used, which increased the overall specific energy of the battery pack, maintaining the same energy and specific power. Moreover, cells spacing, inlet dimension, fan positioning and configuration have been evaluated and improved to optimise the cooling system and enhance the battery pack performance. In addition, it was adopted a new cell bonding technology which enhanced the overall performance, the reliability and safety of the battery pack. Compared to the other techniques available, it also simplified the manufacturing and assembly processes and it contributed to a decrease of the costs.

During summer the PoliTo racing team participated to two competitions, in Varano de Melegari (Italy) and in Barcelona (Spain). The Traction Battery showed its ability to withstand the maximum power request during all dynamic events and store enough energy to complete the endurance event with remarkable results in efficiency. Indeed, we scored the second place in Italy and 13th In Spain.

Overall this project can be considered as one of the key elements which contributed to the team achievements of 2018. It is worth mentioning that, compared to 2016, the team shifted from the 42nd position to the 24th in the overall world ranking. The battery pack constituted a revolutionary element of the vehicle and it used cutting-edge technologies of the automotive racing field. Even though improvements in the cooling effectiveness can still be achieved, this project surely represents an important starting point for future design and experimental research.

Bibliography

[1] SAE International, "Formula SAE Rules 2019," no. July 2018, pp. 1–134, 2018.

[2] Mazur, "Formula Student Electric - World Ranking List." [Online]. Available: https://mazur-events.de/fs-world/E/. [Accessed: 30-Sep-2019].

[3] S. T. Revankar, "Chemical Energy Storage," *Storage Hybrid. Nucl. Energy*, pp. 177–227, Jan. 2019.

[4] P. Du, N. Lu, M. Beaudin, H. Zareipour, A. Schellenberg, and W. Rosehart, "Energy Storage for Mitigating the Variability of Renewable Electricity Sources," *Energy Storage for Smart Grids*, pp. 1–33, Jan. 2015.

[5] H. Budde-Meiwes, J. Drillkens, B. Lunz, J. Muennix, S. Rothgang, J. Kowal, and D. U. Sauer, "A review of current automotive battery technology and future prospects," *Proc. Inst. Mech. Eng. Part D J. Automob. Eng.*, vol. 227, no. 5, pp. 761–776, 2013.

[6] T. Christen and M. W. Carlen, "Theory of Ragone plots," *J. Power Sources*, vol. 91, no. 2, pp. 210–216, Dec. 2000.

[7] R. Korthauer, *Lithium-ion batteries: Basics and applications*. Germany: Springer-Verlag GmbH, 2018.

[8] D. Deng, "Li-ion batteries: Basics, progress, and challenges," *Energy Sci. Eng.*, vol. 3, no. 5, pp. 385–418, 2015.

[9] Panasonic, "Overview of Lithium-Ion Batteries," 2011. [Online]. Available: https://web.archive.org/web/20111107060525/http://www.panasonic.com/industrial/includes/pdf/Panasonic_LiIon_Overview.pdf. [Accessed: 09-Sep-2019].

[10] Sanyo, "Lithium Ion," 2016. [Online]. Available: https://web.archive.org/web/20160303212922/http://www.rathboneenergy.com/articles/sanyo_lionT_E.pdf. [Accessed: 09-Sep-2019].

[11] D. Dutt, "Life cycle analysis and recycling techniques of batteries used in renewable energy applications," in *2013 International Conference on New Concepts in Smart Cities: Fostering Public and Private Alliances (SmartMILE)*, 2013, pp. 1–7.

[12] SANYO, "CADNICA® Batteries Handling Precautions." SANYO Electric Co., 2004.

[13] D. Aurbach, Y. Talyosef, B. Markovsky, E. Markevich, E. Zinigrad, L. Asraf, J. S. Gnanaraj, and H. J. Kim, "Design of electrolyte solutions for Li and Li-ion batteries: A review," *Electrochim. Acta*, vol. 50, no. 2-3 SPEC. ISS., pp. 247–254, 2004.

[14] "Limitations of Internal Protective Devices in High-Voltage/High- Capacity Batteries Using Lithium-Ion Cylindrical Commercial Cells," *NASA Eng. Saf. Cent.*, vol. 9, no. 2, p. 1998, 1998.

[15] I. Wagner, "Global market share of lithium ion battery makers in the 1st quarter of 2018," 2018. [Online]. Available: https://www.statista.com/statistics/235323/lithium-batteries-top-manufacturers/. [Accessed: 10-Sep-2019].

[16] D. Chung, E. Elgqvist, and S. Santhanagopalan, "Automotive Lithium-ion Cell Manufacturing: Regional Cost Structures and Supply Chain Considerations," 2016.

[17] A. Nikolian, Y. Firouz, R. Gopalakrishnan, J.-M. Timmermans, N. Omar, P. Van Den Bossche, and J. Van Mierlo, "Lithium Ion Batteries — Development of Advanced Electrical Equivalent Circuit Models for Nickel Manganese Cobalt Lithium-Ion," *Energies*, vol. 9, no. 360, pp. 1–23, 2016.

[18] Z. Chu, X. Feng, L. Lu, J. Li, X. Han, and M. Ouyang, "Non-destructive fast charging algorithm of lithium-ion batteries based on the control-oriented electrochemical model," *Appl. Energy*, vol. 204, pp. 1240–1250, Oct. 2017.

[19] Q.-K. Wang, Y.-J. He, J.-N. Shen, Z.-F. Ma, and G.-B. Zhong, "A unified modeling framework for lithium-ion batteries: An artificial neural network based thermal coupled equivalent circuit model approach," *Energy*, vol. 138, pp. 118–132, Nov. 2017.

[20] X. Zhang, J. Lu, S. Yuan, J. Yang, and X. Zhou, "A novel method for identification of lithium-ion battery equivalent circuit model parameters considering electrochemical properties," *J. Power Sources*, vol. 345, pp. 21–29, Mar. 2017.

[21] L. Lu, X. Han, J. Li, J. Hua, and M. Ouyang, "A review on the key issues for lithium-ion battery management in electric vehicles," *J. Power Sources*, vol. 226, pp. 272–288, Mar. 2013.

[22] H. Blanke, O. Bohlen, S. Buller, R. W. De Doncker, B. Fricke, A. Hammouche, D. Linzen, M. Thele, and D. U. Sauer, "Impedance measurements on lead–acid batteries for state-of-charge, state-of-health and cranking capability prognosis in electric and hybrid electric vehicles," *J. Power Sources*, vol. 144, no. 2, pp. 418–425, Jun. 2005.

[23] D. Wang, Y. Zhao, F. Yang, and K.-L. Tsui, "Nonlinear-drifted Brownian motion with multiple hidden states for remaining useful life prediction of rechargeable batteries," *Mech. Syst. Signal Process.*, vol. 93, pp. 531–544, Sep. 2017.

[24] X. Dang, L. Yan, K. Xu, X. Wu, H. Jiang, and H. Sun, "Open-Circuit Voltage-Based State of Charge Estimation of Lithium-ion Battery Using Dual Neural Network Fusion Battery Model," *Electrochim. Acta*, vol. 188, pp. 356–366, Jan. 2016.

[25] L. Zhang, H. Peng, Z. Ning, Z. Mu, and C. Sun, "Comparative research on RC equivalent circuit models for lithium-ion batteries of electric vehicles," *Appl. Sci.*, vol. 7, no. 10, 2017.

[26] J. P. Christopherson, "Battery Test Manual forHybrid Electric Vehicles," *Idaho Operations Office*. Idaho Falls, pp. 1–67, 2015.

[27] P. Ramadass, B. Haran, R. White, and B. Popov, "Capacity fade of Sony 18650 cells cycled at elevated temperatures, Part I. Cycling performance," *J. Power Sources*, vol. 112, no. 2, pp. 606–613, 2002.

[28] H. Liu, Z. Wei, W. He, and J. Zhao, "Thermal issues about Li-ion batteries and recent progress in battery thermal management systems: A review," *Energy Convers. Manag.*, vol. 150, pp. 304–330, Oct. 2017.

[29] G. Xia, L. Cao, and G. Bi, "A review on battery thermal management in electric vehicle application," *J. Power Sources*, vol. 367, pp. 90–105, Nov. 2017.

[30] T. Wang, K. J. Tseng, J. Zhao, and Z. Wei, "Thermal investigation of lithium-ion battery module with different cell arrangement structures and forced air-cooling strategies," *Appl. Energy*, vol. 134, pp. 229–238, Dec. 2014.

[31] A. H. Weston, "Liquid cooling manifold with multi-function thermal interface," US20100104938A1, 2010.

[32] M. J. Brand, P. A. Schmidt, M. F. Zaeh, and A. Jossen, "Welding techniques for battery cells and resulting electrical contact resistances," *J. Energy Storage*, vol. 1, no. 1, pp. 7–14, 2015.

[33] H. Zhang and J. Senkara, "Electrothermal Process of Welding," in *Resistance Welding: Fundamentals and Applications*, 2nd editio., Boca Raton: Taylor & Francis Group, 2012, pp. 53–101.

[34] G. Shannon, "Improve Tab to Terminal Connections in Battery Pack Manufacturing," *Amada Miyachi Am. Inc.*, 2016.

[35] J. L. Caron and J. W. Sowards, *Weldability of Nickel-Base Alloys*, vol. 6, no. October. 2014.

[36] A. Das, D. Li, D. Williams, and D. Greenwood, "Joining technologies for automotive battery systems manufacturing," *World Electr. Veh. J.*, vol. 9, no. 22, Aug. 2018.

[37] I. Mys and M. Schmidt, "Laser micro welding of copper and aluminum," 2006, vol. 6107, p. 610703.

[38] A. O' Brien, "Ultrasonic Welding of Metals," in *Welding Handbook Volume 3 - Welding Processes, Part 2*, 9th ed., Miami: American Welding Society, 2007.

[39] E. A. Neppiras, "Ultrasonic welding of metals," *Ultrasonics*, vol. 3, no. 3, pp. 128–135, Jul. 1965.

[40] G. Pistoia, *Lithium-Ion Batteries Advances and Applications*. Elsevier, 2014.

[41] "LEONI Automotive Cables," *LEONI Kabel GmbH 2019*, 2019.

[42] "Fuses." [Online]. Available: http://www.glodark.com/fuses.htm. [Accessed: 24-Sep-2019].

[43] E. V. Olsen and H. G. Lemu, "Mechanical Testing of Composite Materials for Monocoque Design in Formula Student Car," *Int. Sch. Sci. Res. Innov.*, vol. 10, no. 1, pp. 1–8, 2016.